

*Preparation and electrospinning of chitosan
from waste Black Soldier Fly biomass*



A thesis submitted in partial fulfilment of the requirement for the Degree of Magister Scientiae
in Nanoscience in the Department of Chemistry at the
University of the Western Cape
South Africa.

Supervisor
Professor Leslie Petrik

Co-supervisor
Doctor Olanrewaju Fatoba

ABSTRACT

Black soldier flies are important in sustainability because of their ability to voraciously degrade organic waste without constituting a nuisance to the environment. In South Africa, Agriprotein Ltd, a company producing high-protein animal feed is rearing black soldier fly (*Hermetia illucens*, BSF) larvae on organic waste that would otherwise go into landfills. During the process of mass rearing large quantities of dead adult BSF flies and pupae shells are being generated. This motivated the extraction of chitin from the waste materials generated by Agriprotein. This waste can be utilised as an economic source of chitin and its derivative chitosan. Hence, this is the first study to be focused on the chemical extraction of chitin from the pupae shells and adult BSF biomass waste, the conversion of the extracted chitin to chitosan and to fabricate nanofibers from the commercial chitosan by electrospinning technique.

Chitin was optimally extracted from both the pupae shells and adult BSF through demineralisation, deproteinisation and decolouration processes. The extracted chitins were optimally converted to chitosan by deacetylation process. The commercial chitosan were electrospun into nanofibers by optimising the concentration, voltage, flow rate and tip-to-collector distance. The synthesised and fabricated products were characterised using different analytical techniques such as FTIR to examine the spectral patterns and peaks corresponding the stretching and vibrations of various functional groups, XRD to examine the crystalline structure, SEM to examine the morphology and TGA to investigate the thermal stability. Elemental analysis was carried out to determine the degree of acetylation and degree of deacetylation. The commercial shrimp chitin and chitosan were compared to determine the purity of the extracted products. The electrospun chitosan nanofibers were compared to the bulk chitosan to determine how the structure, crystallinity and thermal stability had been altered after the electrospinning process.

The best optimum conditions obtained at 1 M HCl, 100 min and 50 °C for demineralisation and 1 M NaOH, 10 h and 85 °C for deproteinisation yielded the highest final dry weight yield of 13% and 5% for pupae shells and adult BSF chitin respectively. The best optimum conditions obtained at 70% NaOH, 5 h and 100 °C for deacetylation yielded the highest final dry weight

yield of 11% and 2% for pupae shells and adult BSF chitosan respectively. The elemental analysis results revealed that both chitins with a degree of acetylation of 115.1% for pupae shells and 91.5% for adult BSF are of acceptable purity. In addition, both chitosans with a degree of deacetylation of 67% for pupae shells and 69% for adult BSF are of acceptable purity. FTIR, TGA and XRD analysis results demonstrated that the chitins from both pupae shells and adult BSF were in the α -form. Both chitins extracted proved to be fibrous in nature with no porosity, whereas the pupae shells and adult BSF chitosan were characterised without any nanofibers and/or nanopores. The MW of chitosan samples was 217 kDa for pupae shells and 216 kDa for adult BSF. The optimum conditions of the electrospun commercial chitosan nanofibers were obtained at 6 wt% commercial chitosan in TFA, an applied voltage of 25 kV, a tip to collector distance of 10 cm and a flow rate of 0.1 mL/h. The morphology of the optimised commercial chitosan nanofibers had a regular smooth morphology with some small variations in fiber diameter in a bead free network with an average diameter of 130 nm in a range of 60 nm to 200 nm. FTIR analysis revealed that the chemical nature of the polymer during the electrospinning process was not altered. The XRD analysis revealed that the electrospun nanofibers are amorphous and TGA showed that the bulk chitosan (310 °C) was more thermally stable than the electrospun commercial chitosan nanofibers (272 °C).

The chitin and chitosan extracts from pupae shells and adult BSF were similar in quality and purity as commercially produced chitin and chitosan from shrimp, making it a promising new alternative source and an alternative in terms of utilisation and applications. The present study also report on the successful optimisation and fabrication of chitosan nanofibers from commercial chitosan by electrospinning.

DECLARATION

I, the undersigned, hereby declare that the work contained in this thesis titled **Preparation and electrospinning of chitosan from waste black soldier fly biomass** is my own work and has not previously been submitted for any degree or assessment at any university. All the sources that I have used or quoted have been indicated and acknowledged by means of complete references.

M.N. Zimri

Date

DEDICATION

I dedicate this thesis to

My late father, Mr Nelson Demas for all the sacrifices and giving me the opportunity to pursue my degree.

&

My caring mother, Mrs Margaret Demas for her never-ending love, motivation and support throughout the storms of life, believing in me and inspiring me to achieve more.

ACKNOWLEDGEMENT

I would like to extend my sincere gratitude and thanks to:

God Almighty for giving me patience and strength to endure all the difficulties and distress encountered through the process of completing this work.

Prof Leslie Petrik for her guidance, positive criticism and allowing me to grow as a researcher. I believe that her wealth of experience and knowledge has steered me on the path to achieve even greater heights in my career.

To my co-supervisor Dr Olanrewaju Fatoba I would like to thank you for the guidance, support and dedication you have shown towards this project.

Mr. Cosmas Uche, you are truly a special person. I would never have guessed that I would gain the presence of a human being whose silent strength would support me so much. Thank you for all the lessons, tips and advice. For a wonderful friendship filled with laughter.

I appreciate and thank all the ENS members and researchers for your input and being the best colleagues ever to date. I will always cherish the good moments shared in the lab.

My thanks also go to my dearest family and friends for all their help, prayers and support throughout my studies.

I gratefully acknowledge the financial assistance of the DST/National Nanoscience Postgraduate Teaching and Training Programme (NNPTTP) of South Africa towards this research.

I would like to thank Mr. Adrian Josephs (Scanning Electron Microscopy Unit, Department of Physics at University of the Western Cape) for assistance with the SEM. I would also like to acknowledge Dr. Remy Bucher at iThemba LABS (South Africa) for assistance with XRD. In

addition, I would also like to thank Mr. Yunus Kippie at the Pharmacy Department of the University of the Western Cape for assistance with FTIR and TGA.

Finally to Mrs. Valencia Jamali and Mrs. Chyril Abrahams, thank you for always availing yourselves to me for inquiries, fighting with suppliers and sometimes just allowing a small chat.

TABLE OF CONTENTS

ABSTRACT.....	i
DECLARATION	iii
DEDICATION.....	iv
ACKNOWLEDGEMENT	v
LIST OF TABLES.....	xi
LIST OF FIGURES	xiii
LIST OF ABBREVIATIONS.....	xv
LIST OF SYMBOLS AND UNITS.....	xvii
CHAPTER 1	1
INTRODUCTION	1
1.1 Background.....	1
1.2 Problem statement.....	4
1.3 Research questions.....	5
1.4 Aims and objectives.....	5
1.5 Scope and delimitations	6
1.6 Research approach	7
1.7 Outline of the thesis	8
CHAPTER 2	9
LITERATURE REVIEW	9
2.1 <i>Hermetia illucens</i>	9
2.1.1 The origin of <i>Hermetia illucens</i>	9
2.1.2 Feeding and environmental conditions	10
2.1.3 Different applications of black soldier fly	11
2.1.3.1 Alternative protein source	11
2.1.3.2 Waste management and fertilisers.....	12
2.1.3.3 Biodiesel	12
2.1.3.4 Forensics.....	13
2.1.3.5 Antimicrobial properties.....	13
2.2 Insect chitin.....	14
2.3 Chitin and chitosan	15

2.3.1 Structural properties of chitin and chitosan	16
2.3.2 Physiochemical importance of insect chitin and chitosan	18
2.4 Extraction of chitin	20
2.4.1 Chemical methods	20
2.4.2 Biological treatments	23
2.5 Chitosan Deacetylation	24
2.5.1 Alkaline methods	24
2.5.2 Enzymatic methods.....	25
2.6 Applications	25
2.7 Electrospinning	26
2.7.1 Principle of electrospinning.....	27
2.7.2 Polymers used in electrospinning	28
2.8 Electrospinning of chitosan.....	28
2.9 Effects of various parameters on electrospinning.....	29
2.9.1 Solution parameters.....	30
i. Concentration	30
ii. Molecular weight.....	31
iii. Viscosity.....	31
iv. Surface tension	32
v. Conductivity	32
2.9.2 Process parameters	33
i. Applied voltage	33
ii. Flow rate.....	34
iii. Tip to collector distance	34
2.9.3 Ambient conditions.....	35
2.10 Applications	35
2.11 Characterisation techniques for chitosan and its based materials.....	36
2.11.1 Microscopic techniques.....	36
2.11.2 X-ray Diffraction.....	37
2.11.3 Thermogravimetric Analysis.....	37
2.11.4 Spectroscopic techniques	38
i. Fourier Transform Infrared Spectroscopy	38

ii. ¹³ Carbon-Nuclear Magnetic Resonance Spectroscopy.....	39
2.12 Summary of review.....	40
CHAPTER 3	42
MATERIALS & METHODS	42
3.1 Sample collection, preparation and materials	42
3.2 Chitin isolation from black soldier flies.....	42
i. Demineralisation.....	43
ii. Deproteinisation	43
iii. Decolourisation	44
3.3 Chitosan production.....	44
3.3.1 Deacetylation	44
3.4 Yield.....	45
3.5 Electrospinning of chitosan nanofibers.....	46
3.6 Sample preparation for characterisation analysis	46
3.6.1 Elemental analysis	47
3.6.2 Fourier transform infrared spectroscopy (FTIR)	47
3.6.3 Thermogravimetric analysis (TGA)	47
3.6.4 X-ray diffraction (XRD).....	48
3.6.5 Scanning electron microscopy (SEM).....	48
3.7 Viscosimetric determination of chitosan's molecular weight.....	48
3.8 Summary of materials and methods.....	49
CHAPTER 4	50
RESULTS & DISCUSSION.....	50
4. Physiochemical characterisation of chitin and chitosan	50
4.1 Yield of chitin	51
4.1.1 Demineralisation and Deproteinisation	51
4.2 Yield of chitosan	53
4.2.1 Deacetylation	53
4.3 SEM Analysis	55
4.4 Elemental analysis	60
4.5 FTIR Analysis.....	64
4.6 TGA analysis	71

4.7 XRD analysis	79
4.8 Determination of the optimum chitosan's molecular weight.....	83
4.9 Electrospinning of chitosan nanofibers.....	85
4.9.1 The optimisation of chitosan nanofibers	86
4.9.1.1 Effect of applied voltage and flow rate	86
4.9.1.2 Effect of tip-to-collector distance	90
4.9.1.3 Effect of concentration on chitosan nanofibers	92
4.9.2 Characterisation of optimum chitosan nanofibers.....	94
4.9.2.1 Morphology and size distribution of optimised chitosan nanofibers	94
4.9.2.2 Structural analysis of optimised chitosan nanofibers	97
4.9.2.3 Crystalline structure of the optimised chitosan nanofibers	101
4.9.2.4 Thermal degradation behaviour of the optimised chitosan nanofibers.....	102
4.10 Summary of results and discussion.....	105
CHAPTER 5	107
CONCLUSION AND FUTURE RECOMMENDATIONS	107
5.1 Conclusion	107
5.2 Future work and recommendations.....	111

LIST OF TABLES

CHAPTER 2.....	9
Table 2.1: Comparison of the process conditions of chitin produced according to previous studies.....	21
CHAPTER 3.....	42
Table 3.1: The chitin production conditions were optimised by varying temperature of demineralisation, demineralisation time and concentration of pupae shells and adult BSF as independent variables	43
Table 3.2: The chitin production conditions were optimised by varying temperature of deproteinisation, deproteinisation time and concentration of pupae shells and adult BSF as independent variables	44
Table 3.3: The chitosan production conditions were optimised by varying temperature of deacetylation, deacetylation time and concentration of pupae shells-chitin and adult BSF-chitin as independent variables.....	45
Table 3.4: Process parameters optimised for chitosan nanofiber fabrication	46
CHAPTER 4.....	50
Table 4.1: The % yield of extracted chitin from demineralisation with HCl	51
Table 4.2: The % yield of extracted chitin from deproteinisation with NaOH.....	51
Table 4.3: The % yield of extracted chitosan from deacetylation with NaOH.....	54
Table 4.4: Elemental analysis, DA and DD of chitin and chitosan from pupae shells and adult BSF compared to commercial shrimp chitin and chitosan.....	60
Table 4.5: The FTIR assignment bands (cm^{-1}) of chitin isolated from pupae shells and adult BSF, <i>H. illucens</i>	65
Table 4.6: The FTIR assignments of bands (cm^{-1}) of chitosan isolated from the pupae shells and adult BSF, <i>H. illucens</i>	69
Table 4.7: Thermogravimetric results of commercial shrimp chitin and chitin extracted from pupae shells and adult BSF.....	73
Table 4.8: Thermogravimetric results of commercial shrimp chitosan and chitosan extracted from pupae shells and adult BSF.....	77

Table 4.9: X-ray diffraction data of commercial shrimp chitin and chitins isolated from pupae shells and adult BFS.....	80
Table 4.10: Intrinsic viscosity, Mark-Houwink constants and average molecular weight of pupae shells-chitosan, adult BSF-chitosan and commercial shrimp-chitosan.....	84
Table 4.11: The FTIR assignments of bands (cm^{-1}) of the commercial shrimp chitosan nanofibrous mat and bulk commercial chitosan.....	99

LIST OF FIGURES

CHAPTER 1.....	1
Figure 1: Flow chart of the research of this study.....	7
CHAPTER 2.....	9
Figure 2.1: Schematic depicting chemical structure of chitin (Younes & Rinaudo, 2015).....	16
Figure 2.2: Schematic depicting chemical structure of chitosan (Younes & Rinaudo, 2015).....	17
Figure 2.3: Schematic diagram of the typical electrospinning setup (Mazoochi & Jabbari, 2011).....	27
CHAPTER 4.....	50
Figure 4.1: Scanning electron micrographs (SEM) of a) chitin from pupae shells, b) chitin from adult BSF and c) commercial shrimp chitin (Sigma Aldrich)	56
Figure 4.2: Scanning electron micrographs (SEM) of a) chitosan from pupae shell-chitin, b) chitosan from adult BSF-chitin and commercial chitosan (Sigma Aldrich).....	58
Figure 4.3: FTIR spectra of extracted chitins from adult BSF and pupae shells compared to commercial shrimp chitin (Sigma Aldrich).....	64
Figure 4.4: FTIR spectra of extracted adult BSF and pupae shells chitosan compared to the commercial shrimp chitosan (Sigma Aldrich).....	68
Figure 4.5: TGA (A) and DTG (B) thermograms of the extracted adult BSF-chitin and pupae shells-chitin compared to the commercial shrimp chitin (Sigma Aldrich).....	72
Figure 4.6: TGA (A) and DTG (B) thermograms of the extracted pupae shells-chitosan and adult BSF-chitosan compared to the commercial shrimp chitosan (Sigma Aldrich).....	76
Figure 4.7: X-ray Diffractograms of the extracted adult BSF-chitin and pupae shells-chitin compared to the commercial shrimp chitin (Sigma Aldrich).....	79
Figure 4.8: X-ray Diffractograms of the extracted adult BSF-chitosan and pupae shells-chitosan compared to the commercial shrimp chitosan (Sigma Aldrich).....	82
Figure 4.9: SEM micrographic images depicting the differences in voltage of commercial chitosan nanofibers: 20 kV (a), 22 kV (b) and 25 kV (c). In all experiments 5 wt% of commercial chitosan in TFA, a flow rate of 0.1 mL/h and 10 cm tip to collector distance were used.....	87

Figure 4.10: SEM micrographic images depicting the differences in electrospinning flow rate of commercial chitosan nanofibers: 0.06 mL/h (a), 0.08 mL/h (b) and 0.1 mL/h (c). In all experiments 5 wt% of commercial chitosan in TFA, a voltage of 25 kV and 10 cm tip to collector distance were used.....89

Figure 4.11: SEM micrographic images depicting the differences in tip-to-collector distance during electrospinning of commercial chitosan nanofibers: 7 cm (a), 10 cm (b) and 12 cm (c). In all experiments 5 wt% of commercial chitosan in TFA, a voltage of 25 kV and a flow rate of 0.1 mL/h were used.....91

Figure 4.12: SEM micrographic images depicting the differences in solution concentration used to prepare commercial chitosan nanofibers: 3 wt% (a), 5 wt% (b) and 6 wt% (c). In all experiments a voltage of 25 kV, a flow rate of 0.1 mL/h and 10 cm tip to collector distance were used.....92

Figure 4.13: SEM micrographs (a) and the corresponding histogram (a') of the commercial chitosan nanofibers at optimised electrospinning conditions (6 wt% commercial chitosan in TFA, a voltage of 25 kV, a flow rate of 0.1 mL/h and 10 cm tip to collector distance).....95

Figure 4.14: FTIR spectra of the nanofibrous mat fabricated from commercial chitosan at optimum conditions (6 wt% of commercial chitosan in TFA, 25 kV applied voltage, a flow rate of 0.1 mL/h and 10 cm tip to collector distance) compared to bulk commercial chitosan.....98

Figure 4.15: X-ray Diffractograms of the nanofibrous mats fabricated from commercial chitosan at optimum conditions (6 wt% of commercial chitosan in TFA, 25 kV applied voltage, a flow rate of 0.1 mL/h and 10 cm tip to collector distance) compared to the bulk commercial chitosan.....101

Figure 4.16: TGA (A) and DTG (B) thermograms of the electrospun commercial chitosan nanofiber fabricated from commercial chitosan at optimum conditions (6 wt% of commercial chitosan in TFA, 25 kV applied voltage, a flow rate of 0.1 mL/h solution and 10 cm tip to collector distance) compared with the bulk commercial chitosan.....104

LIST OF ABBREVIATIONS

A	Absorbance
BSF	Black soldier fly
BSFL	Black soldier fly larvae
C	Carbon
CrI	Crystallinity index
CP	Cross-polarisation
C-NMR	Carbon Nuclear Magnetic Resonance
DA	Degree of acetylation
DD	Degree of deacetylation
DMSO	Dimethyl sulfoxide
DTG	Differential thermogravimetric
FTIR	Fourier Transform Infra-Red
FBC	Fat-binding capacity
<i>H. illucens</i>	<i>Hermetia illucens</i>
HCl	Hydrochloric acid
H-NMR	Hydrogen Nuclear Magnetic Resonance
MAS	Magic-angle spinning
MW	Molecular weight
N	Nitrogen
N/A	Not applicable
NMR	Nuclear Magnetic Resonance
pH	Potential of hydrogen
PM	Peritrophic matrix
PVA	Poly vinyl alcohol
PEO	Poly ethylene oxide
PCL	Poly caprolactone
rpm	Revolutions per minute
SDS	Sodium dodecyl sulfate
SEM	Scanning Electron Microscopy

TGA	Thermogravimetric Analysis
TFA	Trifluoroacetic acid
TEM	Transmission electron microscopy
UV-VIS	UltraViolet Visible
WBC	Water-binding capacity
XRD	X-ray Diffraction

LIST OF SYMBOLS AND UNITS

α	alpha
β	beta
γ	gamma
%	percentage
$^{\circ}\text{C}$	degree Celsius
>	greater than
<	smaller than
$[\eta]$	Intrinsic viscosity
θ	Degree
Ω	Omega
μM	MicroMeter
cm	centimeter
g	Gram
g/mol	Gram per mole
Da	Daltons
h	Hour
kV	Kilovolt
kDa	KiloDalton
mL	Milliliter
min	Minute
mL/h	Milliliter per hour
mg	Milligram
mL/min	Milliliter per minute
M	Molar
mL/g	Milliliter per gram
mV	millivolts
nm	nanometer
v:v	Volume per volume
wt%	Weight percentage
w:v	Weight per volume

CHAPTER 1

INTRODUCTION

Summary

This chapter presents a brief background to the study which highlights, amongst other items, the extraction of chitin from black soldier fly biomass, the conversion of chitin to chitosan and the importance of characterising the physiochemical properties of chitin and chitosan. The emphasis is on the electrospinning of the chitosan into chitosan nanofibers. The problem and its significance, the research's aim, objectives and framework, scope and delimitations, as well as the thesis outline are further discussed.

1.1 Background

Chitin (β -(1–4)-poly-N-acetyl-D-glucosamine) is widely distributed in nature and is the second most abundant polysaccharide after cellulose. Chitin, which occurs in nature as ordered microfibrils, is a major structural component in the exoskeletons of insects and crustaceans shells, in fungal cell walls and some microorganisms (Erdogan & Kaya, 2016; Kaya *et al.*, 2016; Kaya *et al.*, 2015; Kaya *et al.*, 2014). Chitin and its derivative chitosan have been receiving increasing attention as extremely useful biopolymers over the last few years. They are known as natural polysaccharide biopolymers that are non-toxic, renewable, biodegradable, biocompatible, with high porosity, free from antigenic effects and polar in nature (Philibert *et al.*, 2017; Erdogan & Kaya, 2016). For the past few years chitin has been isolated from waste marine food products such as shrimp, crab and prawn shells and these have since been the main commercial source (Philibert *et al.*, 2017). The physiochemical properties of chitin vary from batch to batch due to seasonality of the raw material, the quality of the raw material, species present, climate and difficulties in process control. This has led to expanded interest in the production of chitin and chitosan from different sources such as the exoskeletons of insects and cell walls of fungi, etc. (Kaya *et al.*, 2014, Kaya *et al.*, 2015).

Chitin together with proteins found in insects give their cuticles mechanical strength and integrity (Ehrlich, 2010), whereas chitin found on the inner surface of insect gut gives mechanical strength and provides protection against reactive oxygen species and microbial

invasion (Kaya *et al.*, 2016). In addition, chitin from insects attracts interests due to its fundamental role in the insect physiology. It is well established in literature that the isolation of chitin is highly dependent on the source. The different sources of chitin differ in structure for example in terms of yield, crystallinity index, purity, morphology and thermal stability (Ofem *et al.*, 2017). Recent reports (Erdogan & Kaya, 2016; Kaya *et al.*, 2016; Kaya *et al.*, 2014) have expounded the changes in the features of chitin in an organism at different developmental stages. For example, chitin content and thermal stability of chitin in an organism differ greatly from one developmental stage to another (Erdogan & Kaya, 2016; Kaya *et al.*, 2014). Kaya *et al.* (2016) in their study on *Vespra Crabro* reported that there is a nearly 3-fold increase in chitin content during its transition from larva to pupae stage (Kaya *et al.*, 2016). However, despite the recent attempts on extracting chitin, structural modifications in chitinous matrix accompanying the growth of the organism (for example larvae, pupae and adult), should be studied in detail. Chitin has become of great interest over the years due to worldwide demand and is rapidly growing as potential new applications are discovered virtually every day. In addition, it is known that at least 10^{11} tons of chitin are produced and degraded annually in the aquatic biosphere alone (Zaku *et al.*, 2011), however, only over 150 000 tons of chitin is made available for commercial use. Due to the intractable molecular structures of chitin, it still remains primarily an underutilised resource despite its availability and huge annual production.

Chitosan is a linear copolymer of β -(1-4) linked 2-acetamido-2-deoxy- β -D-glucopyranose and 2-amino-2-deoxy- β -D-d-glucopyranose (Elsabee *et al.*, 2012). It is obtained by deacetylation of chitin, a polysaccharide widely distributed in nature. The main characteristics that define the chitosan biopolymer are its molecular weight (MW) and degree of deacetylation (DD). These characteristics are fundamental to ensure the chitosan properties, including solubility, polycationic character, antimicrobial properties, biocompatibility and bioadhesivity (Philibert *et al.*, 2017; Elsabee *et al.*, 2012). The DD of chitosan, which is an indication of the number of amino groups along the chains, is calculated as the ratio of D-glucosamine to the sum of D-glucosamine and N-acetyl-D-glucosamine. Chitosan DD greatly varies between 60 and 100% while its MW typically ranges from 300 to 1000 kDa, depending on the source and preparation (Philibert *et al.*, 2017). Chitosan is also widely applied for the removal of toxic metal ions from aqueous solutions, due to the presence of amino and hydroxyl groups in its structure. Therefore,

it is used for the treatment of wastewaters, purifying them by recovering toxic metals. Chitosan offers advantages, being processed into gels, membranes, beads, microparticle, nanoparticles, scaffolds, sponges and nanofibers (Kaya *et al.*, 2016; Hang *et al.*, 2010; Prabakaran & Jayakumar, 2009; Jayakumar *et al.*, 2007; Marreco *et al.*, 2004). Thus, chitosan and its derivatives can be used in various industrial fields. Chitin and chitosan are currently used in multiple applications in various fields such as textiles, biotechnology, medicine, agriculture and wastewater treatment (Philibert *et al.*, 2017; Bae *et al.*, 2013; Hang *et al.*, 2010; Renault *et al.*, 2009). Data published on the worldwide chitosan market estimated it to be 13,730 metric tons in 2010, but the demand for chitosan is growing rapidly, where the market is expected to reach 40,465 metric tons annually by 2018 (Philibert *et al.*, 2017). To further extend the application, the significance of the diversity of these remarkable biopolymers has yet to be determined.

In South Africa, Agriprotein Ltd, a company producing high-protein animal feed is rearing black soldier fly (BSF, *Hermetia illucens*) larvae on organic waste that would otherwise go into landfills. On a daily basis 30 kg of dead adult flies and 15 kg of pupae shells are being produced by *H. illucens* at AgriProtein and this has resulted in the generation of large quantities of waste (Sripontan *et al.*, 2017). Studies have shown that the pupae shells of insects contain chitin. Therefore, the waste pupae shells and dead adult BSF flies generated by AgriProtein could be a good source of chitin which can be converted to chitosan for different applications. Hence, this study focuses on the extraction of chitin from the pupae shells and dead adult BSF flies due to its composition and availability as waste. Waśko *et al.* (2016) recently reported the physiochemical properties of chitin extracted from larvae and adult of *H. illucens*. However, up to the present, there have been no studies on the physiochemical characterisation and content of chitin and chitosan obtained from pupae shells and adult BSF.

In this study, different chitin extraction techniques were explored and optimised before the chitin was converted to chitosan. In literature, chitosan is well recognised as a versatile polymer for nanofiber production by electrospinning. In the last decade, nanofibers from chitosan (Kaya *et al.*, 2016; Mazoochi & Jabbari, 2011) or chitosan-synthetic blends (Homayoni *et al.*, 2009) have been prepared by electrospinning. Chitosan's free amino groups which make it a positively-charged polyelectrolyte in pH below 2-6 and which contribute to its higher solubility in

comparison to chitin. However, this property makes chitosan solutions highly viscous and complicates its electrospinning. Furthermore, the formation of strong hydrogen bonds in a 3-D network prevents the movement of polymeric chains exposed to the electrical field. Electrospinning is an efficient fabrication technique that enables the mass production of polymer nanofibers with unique properties (Bhardwaj & Kundu, 2010). Electrospun nanofibers exhibit some special characteristics, such as high specific surface area, high porosity, and very small pore structures between the fibrous matrix. Nanofibers fabricated from natural polymers are applied in a broad spectrum of operations in fields like tissue engineering (Ma *et al.*, 2012), drug delivery (Zhang *et al.*, 2005), nanofiltration (Cooper *et al.*, 2013), toxic metal removal (Haider & Park, 2009) and biosensor design (Ding *et al.*, 2014). The present study thus report on the optimisation and fabrication of chitosan nanofibers from the commercial shrimp chitosan by electrospinning.

The hypothesis for this study is that the pupae shells and adult BSF do indeed contain chitin, that the extracted chitin can be converted to chitosan and that the commercial chitosan can be electrospun into nanofibers.

1.2 Problem statement

The human population is growing at a rapid rate with the global population standing at more than 7.3 billion people, and numbers are expected to reach 9.7 billion by 2050 (Brits, 2017). The two primary concerns arising as the population increases, are the inevitable stress that is being put on global food security, and waste management (Salomone *et al.*, 2017; Alooh, 2015). AgriProtein's Technology has come up with a green process to produce animal feed thus not only solving the food security problem but also healing our planet in the process by recycling organic waste.

AgriProtein, the world's biggest fly-farmer, has developed a blueprint for mass-production of sustainable animal feeds as an alternative to fishmeal widely used in aquaculture and agriculture. Likewise, AgriProtein Technology also helps tackle local waste disposal issues by rearing black soldier flies on organic waste that would otherwise go to landfills. An AgriProtein fly farm has a population of 8.5 billion black soldier flies which are used to convert 250 tonnes of organic waste per day into animal feed, with a similar amino acid and protein profile to fishmeal. In addition, the AgriProtein industry has been rapidly increasing with the growing of cultured black

soldier fly larvae production, whereby 5000 tonnes of Magmeal™ and 2000 tonnes of Magoil™ rich in high-quality protein and lipids are produced per year. During the process of rearing black soldier fly larvae on organic waste in order to manufacture a high quality-protein feeds, bio-waste of dead pupae shells and adult BSF flies are being generated along the line. As result of the large quantity of waste generated, the disposal of the waste has resulted in the introduction of an unpleasant odour and aesthetic damage to the environment. In order to avoid this, beneficial use of the waste materials is considered necessary. This motivated the extraction of chitin from the waste materials generated by AgriProtein. The conversion of the waste into a useful product like chitosan can potentially add economical value to the rearing of black soldier flies and the chitin and chitosan industry.

1.3 Research questions

- a. Do pupae shells and dead adults of BSF contain chitin?
- b. Is the chitin content of pupae shells and dead adults of BSF extractable?
- c. Can the extracted chitin from pupae shells and dead adults of BSF be converted to chitosan?
- d. What is the percent yield of chitin and chitosan from both pupae shells and adult BSF?
- e. What are the molecular weights of BSF pupae shells and adult-based chitosan?
- f. Can the chitosan be electrospun into nanofibers?

1.4 Aims and objectives

The aims of this study are to extract chitin from the adult BSF and pupae shells waste, to convert the extracted chitin to chitosan and to fabricate nanofibers from the chitosan by electrospinning technique.

The objectives of this study are as follows:

- a. To find the best route to extract chitin from black soldier fly waste.
- b. To optimally convert the extracted chitin into chitosan.
- c. To characterise the chitin and chitosan using different analytical techniques such as elemental analysis, FTIR, XRD, TGA, and SEM.
- d. To determine the optimised condition for the electrospinning of chitosan nanofibers.

- e. To characterise the electrospun chitosan nanofiber membranes using different analytical techniques such as SEM, FTIR, XRD, and TGA.

1.5 Scope and delimitations

This study aimed specifically at addressing the waste problem by extracting chitin from pupae shells and adult BSF and converting it into chitosan through demineralisation, deproteinisation, decolouration and deacetylation processes. Both chitin and chitosan yield was determined from dry weight. This study then compared the physiochemical properties of chitin and chitosan to commercial shrimp chitin and chitosan products. Both the chitin and chitosan were characterised by different analytical techniques including FTIR, SEM, TGA, XRD and elemental analysis. The extracted chitosan's molecular weight was determined with the viscometry method. Furthermore, the commercial chitosan was electrospun into chitosan nanofibers by optimising the concentration, voltage, flow rate and tip to collector conditions and then characterised by SEM, FTIR, XRD and TGA.

The study is limited to the design of potential applications of the extracted chitins and chitosans. Furthermore, this study did not cover the electrospinning of pupae shells and adult BSF chitosan due to limited time. In addition, this study did not cover the neutralisation and stabilisation of the commercial chitosan nanofibers and it also did not include the application of the fabricated chitosan nanofibers. Moreover, a few characterisation techniques were not included such as nuclear magnetic resonance (NMR), raman spectroscopy and ultraviolet-visible (UV-VIS) spectroscopy.

1.6 Research approach

The research approach of this study is identified as follows:

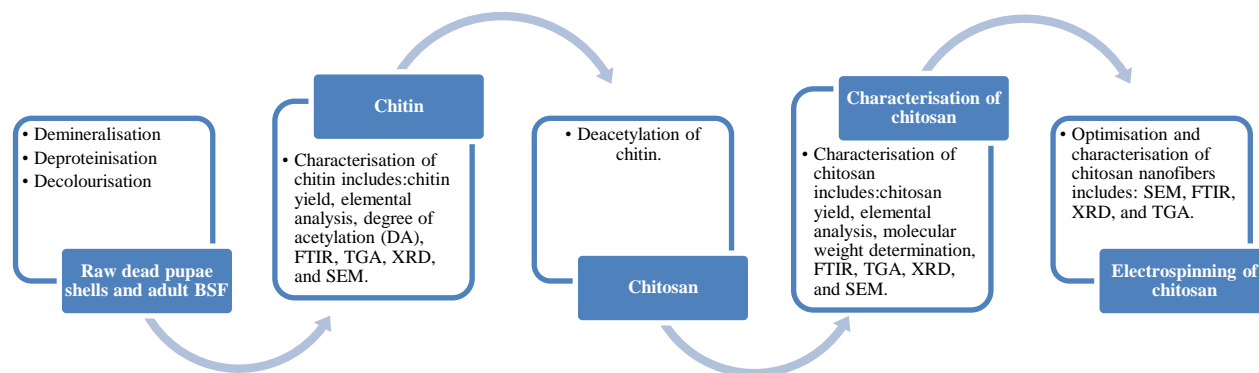


Figure 1: Flow chart of the research of this study.

Figure 1 shows the flow chart of the research approach of this study. In this study, the pupae shells and adult BSF waste were obtained from AgriProtein farm. The pupae shells and adult BSF wastes were then processed to powder form through drying and grinding. The pupae shells and adult BSF waste powder then underwent demineralisation by using dilute (1 M) hydrochloric acid (HCl) to remove minerals. The residue obtained was then filtered, rinsed until neutral pH and dried in an oven. This was followed by deproteinisation using dilute alkali (1 M) sodium hydroxide (NaOH) to remove protein. Once again, the residue was filtered, rinsed until neutral pH and dried in an oven. Next, the chitin was decolourised by 3% sodium hypochlorite (NaClO), filtered, rinsed until neutral pH and dried in an oven. The chitin then underwent deacetylation by using 70% NaOH to convert it to chitosan. The residue obtained was then filtered, rinsed until neutral pH was attained and dried in an oven. The chitin and chitosan products obtained from these processes were characterised using various characterisation techniques and compared to the commercial products. The commercial chitosan was electrospun into chitosan nanofiber membrane by varying solution concentration, applied voltage, flow rate and tip to collector distance. The obtained chitosan nanofibers were then characterised by different analytical techniques by comparing to the bulk commercial chitosan.

1.7 Outline of the thesis

The thesis outline of this study is as follows:

Chapter 1: This chapter presents a brief background of the main aspects of the study, that is: black soldier fly waste, extraction of chitin from black soldier fly waste, conversion of chitin to chitosan, and the fabrication of chitosan nanofibers. The problem and its significance, the research questions, the research's aim and objectives and the scope and delimitations are also discussed. Furthermore, a brief outline of the research approach and thesis chapters is also included.

Chapter 2: This chapter presents an extensive literature review on the concepts of the study which were briefly introduced in the previous chapter. The concepts, discussed amongst others, include: what is black soldier fly, different types of sources and morphology of chitin, chemical and biological extraction methods of chitin, various characteristics of chitosan for example molecular weight, viscosity etc., chemical and enzymatic deacetylation methods of chitosan. This is followed by the working principles and the different parameters in the electrospinning process, solvents used in the electrospinning process, different types of analytical techniques to characterise the physiochemical properties of chitin and chitosan based material. Applications of nanofibers in different fields are discussed and then a summary of the need for this study.

Chapter 3: This chapter provides the detailed experimental procedures, the chemical reagents, materials and instruments which facilitated the successful synthesis, characterisation and finally fabrication of desired nanofibers.

Chapter 4: This chapter presents and discusses the results from various characterisation techniques employed to validate the successful extraction of chitin and chitosan, and the fabrication of chitosan nanofibers.

Chapter 5: This chapter summarises the main points and findings of the study with final conclusion, future work and recommendations.

References

This section presents a list of all the references cited in this study.

CHAPTER 2

LITERATURE REVIEW

Summary

This chapter presents a literature review of the concepts of the study which were briefly introduced in the previous chapter. The concepts, discussed amongst others, include: black soldier fly origin, classification of different types of chitin sources, chemical and biological methods, characteristics of chitosan and applications of chitin and chitosan. This followed by the working principles and the different parameters in electrospinning process. Applications of nanofibers are further described, with the characterisation techniques applied in this study finalising this chapter.

2.1 *Hermetia illucens*

2.1.1 The origin of *Hermetia illucens*

The black soldier fly (BSF), *Hermetia illucens*, is a true fly (Diptera) of the family Stratiomyidae. Black soldier fly originates from Central America (Benelli *et al.*, 2014; Brits, 2017), however it now occurs worldwide in tropical and temperate regions (Benelli *et al.*, 2014; De Groot & Veenvliet, 2011; Heo *et al.*, 2008). Black soldier fly is a holometabolous insect which undergoes a complete metamorphosis.

Hermetia illucens is considered a non-pestilent fly as the adults do not have functional mouth parts or digestive organs to consume waste (Brits, 2017). They are not found in human settlements, except in exposed pit latrines or on animal farms where they utilise manure as food (Yu *et al.*, 2011; Newton *et al.*, 2005). Since the larvae rarely encounter humans, they are not considered a pest or disease vector thus this limits the possibility of disease transmission or nuisance habits compared to the housefly (*Musca domestica*). To further emphasise their non-pest status *H. illucens* larvae have been shown to produce antimicrobial substances that fight disease (Gabler *et al.*, 2014). Black soldier fly's biggest advantage over other insects is their ability to convert waste into food, generating value and closing nutrient loops as they reduce pollution and costs.

2.1.2 Feeding and environmental conditions

Black soldier fly larvae (BSFL) are voracious feeders of a wide range of organic materials including manure, decaying plant materials and carrion (Wang & Shelomi, 2017; Newton *et al.*, 2005). The diversity of substrates they can process and the efficiency with which they do so may be the highest among the flies. These insects could bioconvert more than 30% of the substrates into their own body mass under optimal conditions (Holmes *et al.*, 2016). BSFL are also edible, and have been studied as such. Their larval feed conversion ratios are known to be superior to both crickets and mealworms and compared to those two BSFL survival rate and nitrogen and phosphorous compositions do not vary highly with diet (Wang & Shelomi, 2017). BSFL accumulate lipids from their diet to use as energy by the non-feeding adult, to the point that the lipids can be converted to biodiesel (Brits, 2017; Wang & Shelomi, 2017). The rest that they do not consume, combined with their nitrogen-rich frass, can be used as fertiliser (Brits, 2017). Their larval development time of over three weeks is longer than that of house and carrion flies, indicating a single larva will consume a larger amount of substrate and produce larger pupae (Wang & Shelomi, 2017). Several enzymes have been identified in BSF that assist in breaking down the three major macronutrients using amylases, proteases and lipases (Park *et al.*, 2012; Kim *et al.*, 2011).

The larvae have been shown to withstand temperatures ranging from 16-40 °C (Holmes *et al.*, 2016). In addition to temperature, a relative humidity of between 60-90% is a common practice in the *H. illucens* lifecycle and has been shown to have significant effects on the pupal and adult stages (Holmes *et al.*, 2016). One adult *H. illucens* will take a maximum of 55 days to complete its lifecycle (Tomberlin *et al.*, 2009). The duration from egg hatch to prepupae is approximately 21 days (Tomberlin *et al.*, 2009). Nutritionally the larvae consist of 44.1±9.1% protein and 27.6±9.6% lipids and larvae tend to feed in mediums with similar macronutrient balances (Surendra *et al.*, 2016). All these benefits make BSFL a suitable tool to valorise wastes, plus a sustainable animal feed. The rest of this section will look at many uses of this fly species.

2.1.3 Different applications of black soldier fly

2.1.3.1 Alternative protein source

Recently, there has been a significant increase in the demand for protein and lipid sources for animal feed throughout most developed and developing countries due to the rapid increase in global human population and/or climate change (Wang & Shelomi, 2017). Insects are rich sources of proteins, fats, and certain trace elements (van Huis, 2013). Their biggest advantage over other animal meats, is their lower environmental impact (Wang & Shelomi, 2017). Insects have a lower feed-to-protein conversion ratio than cattle or swine and even poultry according to some sources, and produce fewer greenhouse gases and lower ammonia emissions than any conventional livestock (Wang & Shelomi, 2017; van Huis, 2013).

The increasing price of fishmeal and fish oil (e.g. lipids) required for aquaculture, due to overexploitation, may lead to making fish inaccessible for human consumption. In order to avoid shortage of fish for human consumption, alternative feed stocks have been sought for aquaculture, which includes plant and insect-based feeds (Wang & Shelomi, 2017; Karapanagiotidis *et al.*, 2014). This alternative feedstock would allow fish to be cultured in greater amounts for human consumption. Black soldier flies are a good example of insects that are capable to compost and bioconvert organic wastes into useful products such as a protein source.

According to studies both reared and wild specimens of BSFL are a good source of proteins and lipids (Wang & Shelomi, 2017). Experiments with African catfish, *Clarias gariepinus*, found total BSFL substitution of fishmeal in diets had no effect in terms of growth rate and nutrient utilisation indices, so BSFL were recommended as an alternative due to their lower cost (Okey *et al.*, 2009). BSFL has also been used in poultry feed as partial replacement for maize or soy-based feeds, mainly because the species naturally colonise and breaks down poultry manure. Populations are often kept by poultry farms for the purpose of waste management and pollution reduction (Wang & Shelomi, 2017). Black soldier flies are also known to reduce the mass and nutrient content of swine manure (Nguyen *et al.*, 2015) at efficiencies similar to poultry manure, with benefits for improved farm hygiene, reduced pest fly populations and reduced nutrient pollution in runoff. BSFL's ability to efficiently produce protein-rich edible biomass from potentially protein-poor organic wastes has led many authors to conclude that BSFL can contribute to sustainable aquaculture as partial or total meal replacement (Magalhães *et al.*, 2017;

Diener *et al.*, 2009; Bondari & Sheppard, 1981). This may apply for aquatic invertebrates such as shrimp (Cummins *et al.*, 2017). It is therefore well established that BSFL can be used to feed many vertebrates and can use various vertebrate wastes as a substrate, with significant positive implications for sustainable and lower input agriculture in the developing world (Wang & Shelomi, 2017). The BSFL is thus a natural and cost-effective alternative to fishmeal in agriculture and aquaculture.

2.1.3.2 Waste management and fertilisers

Hermetia illucens larvae were first known to inhabit manure and gained a lot of interest indirectly, due to fly control studies, but also due to their ability to reduce the amount of waste present therefore acting as manure management agent in confined animal feeding operations (Wang & Shelomi, 2017). This has been reviewed and studied since the 1970s. The use of BSFL has since been expanded to the management of organic wastes such as kitchen wastes, palm kernel waste, biodiesel fractions and vegetable wastes to name a few (Salomone *et al.*, 2017; Wang & Shelomi, 2017; Nguyen *et al.*, 2015). The larvae are able to efficiently reduce waste by as much as 60% and the leftover residue is suitable and safe as a fertiliser for use in plant growth (Brits, 2017; Green & Popa, 2012), especially when exuviae of the larvae are added to the fertiliser (Lee *et al.*, 2013). Additionally, this fertiliser can reduce the number of organic leachates produced from organic wastes, which if not treated with *H. illucens*, could have caused major environmental impacts for surrounding and immediate ecosystems (Green & Popa, 2012).

2.1.3.3 Biodiesel

Biodiesel is a promising alternative, renewable and environmental friendly liquid diesel fuel which has increased worldwide in a number of countries including China and South America (Brits, 2017). However, the feedstock, mainly crop oil including soybean oil, rapeseed oil, and sunflower oil, is a limited and expensive food resource which prevents large scale application of biodiesel. Development of non-food feedstocks is, therefore needed to fully utilise biodiesel's potential. The larvae of a high fat containing insect, BSFL, were evaluated for biodiesel production. When fed on the organic fraction, dairy manure or organic kitchen wastes BSFL have been shown to be high in lipids that are a good source for high-grade biodiesel (Leong *et*

al., 2016). The lipid yield can produce as much as 96% biodiesel yield when processed (Brits, 2017). A study conducted by Li *et al.* (2011), reared BSFL on organic waste (chicken manure) to raise a high fat-BSFL insect for biodiesel production, which yielded 91.4 g of biodiesel with a biodiesel yield of 93% from the crude fat contents of BSFL. The fuel properties of the BSFL fat-based biodiesel were comparable to those of rapeseed oil-based biodiesel and met the European biodiesel standard (Li *et al.*, 2011). The BSFL fat-based biodiesel has two advantages over those of crop oil-based biodiesel, firstly, it does not compete with food resources or land use, and secondly, it maximizes the benefits of waste management by using waste nutrients for insect growth.

2.1.3.4 Forensics

Black soldier fly has been found on many cadavers through much of the Central Americas (Pujol-Luz *et al.*, 2008) and has been used in numerous forensic investigations (Ndueze *et al.*, 2013). The flies preferentially colonise later stages of corpse decomposition (Ndueze *et al.*, 2013). However, Tomberlin *et al.* (2005) showed that it can occur as early as the first week of decomposition (Tomberlin *et al.*, 2005). Black soldier flies have been used for forensic purposes in the United States, South America, Europe, Africa and South East Asia (Ndueze *et al.*, 2013; Pujol-Luz *et al.*, 2008; Brits, 2017).

2.1.3.5 Antimicrobial properties

Like many fly larvae, BSFL have several antimicrobial properties of benefit when feeding in a waste medium or in the presence of specific pathogens (Leong *et al.*, 2015; Gabler *et al.*, 2014). Their distinct effect on *Salmonella* spp. in chicken manure and other wastes have been studied several times (Gabler *et al.*, 2014). Choi *et al.* (2012) also showed that extracts of BSFL were effective at reducing general gram-negative bacteria (Choi *et al.*, 2012). In addition, the fatty acid profile of BSF prepupae is, in general, high in the medium-chain fatty acid lauric acid. The fat of prepupae reared on organic waste streams with high amounts of starch contains up to 60% lauric acid (Spranghers *et al.*, 2017). The medium-chain fatty acids are well known for their antimicrobial effects on gut microbiota, while lauric acid is particularly active against gram-positive bacteria (Skřivanová *et al.*, 2005; Spranghers *et al.*, 2018). Likewise Leong *et al.* (2015)

showed that the larvae of BSF contain high levels of lauric acids that have antimicrobial and antifungal properties and therefore could be useful for detergent and soap production (Leong *et al.*, 2015).

2.2 Insect chitin

The evolutionary success of insects is attributable to the development of the cuticle, which is a complex exoskeleton with diverse functions. The composition of the cuticle is dictated by the desired physiochemical and mechanical properties for each anatomical part of the organism. The main structural components of the cuticle are chitin, a large assortment of cuticular proteins, lipids, catecholamines, and minerals. Cuticular proteins and potentially chitin are cross-linked by o-quinones, which are oxidised catecholamines derived from the amino acid tyrosine through the action of different enzymes, including laccase-2 (Zhu *et al.*, 2016). The exoskeleton supports muscle attachment for locomotion, prevents physical and chemical damage, and protects against infectious diseases and water loss. Chitin is also found in the internal structure of many insects and other arthropods, including the inner cuticular linings of the alimentary canal, tracheal system, genital ducts, and the ducts of the various dermal glands (Zhu *et al.*, 2016).

The alimentary canals of most insects contain a chitinous peritrophic matrix (PM), which is an acellular, porous tube lining the midgut epithelium. The PM is an essential component of the insect intestinal tract that surrounds the food bolus and compartmentalises digestion. It also protects the underlying epithelial cells from mechanical damage by rough food particles, from chemical damage by toxins, and from infection by microorganisms (Lehane, 1997; Zhu *et al.*, 2016). Due to the fact that chitin forms a significant portion of the cuticular exoskeleton and PM that is regularly shed and replaced by new materials, synthesis and turnover of chitin are crucial for growth and development of arthropods.

During insect development and metamorphosis, the chitin content of the cuticle fluctuates as a complex function of the activities. All these processes can occur simultaneously during moulting, when the old cuticle is degraded and replaced with the new cuticle formed by the underlying epidermal cells. Similarly, the PM also appears to be degraded and discarded periodically and replaced with a new PM at the time of moulting to allow for intestinal growth and maturation (Shao *et al.*, 2001).

2.3 Chitin and chitosan

Over the years chitin and its derivative chitosan have been receiving increasing attention as valuable biopolymers. Chitin can be found naturally as supporting materials in many aquatic organisms, terrestrial organisms, and some microorganisms, and is also present in vertebrates and is known to give living organisms a strong structure (Elieh-Ali-Komi & Hamblin, 2016; Younes & Rinaudo, 2015; Daraghmeh *et al.*, 2011). Depending on the source, chitin occurs combined with proteins, carbonates, silicates, lipids and pigments in different proportions, the chitin content ranging over a relatively ample interval (5%-40%) as a consequence. Chitin and chitosan are considered to be materials with desired properties and functions that would increase their applications in diverse commercial and scientific areas. The value of chitosan has increased due to its versatile properties which can be employed in food, agriculture, medicine, pharmaceuticals, personal care products and the environmental sectors (Philibert *et al.*, 2017; Elieh-Ali-Komi & Hamblin, 2016; Younes & Rinaudo, 2015). Chitin is highly hydrophobic and therefore its water-insoluble property is probably due to intra- and intermolecular hydrogen bonds that makes chitin a rigid material with adjacent –NH or –OH functional groups formed by the oxygen of the acetamido group (Daraghmeh *et al.*, 2011). Hence, researchers have decided to transform this complex chitin substance into its derivatives with low viscosity and relatively small molecular sizes which in turn make them water soluble and readily absorbed (Elieh-Ali-Komi & Hamblin, 2016). Industrially, chitin and chitosan are obtained from shrimp and crab shells, which are wastes from the seafood industries. First, the crustacean wastes are submitted to demineralisation, deproteinisation, decolouration and drying steps, in order to obtain chitin. Afterwards, the chitin is deacetylated, purified and dried to obtain chitosan. This process is economically feasible since the raw material has zero cost and can include the recovery of a naturally occurring carotenoid, mainly astaxanthin antioxidant. Nowadays, chitosan is commercially produced in Japan, India, China, Italy, Canada, Chile, Poland, Norway, USA and Brazil (Younes & Rinaudo, 2015). Furthermore, the physicochemical characteristics of chitin and chitosan vary from batch to batch due to seasonality of raw materials, the quality of the source, climate, and difficulties in process control. This has led to an expanded interest in chitin and chitosan from different sources such as exoskeleton of insects and cell walls of fungi, microorganisms etc. (Kaya *et al.*, 2015; Kaya *et al.*, 2014).

2.3.1 Structural properties of chitin and chitosan

Chemically, chitin is a linear, uncharged polysaccharide polymer made of numerous units of N-acetyl- β -D-glucosamine (GlcNAc) linked by β -1,4 glycosidic bonds, but some 2-amino-2-deoxy-D-glucopyranose (GlcN) units can occur depending on the biomass and on the procedures used to extract chitin from it. However, chitin from natural sources is a heteropolymer of GlcNAc and glucosamine (GlcN) residues at various proportions (Kumar, 2000).

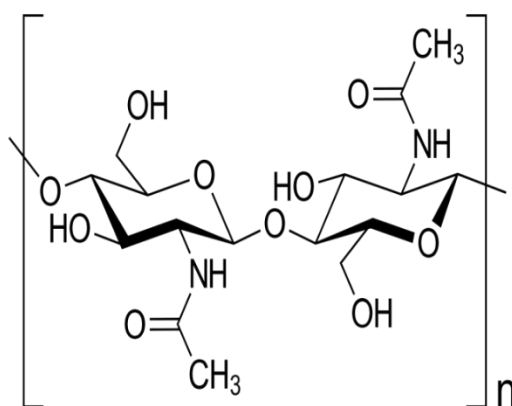


Figure 2.1: Schematic depicting chemical structure of chitin (Younes & Rinaudo, 2015).

Structurally, chitin is similar to cellulose except for the substitution of the 2-hydroxyl group with an acetyl amino group on each monomer. The presence of the acetyl amino group allows for increased hydrogen bonding between adjacent chitin chains, thereby increasing the strength of the fibrillary scaffold, which is made up of multiple chitin chains. As the chitin polymer is synthesised, individual chitin chains assemble in different ways to form crystalline microfibrils through hydrogen bonds between the N-H and the C=O groups, and between adjacent chains. Chitin is a semi-crystalline polymer and, depending on the organism in which it occurs and on its function, the chitin chains adopt different allomorphs in the solid state, namely α -, β -, and γ -chitin. Alpha-chitin, the more stable and wide spread allomorph, occurs where rigidity and mechanical resistance are required, such as in the shells of crustaceans and insects, and it adopts a dense packing due to numerous inter, intra-chains and interlamellar hydrogen bonds, strongly favoured by the anti-parallel orientation of polymeric chains in the ordered domains (Philibert *et al.*, 2017). In beta-chitin, which occurs where flexibility and toughness are important, such as in

squid pens, the polymer chains are disposed in parallel orientation, disfavours the establishment of hydrogen bonds involving chains pertaining to different lamellae and resulting in a less dense packing compared to alpha-chitin (Kaya *et al.*, 2017; Philibert *et al.*, 2017; Daraghmeah *et al.*, 2011). Gamma chitin on the other hand, is much rarer than the other two chitins and some authors claim that it has characteristics of both alpha- and beta-chitin (Kaya *et al.*, 2017).

Chitosan on the other hand is a linear polysaccharide composed of repeated units of N-acetyl-2-amino-2-D-glucopyranose and 2-amino-2-deoxy-D-glucopyranose, which are linked by β -(1-4)-glycosidic bonds. It is known that the amino (NH_2) and hydroxyl (OH) groups in its structure are mainly responsible for its properties and potential applications (Mati-Baouche *et al.*, 2014).

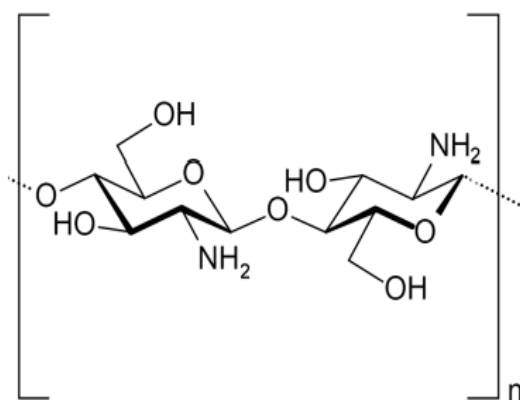


Figure 2.2: Schematic depicting chemical structure of chitosan (Younes & Rinaudo, 2015).

The main characteristics that define the chitosan biopolymer are its molecular weight (MW) and degree of deacetylation (DD). The average MW of chitosan is usually obtained from intrinsic viscosity, exclusion chromatography and matrix-assisted laser desorption/ionization-mass spectrometer. The DD can be determined by different techniques, such as elemental analysis, infrared spectroscopy, potentiometric titration and more advanced methods like hydrogen nuclear magnetic resonance ($^1\text{H-NMR}$) liquid state and solid state carbon nuclear magnetic resonance ($^{13}\text{C-NMR}$). In addition, DD and MW are fundamental to the chitosan properties, including both chemical (solubility, viscosity, flexibility, polymer conformation, crystallinity, high surface area, porosity, tensile strength, thermal stability, conductivity, photoluminescence)

and biological properties (biodegradability, biocompatibility, mucoadhesion, hemostatic, analgesic, adsorption enhancer, antimicrobial, anticholesterolemic, and antioxidant), which vary with process conditions (Philibert *et al.*, 2017; Elieh-Ali-Komi & Hamblin, 2016; Mati-Baouche *et al.*, 2014). Furthermore, the abovementioned characteristics are responsible for determining what chitosan based material could be prepared (films, nanofibers, nanoparticles, nanocapsules, scaffolds, hydrogels) and what the possible application of the biopolymer will be (water treatment, food industry, agriculture, biomedicine). In addition, chitosan also has the ability to chelate with various metal ions, due to the neutral or negatively charged hydroxyl groups of D-glucosamine, GlcN (2-acetamido-2-deoxy-D-glucopyranose) residues and amino groups (Philibert *et al.*, 2017; Younes & Rinaudo, 2015; Vasiliev, 2015). One of the advantages of cationic chitosan polymer is its solubility at neutral and acidic conditions due to its NH_3^+ positive charges at $\text{pH} < 6.5$. Furthermore, alkali concentration, chemical form of the polymer, type of chitin and polymorph type, chitin particle size, heterogeneous or homogeneous N-deacetylation, single or multiple process, and incubation time have been reported to influence chitosan properties (Philibert *et al.*, 2017; Kardas *et al.*, 2012; Aranaz *et al.*, 2009).

2.3.2 Physiochemical importance of insect chitin and chitosan

Insects are a promising source of new biomass because of their constitution (rich in proteins, fats and biopolymers), their cultivation possibilities (grow on organic biological waste streams), and with high percentage of dry matter (20–60%) (Philibert *et al.*, 2017). The procedure for extraction of chitin and chitosan from the cuticle of insects is similar to that of crustacean sources; however, their demineralisation and deacetylation requires a higher concentration than that of aquatic crustacean material. The chemical structure and physiochemical properties of commercial α -chitin from shrimp and seven orthoptera insect species (including *Ailopus simulatrix*, *Ailopus strepens*, *Duroniella fracta*, *Duroniella laticornis*, *Oedipoda miniata*, *Oedipoda caerulescens*, and *Pyrgomorpha cognata*) were reported to be similar and chitin yield varied between 5.3 and 8.9%. Therefore, these species were an alternative chitin source (Kaya *et al.*, 2015; Liu *et al.*, 2012). Moreover, *Hydrophilus piceus* has shown the highest chitosan dry weight productivity, while *Ranatra linearis* and *Notonecta glauca* have shown higher chitin and chitosan thermal stabilities, respectively. Additionally, α -chitin extracted from different insect

species was observed by SEM, TGA, XRD and FTIR with surface morphology of nanofiber structures and the crystalline index value between 76.4 and 90.6% (Kaya *et al.*, 2016; Kaya *et al.*, 2014). Four grasshopper species exhibited a quantity of chitin with dry weight ranging from 4.71 to 11.84%; the male grasshopper chitin surface structure contained 25–90 nm-wide nanofibers and 90–250 nm nanopores. Moreover, the elemental analysis, thermal properties, and crystalline index values for chitin were similar in males and females. Compared with commercial chitin digestion rate, neither sex showed a big difference, respectively (Kaya *et al.*, 2015). The dry bat guano from bat species *Rhinolophus hipposideros* had 28% α -chitin yield and a chitosan yield of 21%. In addition, the crystallinity index of chitin was 85.49% and for chitosan it was 58.51%. Chitin nanofibers of some insects are very similar to those of crustaceans, but the widths of chitin nanofibers extracted from *Melolontha* were observed to be much higher than those of nanofibers isolated from crab, prawn, and fungi species (Kaya *et al.*, 2014). *Schistocerca gregaria* had the highest yield of chitin at 12.2% compared with *Calosoma rugosa* and *Apis mellifera*, and these insects showed a good characteristic of DD, water-binding capacity (WBC) and fat-binding capacity (FBC), ash content, and moisture content compared with shrimp (Philibert *et al.*, 2017). Moreover, the dry weight chitin content of adult potato beetle and larva were 20 and 7%, with a chitosan yield of 72 and 67%, respectively, therefore the adult potato beetle can be utilised as an alternative chitin and chitosan source (Kaya *et al.*, 2014). Recently, six different common insect species including *Shistocerca gregaria*, *Forsskal*, green bugs, German cockroach, *Vespid wasp*, and *Fuessly* have been identified to be sources of chitin with an effective yield in comparison with crustaceans, and these chitins exhibited similar chemical structures and physiological properties (Badawy & Mohamed, 2015). With that, the grasshopper could be an alternative source of chitin. Insects and other arthropods make up the largest and most biodiverse group of organisms on the planet. Therefore, insects are a suitable alternative chitin and chitosan source being the richest and most unexplored reservoirs of potentially useful chitin and chitosan resources for commercialisation. Obviously, many of these insects have an environmental utility in their niche area and harvesting excessive amounts from nature could have unforeseen consequences, whereas a new source from BSF does not raise this concern.

2.4 Extraction of chitin

Two types of methods are used to obtain chitin: chemical and biological methods. Despite the fact that chemical methods have a few disadvantages (eco-unfriendly and may negatively affect the physiochemical properties of chitin), the short processing time still makes it the most commonly used treatment commercially. Another drawback of chemical chitin purification is that the removed proteins and minerals, although potentially valuable supplements for human foods and animal feeds, are sufficiently damaged that they are no longer appropriate for human and animal related applications (Younes & Rinaudo, 2015; Daraghme *et al.*, 2011).

2.4.1 Chemical methods

The traditional chemical methods for obtaining chitin involve three steps: demineralisation, deproteinisation, and decolouration (Waško *et al.*, 2016; Kaya *et al.*, 2015; Liu *et al.*, 2012). In the first step the powdered raw material undergoes an acidic treatment with hydrochloric acid (HCl), the preferred reagent. The purpose is to remove mineral constituents such as calcium carbonate and calcium phosphate into water-soluble calcium salts with the release of carbon dioxide. The excess salts are then separated by filtration of the chitin solid phase followed by rinsing using deionised water. An alkali treatment is used for deproteinisation to remove proteins with sodium hydroxide (NaOH) of the demineralised residue followed by rinsing using deionised water. The last step is the decolouration to remove pigments and lipids. Acetone or organic solvent mixtures are used to remove the pigments such as carotenoids (Simionato *et al.*, 2014; Liu *et al.*, 2012). All these treatments must be adapted to the chitin source, owing to differences in the ultrastructure of the initial material. Several demineralisation, deproteinisation and decolouration treatments were previously used, involving various reaction conditions. Typical process conditions that have been applied by other studies i.e. molarities, temperatures and times are displayed in Table 2.1. Among such methods are those of Kaya *et al.* (2014), Soon *et al.* (2018), Erdogan *et al.* (2017) (Table 2.1). However, no process conditions are available for extracting chitin from pupae shells and adult BSF nor are the yields reported.

Table 2.1: Comparison of the process conditions of chitin produced according to previous studies.

Organism	Demineralisation	Deproteinisation	Decolourisation	Chitin yield (%)	Reference
Crustaceans					
<i>Oniscus ascellus</i> (common woodlouse)	4 M HCl, 75 °C, 2 h	4 M NaOH, 150 °C, 18 h	4:2:1 (water, methanol, chloroform), 25 °C. 20 min	6-7	(Kaya <i>et al.</i> , 2014)
<i>Oreochromis niloticus</i> (nile tilapia scales)	0.5 M HCl, 25 °C, 2 h	0.25 M NaOH, 50 °C, 3 h	1% NaClO, 25 °C, 2h	20	(Boarin-Alcalde & Graciano-Fonseca, 2016)
<i>Paranephrops planifrons</i> (crawfish shells)	1 M HCl, 25 °C, 30 min	3.5% NaOH, 65 °C, 2 h	0.315% NaClO, 25 °C, 5 min	23.5	(No <i>et al.</i> , 1989)
Insects					
<i>Palomena prasina</i> (green shield bug)	2 M HCl, 100 °C, 2 h	2 M NaOH, 140 °C, 20 h	4:2:1 (water, methanol, chloroform), 25 °C. 2 h	10.8	(Kaya <i>et al.</i> , 2015)
<i>Dociostaurus maroccanus</i> (grasshopper)	2 M HCl, 55 °C, 1 h	2 M NaOH, 50 °C, 18 h	2:1:4 (methanol, chloroform, water), 25 °C	12-14	(Erdogan & Kaya, 2016)
<i>Zophobas morio</i> (superworm)	1 M HCl, 35 °C, 30 min	(0.5 M, 1 M, 2 M) NaOH, 80 °C, 20 h	glacial acetone (1:10 of solid to solvent), 25 °C, 30 min	4.77-5.43	(Soon <i>et al.</i> , 2018)
<i>Vespa crabro</i> (european hornet)	1 M HCl, 50 °C, 6 h	1 M NaOH, 60 °C, 16 h	4:2:1 (water, methanol, chloroform), 25 °C. 40 min	2.1	(Kaya <i>et al.</i> , 2016)
<i>Leptinotarsa decemlineata</i> (potato beetles)	2 M HCl, 65-75 °C, 2 h	2 M NaOH, 80-90 °C, 16 h	1:2:4 (chloroform methanol, water), 25 °C. 1 h	7-20	(Kaya <i>et al.</i> , 2014)
Fungi					
<i>Fomes fomentarius</i>	2 M HCl, 100 °C, 2 h	2 M NaOH, 140 °C, 20 h	4:2:1 (water, methanol, chloroform), 25	2.4	(Kaya <i>et al.</i> , 2015)

			°C. 2 h		
<i>Lactarius vellereus</i>	2 M HCl, 60 °C, 15 h	2 M NaOH, 85 °C, 24 h	1:2:4 (chloroform methanol, water), 25 °C	11.4	(Erdogan <i>et al.</i> , 2017)
<i>Phyllophora ribis</i>	2 M HCl, 60 °C, 15 h	2 M NaOH, 85 °C, 24 h	1:2:4 (chloroform methanol, water), 25 °C	7.9	(Erdogan <i>et al.</i> , 2017)

* Reactant are expressed in molarity or w/v%

* Yield based on dry basis

2.4.2 Biological treatments

In order to avoid acidic and alkali treatments that could be a source of environmental problems, biological treatments offer an alternative way to extract chitin. The biological extraction of chitin offers high reproducibility in shorter time, simpler manipulation, smaller solvent consumption and lower energy input. The most common biological methods used for chitin extraction are the use of proteolytic enzymes in order to digest the proteins or a fermentation process using microorganism which allows a digestion of both proteins and minerals. Proteolytic enzymes are mainly derived from plant, microbial and animal sources. Many proteases such as alcalase, pepsin, papain and trypsin remove proteins and minimize deacetylation and depolymerisation during chitin isolation (Younes & Rinaudo, 2015). This treatment may be performed either after, or before demineralisation step of the solid material, which modifies the accessibility for the reactants. Both purified and crude extracted proteases are used in deproteinisation step. However, commercially purified enzymes are expensive in contrast to crude proteases, which are not only cheaper but also more efficient due to the presence of coexisting proteases. Fermentation methods could be separated into two major categories: lactic acid fermentation and non-lactic acid fermentation for example lactic or non-lactic bacteria includes *Lactobacillus plantarum*, *Pseudomonas aeruginosa* K-187, *Serratia marcescens* FS-3 or *Bacillus subtilis* (Philibert *et al.*, 2017; Daraghmeh *et al.*, 2011). Lactic acid-producing bacteria reacts with the calcium carbonate component in the biomass waste resulting in the formation of calcium lactate, which can be precipitated and removed by washing during the demineralisation process (Philibert *et al.*, 2017). The efficiency of lactic acid fermentation depends on many factors, mainly the species and quality of inoculums, carbon sources and its concentration, initial pH and pH evolution during fermentation temperature and the duration (Younes & Rinaudo, 2015). For example, Choorit *et al.* (2008) optimised demineralisation efficiency in fermented shrimp shells by testing the following variables: source concentration, initial pH value and soaking time, using *Pediococcus* sp L1/2. Two other bacteria, *Bacillus cereus* and *Exiguobacterium acetylicum*, have shown high activity in both the deproteinisation and demineralisation steps (Philibert *et al.*, 2017; Aranaz *et al.*, 2009). Major microbial fermentation drawbacks includes longer processing time compared to chemical methods and poorer accessibility of proteases caused by the presence of minerals which lead to high residual proteins (Daraghmeh *et al.*, 2011; Philibert *et al.*, 2017; Younes & Rinaudo, 2015). Biological production of chitin can reduce environmental pollution

and depolymerisation of chitin. However, the main drawbacks of the biological process are its lower efficiency and quality of chitin, the extraction process being time consuming and more costly (Younes & Rinaudo, 2015).

2.5 Chitosan Deacetylation

Chitosan can be obtained by deacetylation of chitin through alkaline or enzymatic methods. The purpose is to remove acetyl groups (COCH₃) from the molecular chain of chitin, leaving behind a chitosan with a high degree of chemical reactive NH₂ groups, however the N-deacetylation is almost never complete (Elieh-Ali-Komi & Hamblin, 2016; Younes & Rinaudo, 2015). In addition, deacetylation degree is an important property in chitosan production as it affects the physiochemical and biological properties and hence determines the suitable applications (Yeul & Rayalu, 2013).

2.5.1 Alkaline methods

Raw materials obtained after chitin demineralisation, deproteinisation and decolouration are typically mixed with concentrated NaOH. Chitosans with different degree of deacetylation are generated depending on the reaction temperature, time, and the concentration of the alkali solution (Ahing & Wid, 2016; Kaya *et al.*, 2016; Paulino *et al.*, 2006). NaOH is the preferred reagent and it is applied at concentration ranging from 40% to 60%, at varying temperatures (from 80 °C up to 150 °C) and treatment duration from 2 h up to 10 h (Erdogan & Kaya, 2016; Kaya *et al.*, 2014; Kumari & Rath, 2014). The alkaline treatments hydrolyse the acetyl groups and transform the N-acetyl-D-glucosamine units into D-glucosamine units with free NH₂ groups (Philibert *et al.*, 2017). In some cases the alkali treatment can cause environmental pollution, requires significant energy, and produces poor quality chitosan (Younes & Rinaudo, 2015). Therefore enzymatic methods have been explored to overcome those limitations. However, the alkali treatment is more commonly used for commercial preparation because of economic issues and feasibility for mass production.

2.5.2 Enzymatic methods

The alternative enzymatic method exploiting chitin deacetylase has been explored and it was first found in *Mucor rouxii* in 1974 (Araki & Ito, 1974). The use of chitin deacetylase for the conversion of chitin to chitosan, in contrast to the chemical procedure, offers the possibility of a controlled, non-degradable process, resulting in the production of a well-defined chitosan (Younes & Rinaudo, 2015). Chitin deacetylase catalyses the hydrolysis of N-acetamido bonds in chitin to produce chitosan. The presence of this enzyme activity has been reported in several fungi (Araki & Ito, 1974; Tsigos & Bouriotis, 1995) and insect species (Younes & Rinaudo, 2015). The most well-studied enzymes are those extracted from the fungi *Mucor rouxii* (Araki & Ito, 1974), *Absidia coerulea* (Gao *et al.*, 1995), *Aspergillus nidulans* (Alfonso *et al.*, 1995) and two strains of *Colletotrichum lindemuthianum* (Tsigos & Bouriotis, 1995). All the enzymes are glycoproteins and are secreted either into the periplasmic region or into the culture medium. Furthermore, all enzymes exhibit a remarkable thermal stability at their optimal temperature (50 °C), and exhibit a very strong specificity for β -(1,4)-linked N-acetyl-D-glucosamine polymers. However, the enzymes vary significantly in their MW and carbohydrate content and display a wide range of pH optima. In addition, there are some problems with the use of enzyme-producing fungi such as low yield of deacetylase-producing strains, low enzyme activity and fermentation requirements that are complicated. Therefore chitin deacetylase-producing bacteria (*Serratia* sp. and *Bacillus* sp.) may replace the current fungal strains (Zhou *et al.*, 2010). However to date it has been limited to small-scale production and is very costly.

2.6 Applications

Chitin and chitosan are a potential resource for multiple applications ranging from biomedical, pharmaceutical, food and environmental industries due to their physiochemical and biological properties. There are now currently over 2000 known applications of these versatile biopolymers. A number of potential products have been developed for various areas such as in the food industry, as an anticholesterol and fat binding agent, preservative, packing material, or animal feed additive; in wastewater treatment to remove toxic metal ions, or to flocculate/coagulate dyes and proteins, or for membrane purification processes; in agriculture for seed and fertiliser coating, controlled agrochemical release; in the pulp and paper industry for surface treatment,

photographic paper; in cosmetics as a moisturiser, body cream, bath lotion etc. (Philibert *et al.*, 2017; Krishnaveni & Rangunathan, 2015; Mati-Baouche *et al.*, 2014; Shanmuga *et al.*, 2014; Dash *et al.*, 2011). The most exciting uses of these materials are in the area of medicine and biotechnology owing to their unparalleled biological properties. Medicine takes advantage of their biodegradability, biocompatibility, nontoxicity, physiochemical inertness, remarkable affinity for proteins; their hemostatic, fungistatic, antitumoral and anticholesteremic properties; as drug delivery and controlled release systems; for artificial cells, wound healing ointments and dressings, haemodialysis membranes, contact lenses, artificial skin, surgical sutures and for tissue engineering (Philibert *et al.*, 2017; Elieh-Ali-Komi & Hamblin, 2016; Younes & Rinaudo, 2015). In biotechnology they may find application as chromatographic matrices, membranes for separations and notably as enzyme/cell immobilisation supports (Mohammedi, 2017; Philibert *et al.*, 2017; Hirano, 1996). Developing new sources of chitin and chitosan is thus of considerable commercial interest.

2.7 Electrospinning

In the field of nanotechnology, polymer nanofibers are of great interest for various applications such as filters, skin masks, semi-permeable membranes, clothing and medical materials. Electrospinning is one of the conventional, simple, versatile and efficient methods used to prepare nanofibers. The generated nanofibers have unique characteristics such as large surface area to volume, high porosity, good pore interconnectivity and the possibility to incorporate active components on a nanoscale. Despite several advantages and the success of electrospinning there are some limitations in this process such as small pore size and lack of proper cellular infiltration inside the fibers. Several attempts in these directions are being made to improve the design and cellular migration through multilayering, inclusion of heprasil and blending with polymers with different degradation behaviour (Wang & Hsiao, 2016). Recently, nanofibers have been used in drug delivery systems, tissue engineering scaffolds, vascular grafts, filter formation, sensing applications and biological wound dressings (Ding *et al.*, 2014; Sun & Li, 2011; Bhardwaj & Kundu, 2010). A large number of research groups are dedicated to produce new and improved nanofibers, synthesising and modifying biocompatible materials, in particular using biological materials such as chitosan. The natural polysaccharide chitosan has attracted much attention due to its natural origin, biocompatibility, biodegradability, functionalisability,

antibacterial activity, lack of toxicity and excellent processability (Sun & Li, 2011). Some companies such as Stellenbosch Nanofiber company (SNC) (South Africa), eSpin Technologies (USA), NanoTechnics (Korea) and KATO Tech (Japan) are actively engaged in reaping the benefits of the unique advantages offered by electrospinning.

2.7.1 Principle of electrospinning

Electrospinning is a simple and versatile method which produces fibers ranging from submicron level to several nanometers in diameter in a high voltage electrostatic field (Wang & Hsiao, 2016). This method is a relatively old approach to fiber production, but is currently one of the most advanced techniques in manufacturing high performance nanofibers. These have been introduced into various technological fields due to their distinct characteristics, such as a high surface area to mass ratio, high interfibre porosity and special chemical and physical properties, which result from their unique structure (Wang & Hsiao, 2016; Ding *et al.*, 2014; Bhardwaj & Kundu, 2010). The formation of nanofibers through electrospinning is based on the uniaxial stretching of a viscoelastic solution. A typical electrospinning setup consists of three basic components: a capillary-tube with a needle, a high voltage supply and a collector, as shown in Figure 2.3.

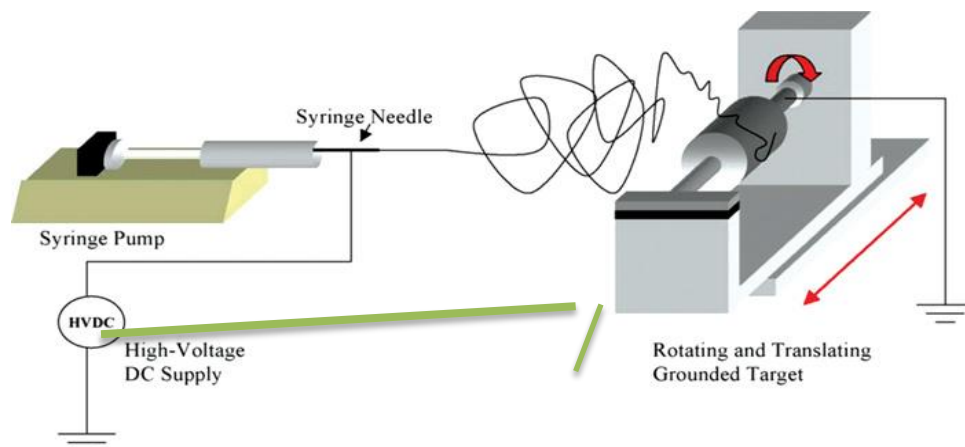


Figure 2.3: Schematic diagram of the typical electrospinning setup (Mazoochi & Jabbari, 2011).

In the electrospinning technique, an electric field is applied between the tip of a syringe and a collector plate. The polymer solution is put into a syringe and mounted on a pump, which produces a consistent flow rate. When the electric field applied between the tip and collector reaches a certain value, at which the repulsive electrostatic and surface tension forces are overcome, the charged fluid jet is ejected from the tip of the conical protrusion, commonly known as a Taylor cone. The jet is continuously lengthened and whipped, resulting in solid nanofibers deposited on the collector with simultaneous rapid evaporation of the solvent (Wang & Hsiao, 2016; Bhardwaj & Kundu, 2010). The diameter, shape and surface morphology of the fibers and the texture of the nonwoven fabric produced by electrospinning depend on a number of parameters, including solution parameters, process parameters and ambient parameters (Sun & Li, 2011).

2.7.2 Polymers used in electrospinning

Currently there are a wide range of polymers used in electrospinning that are able to form fine nanofibers within the nanometer range for various applications. Electrospun nanofibers have been reported as being made from various natural polymers, synthetic polymers or a blend. Over the years, more than 200 polymers have been electrospun successfully and characterised with respect to their applications (Wang & Hsiao, 2016). Natural polymers include chitosan, cellulose, chitin, collagen etc. A few synthetic polymers in literature include, poly (vinyl alcohol) (PVA), poly (ethylene oxide) (PEO), poly (ethylene terphthalate) (PET), polycaprolactone (PCL) etc (Chen *et al.*, 2008; Cooper *et al.*, 2013; Ki *et al.*, 2005; McKee *et al.*, 2004; Rieger *et al.*, 2016; Zheng *et al.*, 2001; Bhardwaj & Kundu, 2010; Wang & Hsiao, 2016). From the list of natural polymers, pure chitosan in particular will be discussed for its use in electrospinning process.

2.8 Electrospinning of chitosan

Over the past years, chitosan has proven challenging to electrospin. Firstly, chitosan's rigid D-glucosamine repeat unit, its high crystallinity and its ability to hydrogen bond lead to poor solubility in common organic solvents. McKee *et al.* (2004) found that in order to electrospin bead-free fibers, the concentration of the polymer must be at least 2 to 2.5 times the entanglement concentration, where the polymer chains significantly overlap one another and

topologically constrain each other's motion (McKee *et al.*, 2004). However, chitosan solutions at these concentrations are often difficult to electrospin due to the high viscosity in solution. With chitosan solutions, even moderate concentrations become too viscous to overcome the electric field and cannot be successfully electrospun. The problem of the high viscosity of chitosan, which limits its spinnability, is resolved through the application of an alkali treatment which hydrolyses chitosan chains and so decreases their MW (Homayoni *et al.*, 2009). Additionally, chitosan is a cationic biopolymer, which also affects the rheology of the solutions. With a typical laboratory electrospinning setup, the viscosity of the solution must be within a certain window for nanofibers to form successfully. Above the upper threshold, the solution becomes too viscous and fiber formation is hindered because the electric field is not strong enough to overcome the viscosity of the solution. Below the lower limit, the polymer chains are not entangled so fiber formation is not possible and polymer beads are often created. Therefore, several research studies have blended chitosan with other polymers in an attempt to improve the electrospinnability of the solutions (Ding *et al.*, 2014). Moreover, it has been shown that fine nanofibers can be obtained in chitosan blends with PVA, gelatin or collagen, polycaprolactone but mainly with PEO (Ding *et al.*, 2014; Sun & Li, 2011; Chen *et al.*, 2008; Zheng *et al.*, 2001).

2.9 Effects of various parameters on electrospinning

The initial step in preparation of electrospinning is the dissolution of the polymer in a suitable solvent and therefore the solvent used in preparing polymer solutions has a significant influence on its spinnability. Basically, a solvent performs two essential roles in electrospinning; first of all to dissolve the polymer molecules for forming the electrified jet and secondly to carry the dissolved polymer molecules towards the collector (Wang & Hsiao, 2016; Bhardwaj & Kundu, 2010). Solvents must have some properties such as high or low vapour pressure, good volatility, low boiling point and should be able to maintain the integrity of the polymer solution (Bhardwaj & Kundu, 2010). Hence, for successful electrospinning the selection of an appropriate solvent system is absolutely necessary. Chitosan is soluble in most acids and has been electrospun using different acid-based solvents (Elsabee *et al.*, 2012; Sun & Li, 2011). Acetic acid, a monobasic organic acid, has been used as a solvent to prepare chitosan solutions at concentration from 90% down to 50% (Bhardwaj & Kundu, 2010; Geng *et al.*, 2005). However, pure chitosan fibers have rarely been obtained in acetic acid because aqueous acetic acid solutions can only dissolve a very

small amount of chitosan, which does not provide sufficient viscosity or polymer chain entanglement required for electrospinning (Kaya *et al.*, 2016). In addition, more concentrated acetic acid in water progressively decreased the surface tension of the chitosan solution and concomitantly increased the charge density of the jet without a significant effect on the solution viscosity (Kaya *et al.*, 2016; Homayoni *et al.*, 2009). Trifluoroacetic acid (TFA) on the other hand is another solvent currently used to electrospin chitosan. TFA is a suitable spinning solvent for chitosan because the amino groups of the chitosan can form salts with TFA, which can effectively destroy the intermolecular interactions between the chitosan molecules and thus facilitate electrospinning (Kaya *et al.*, 2016; Sun & Li, 2011). As the chitosan concentration increases, the morphology of the deposition on the collector changes from spherical beads to interconnected fibrous networks. However, TFA is a volatile, toxic and expensive solvent.

In addition, the electrospinning process is also governed by numerous parameters, classified broadly into solution parameters, process parameters and ambient parameters. Each of these parameters significantly affects the fiber morphology and diameter and by proper manipulation of these parameters one can get nanofibers of desired morphology and diameter for various applications.

2.9.1 Solution parameters

i. Concentration

For fiber formation to occur in the electrospinning process, a minimum solution concentration is required. It has been found that at low solution concentration, a mixture of beads and fibers is obtained and, as the solution concentration increases, the shape of the beads change from spherical beads to spindle-like structures and finally uniform fibers with increased diameters are formed due to the higher viscosity resistance (Wang & Hsiao, 2016; Hagi & Akbari, 2007). It is necessary to determine the optimum solution concentration for the electrospinning process as at too low concentrations, beads are formed instead of fibers and at too high concentrations, the formation of continuous fibers are prohibited. This is due to the inability to maintain the flow of the solution at the tip of the needle resulting in the formation of larger fibers (Bhardwaj & Kundu, 2010). Researchers have attempted to find a relationship between solution concentration and fiber diameter and they found a power law relationship, that by increasing the concentration of solution, the fiber diameter increases in the electrospinning process (Bhardwaj & Kundu,

2010; Ki *et al.*, 2005). Solution surface tension and viscosity also play important roles in determining the range of concentrations from which continuous fibers can be obtained in electrospinning (Wang & Hsiao, 2016; Bhardwaj & Kundu, 2010).

ii. Molecular weight

The molecular weight (MW) of the polymer has a significant effect on rheological and electrical properties such as viscosity, surface tension, conductivity and dielectric strength (Wang & Hsiao, 2016; Bhardwaj & Kundu, 2010; Hagi & Akbari, 2007). Generally high MW polymer solutions have been used in electrospinning and they provide the desired viscosity for the fiber fabrication. It has been observed that too low MW solutions tend to form beads rather than fibers and high MW solutions give fibers with larger average diameters (Bhardwaj & Kundu, 2010). The MW of the polymer reflects the number of entanglements of the polymer chains in a solution, thus solution viscosity. Chain entanglement plays an important role in the processing of electrospinning. In addition, it has been observed that high MW is not always essential for the electrospinning process; therefore acid hydrolysis is done in order to decrease the MW. The chitosan MW from which nanofibers have been obtained varies from 85 kDa up to 570 kDa, nevertheless the real MW is often difficult to obtain precisely due to the presence of aggregates (Wang & Hsiao, 2016; Ding *et al.*, 2014; Bhardwaj & Kundu, 2010). The concentration used for electrospinning is directly related to the chitosan MW which imposes the solution viscosity.

iii. Viscosity

The solution viscosity plays an important role in determining the fiber size and morphology during spinning of polymeric fibers. Over the years it has been found that with very low viscosity there is no continuous fiber formation and with very high viscosity there is difficulty in the ejection of jets from polymer solutions, thus there is a requirement of optimal viscosity for electrospinning (Bhardwaj & Kundu, 2010; Homayoni *et al.*, 2009). Different polymer solutions used for spinning have different viscosity ranges. The viscosity, MW of the polymer and polymer concentration are correlated to each other. At very high viscosity polymer solutions usually exhibit longer stress relaxation times, which could prevent the fracturing of the ejected jets during electrospinning. An increase in solution viscosity or concentration gives rise to a

larger and more uniform fiber diameter (Bhardwaj & Kundu, 2010). In addition, the viscosity of the solution in the electrospinning process plays an important role in determining the range of concentrations from which continuous fibers can be obtained. For solutions of low viscosity, surface tension is the dominant factor and beads only, or beaded fibers are formed while above a critical concentration, a continuous fibrous structure is obtained and its morphology is affected by the concentration of the solution (Sun & Li, 2011). All these findings indicate that there exist polymer-specific, optimal viscosity values for electrospinning and this property has a remarkable influence on the morphology of the fibers.

iv. Surface tension

Surface tension is a function of solvent composition. Thus the solvent plays a critical role in the electrospinning process. By reducing the surface tension of a nanofiber solution; fibers can be obtained without beads. Different solvents contribute to different surface tensions. Generally, the high surface tension of a solution inhibits the electrospinning process due to instability of the jets and the generation of sprayed droplets (Bhardwaj & Kundu, 2010). The formation of droplets, fibers and beads depends on the surface tension of the solution and a lower surface tension of the spinning solution helps electrospinning to occur at a lower electric field (Homayoni *et al.*, 2009; Haghi & Akbari, 2007). However, a lower surface tension of a solvent will not necessarily always be more suitable for electrospinning. Among the surfactants that are typically being used to lower surface tension are SDS (sodium dodecyl sulfate), DMSO (dimethyl sulfoxide) and Triton X-100, ethanol etc. (Ohkawa, 2015; Thongngam & McClements, 2004; Zhou *et al.*, 2013). Basically, surface tension determines the upper and lower boundaries of the electrospinning window if all other variables are held constant (Bhardwaj & Kundu, 2010; Pham *et al.*, 2006).

v. Conductivity

Most polymers are conductive, with a few exceptions of dielectric materials, and the charged ions in the polymer solution are highly influential in jet formation. The conductivity of a solution is mainly determined by the polymer type, solvent used and the availability of ionisable salts. In literature it has been found that with the increase of electrical conductivity of the solution, there is a significant decrease in the diameter of the electrospun nanofibers whereas, with low

conductivity, insufficient elongation of a jet by electrical force to produce uniform fiber and beads may be observed (Wang & Hsiao, 2016; Bhardwaj & Kundu, 2010). Hayati et al. (1987) have indicated that highly conductive solutions are extremely unstable in the presence of strong dielectric fields, which results in a dramatic bending instability as well as a broad diameter distribution (Hayati *et al.*, 1987). Generally, electrospun nanofibers with the smallest fiber diameter can be obtained with the highest electrical conductivity and it has been found that the decrease in size of the fibers is due to the increased electrical conductivity. It was observed that the jet radius varied inversely with the cube root of the electrical conductivity of the solution (Bhardwaj & Kundu, 2010; Haggi & Akbari, 2007). Natural polymers are generally polyelectrolytic in nature because the ions increase the charge carrying capacity of the jet, thereby subjecting it to higher tension with the applied electric field, thus the fiber forming ability of the natural polymer is lower compared to synthetic polymers.

2.9.2 Process parameters

i. Applied voltage

The crucial element in the electrospinning process is the voltage applied to the solution. Only after obtaining the threshold voltage, fiber formation occurs. This induces the necessary charges on the solution along with electric field and initiates the electrospinning process (Bhardwaj & Kundu, 2010). It has been already proved experimentally that the shape of the initiating drop changes with spinning conditions (voltage, viscosity and flow rate). There is some disagreement about the behaviour of applied voltage in the electrospinning process. Researchers have suggested that when higher voltages are applied, there is more polymer ejection and this facilitates the formation of a larger diameter fiber (Wang & Hsiao, 2016; Zhang *et al.*, 2005).

De Vrieze et al. (2007) and Homayoni et al. (2009) have reported that an increase in the applied voltage increases the electrostatic repulsive force on the fluid jet which ultimately favours the narrowing of fiber diameter. In most cases, a higher voltage causes greater stretching of the solution due to the greater columbic forces in the jet as well as a stronger electric field and these effects lead to a reduction in the fiber diameter and also to rapid evaporation of solvent from the fibers. It has been shown that the decrease of fiber diameter by increasing the applied electric field, also influences fiber diameter, however the level of significance varies with the polymer

solution concentration and on the distance between the tip and the collector (Yördem *et al.*, 2008).

ii. Flow rate

The flow rate of the polymer from the syringe is a significant process parameter as it influences the jet velocity and the material transfer rate. A lower feed rate is more desirable as the solvent will get enough time for evaporation (Yuan *et al.*, 2004). There should always be a minimum flow rate of the spinning solution. It has been observed that the fiber diameter and the pore diameter increases with an increase in the polymer flow rate and by changing the flow rate, the morphological structure can be slightly changed. High flow rates result in beaded fibers due to unavailability of proper drying time prior to reaching the collector (Bhardwaj & Kundu, 2010; Yuan *et al.*, 2004).

iii. Tip to collector distance

Varying the tip to collector distance will have a direct influence on both the flight time and the electric field strength, which will affect the electrospinning process and the resultant fibers. For independent fibers to form, the electrospinning jet must be allowed enough time for most of the solvent to be evaporated. When the tip to collector distance is reduced, the jet will have a shorter distance to travel before it reaches the collector plate. Moreover, the electric field strength will also increase at the same time, and this will increase acceleration of the jet to the collector. As a result, there may not be enough time for the solvent to evaporate when it hits the collector and fiber diameter increases. It has been found that a minimum distance is required to give the fibers sufficient time to dry before reaching the collector, however, with distances that are either too close or too far, beads have been observed (Geng *et al.*, 2005; Ki *et al.*, 2005). The effect of tip and the collector distance on fiber morphology is more significant than other parameters and this has been shown with electrospinning of gelatin, chitosan and poly (vinylidene fluoride) (Bhardwaj & Kundu, 2010; Geng *et al.*, 2005; Ki *et al.*, 2005). It has been reported that for polysulfone polymer, closer distances between the tip and collector has yielded smaller fibers (Pham *et al.*, 2006). One important physical aspect of the electrospun nanofibers is their dryness

from the solvent used to dissolve the polymer, thus, there should be an optimum distance between the tip and collector which favours the evaporation of solvent from the nanofibers.

2.9.3 Ambient conditions

Apart from the two parameters mentioned above, there are also ambient parameters that include humidity, air speed, temperature etc. Several studies have been conducted to examine the effects of ambient parameters on the electrospinning process. Mit-Uppatham et al. (2004) have examined the effect of temperature on the electrospinning of polyamide-6 fibers ranging from 25 to 60 °C and found that with increase in temperature, there is a yield of fibers with decreased fiber diameter and they attributed this decline in diameter to the decrease in the viscosity of the polymer solutions at increased temperatures (Mit-uppatham *et al.*, 2004). It has been observed that there is an inverse relationship between viscosity and temperature. As for the variation in humidity, while spinning polystyrene solutions, it has been shown that by increasing humidity there is an appearance of small circular pores on the surface of the fibers; further increasing the humidity leads to the pores coalescing (Casper *et al.*, 2003). In addition, it has been found that at very low humidity, a volatile solvent may dry rapidly as the evaporation of the solvent is faster. Some researchers have suggested that the high humidity can help the discharge of the electrospun fibers. Hence, apart from solution and processing parameters, ambient parameters also affect the electrospinning process (Bhardwaj & Kundu, 2010).

2.10 Applications

Various applications of electrospun nanofibers have been explored over the years due to several unique advantages such as high surface area to volume ratio, very high polarity, easy surface modifications and enhanced physico-mechanical properties. In addition, with the electrospinning process, manipulation of the solution and process parameters can be easily done to get the desired fiber morphology and mechanical strength. Electrospun nanofibers are broadly applied in different sectors such as tissue engineering applications (dressing for wound healing, scaffolds for tissue engineering and in drug delivery); as biosensors: in filtration; in protective clothing; energy generation applications, in immobilisation of enzymes; as affinity membrane and in cosmetics (Wang & Hsiao, 2016; Ding *et al.*, 2014; Cooper *et al.*, 2013; Sun & Li, 2011;

Bhardwaj & Kundu, 2010). Owing to application of these nanofibers in diverse fields, various research and developments are on-going in the fields of electrospinning.

2.11 Characterisation techniques for chitosan and its based materials

All synthesised materials need to be characterised before application. For each type of application there are a number of possible techniques that may be used in order to identify specific material properties and their behaviours during a particular test. Currently a series of chitosan based materials have been synthesised and applied in various fields of science due to the versatility of the materials and their applications (Ding *et al.*, 2014; Elieh-Ali-Komi & Hamblin, 2016; Erdogan & Kaya, 2016; Krishnaveni & Rangunathan, 2015). In literature there are a variety of analytical techniques, including diffraction, microscopy and numerous spectroscopic techniques, currently being used to characterise these materials (Ioelovich, 2014; Kaya *et al.*, 2014; Kaya *et al.*, 2017; Kumari *et al.*, 2017). The following section gives a brief general overview of some of the most commonly applied techniques used in the characterisation of the materials.

2.11.1 Microscopic techniques

Scanning electron microscopy (SEM) is a technique used for the visual confirmation of the morphology and physical state of the surface (Kaya *et al.*, 2017; Krishnaveni & Rangunathan, 2015). SEM can image samples distributed over a surface, size and shape and it can offer surface imaging up to a resolution of <2 nm. In addition to the polymeric material, SEM is better for imaging bulk samples and has a greater depth of field giving rise to better 3D images of the sample. SEM images are capable of resolving the morphology of the fibers and as well as detecting fiber diameters. SEM remains a quick method for observing the fibers produced and it requires a very small sample size for its operation. Transmission electron microscopy (TEM) is another alternative for detecting fiber diameters with extremely small fibers (<300 nm).

2.11.2 X-ray Diffraction

X-ray Diffraction (XRD) is a versatile, non-destructive technique that reveals detailed information about the mineral phase and crystallographic structure of natural and manufactured materials (Ioelovich, 2014). It is also used to interrogate crystal structure and lattice spacing parameters of organic materials. The crystallographic structure present in the material is identified by comparing the fingerprint compiled in the library of XRD with the peaks obtained experimentally.

The crystallinity index value (CrI) of chitin and chitosan can be calculated according to the formula by Liu et al. (2012) as follows:

$$\text{CrI}_{100} = \left[\frac{(I_{110} - I_{am})}{I_{110}} \right] \times 100 \quad \text{Equation 1}$$

I_{110} is the maximum intensity at $2\theta \approx 20^\circ$ and I_{am} is the intensity of amorphous diffraction at $2\theta \approx 16^\circ$.

The crystallinity index shows the comparative content of crystalline fraction in several materials. In addition, it also indicates which of the materials has greater crystallinity and which less crystallinity, however it does not disclose the actual degree of crystallinity.

2.11.3 Thermogravimetric Analysis

Thermal gravimetric analysis (TGA) is a thermal analysis in which changes in physical and chemical properties of the materials such as mass loss are measured as a function of the temperature. TGA provides complementary characterisation information to the most commonly used techniques. TGA measures the amount and rate of change in the mass of a sample as a function of temperature or time in a controlled atmosphere (Kaya *et al.*, 2015; Kaya *et al.*, 2014; Sichina, 2000). The measurements are used primarily to determine the thermal and/or oxidative stabilities of materials as well as their compositional properties. The technique can analyse materials that exhibit either mass loss or gain due to decomposition, oxidation or loss of volatiles such as moisture (Kumari *et al.*, 2017; Sichina, 2000). In case of the polymeric materials, TGA

determines temperature and weight change of decomposition reactions, which allows quantitative composition analysis and thermal stability to be measured.

2.11.4 Spectroscopic techniques

i. Fourier Transform Infrared Spectroscopy

Fourier transform infrared (FTIR) spectroscopy is an effective qualitative analytical technique that is able to detect chemical functional groups and characterise covalent bonding information in the material. FTIR depends on transitions between vibrational energy states stretching and bending of a molecule (Kaya *et al.*, 2014; Cárdenas *et al.*, 2004). The most useful region of infrared lies between 4000 and 625 cm^{-1} . FTIR spectroscopy is one of the most common characterisation methods for chitin and chitosan due to its relative instrument availability, simplicity and independence of sample solubility. FTIR is commonly used to determine the functional groups, differentiate between the two chitin isomorphs, and check for impurities in chitin and chitosan preparation, to determine the degree of acetylation and deacetylation and for control of purification conditions (Cárdenas *et al.*, 2004; Kaya *et al.*, 2015). With the spectrum obtained, the degree of acetylation (DA) of chitin can be calculated using the following formula (Kaya *et al.*, 2015):

$$\text{DA (\%)} = \left(A_{1655} / A_{3450} \right) \times 100 \quad \text{Equation 2}$$

A_{1655} is the absorbance at 1655 cm^{-1} wavelength and A_{3450} is the absorbance at 3450 cm^{-1} wavelength.

As for chitosan the degree of deacetylation (DD) can be calculated according to the following formula (Kaya *et al.*, 2015):

$$\text{DD (\%)} = 100 - \left[\left(A_{1655} / A_{3450} \right) \times 100 \right] \quad \text{Equation 3}$$

A_{1655} is the absorbance at 1655 cm^{-1} wavelength and A_{3450} is the absorbance at 3450 cm^{-1} wavelength.

The molecular structure of a nanofiber can also be characterised by FTIR technique. In the case where two polymers were blended together for the fabrication of nanofibers, not only can the structure of the two materials be detected but the intermolecular interaction can be determined (Pakravan *et al.*, 2012) .

ii. ¹³C Carbon-Nuclear Magnetic Resonance Spectroscopy

There are two kinds of ¹³C carbon-nuclear magnetic resonance (¹³C-NMR) spectroscopy: liquid-state and solid-state. The first one has the same limitations as ¹H hydrogen nuclear magnetic resonance (¹H-NMR) spectroscopy, namely, the insufficient solubility of most analysed materials. Moreover, ¹³C-NMR spectroscopy is much less sensitive than ¹H-NMR spectroscopy owing to the properties of the carbon nucleus and the only 1% abundance of the ¹³C isotope in nature (Hajji *et al.*, 2014; Daraghmeh *et al.*, 2011). Liquid-state ¹³C-NMR spectra are usually recorded from the same kinds of solutions as are used for producing ¹H-NMR spectra, but the number of scans has to be much higher. Solid-state ¹³C-NMR spectroscopy is a much more powerful technique. Chitin can be analysed without any special solubilisation of the polymer. This means that quite a large amount of sample can be used, which solves the problem of the low sensitivity of ¹³C-NMR spectroscopy (Daraghmeh *et al.*, 2011). The ¹³C-NMR spectra of solid samples are generally recorded with magic-angle spinning (MAS) and cross-polarisation (CP). MAS averages out dipolar interactions and chemical shift anisotropy, producing highly resolved spectra. CP considerably increases the sensitivity of the technique by reducing the relaxation delay due to the magnetisation transfer from the ¹H to the ¹³C spins. The intensities of the ¹³C-NMR signals are influenced by the kinetics of the CP process for example different contact times affect the intensities of ¹³C NMR resonances. Hence, it is very important to use the proper contact and relaxation delay times (Guinesi & Cavalheiro, 2006). Apart from UV/VIS (ultraviolet-visible spectroscopy) and FTIR, NMR spectroscopy is the most powerful technique to study the DD and DA. The degree of acetylation (DA) and degree of deacetylation (DD) values of chitin and chitosan can be determined on the basis of integrals from different NMR spectra, for instance, for ¹H and ¹³C-NMR spectra, the DA can be calculated by comparing the integral of the methyl carbon/protons of the acetyl group to the integrals of other carbons/protons from the main chains. Many equations for the DA calculation have been put forward for different

types of NMR spectroscopy. On the basis of carbon atom integrals from solid-state ^{13}C -NMR spectra, DA of chitin is mainly calculated according to equation (Tolaimate *et al.*, 2000):

$$\%DA = \left[\left(\frac{I_{CH3(A)}}{I_{C1-C6(A+D)}} \right) \div 6 \right] \times 100 \quad \text{Equation 4}$$

2.12 Summary of review

The literature on chitin and chitosan in the last three decades is abundant and mainly focused on applications of these polymers and their derivatives. The biological activities displayed by chitosan and its derivatives have attracted the interest of academics and industry, mainly for applications in health-related fields due to their low cytotoxicity, biocompatibility, biodegradability, antibacterial activity, flexibility in surface functionalities and extremely small pore dimensions. Despite the success of several studies, which showed the potential of chitosan based materials in many applications, and the huge number of scientific documents and patents, there are few registered products and yet fewer commercially available products based on chitosan and derivatives, mainly due to poor properties and reproducibility, which thus result in it being very costly. Therefore, exploring the physiochemical properties of chitosan from different sources, should allow the production of chitosan based materials for commercialisation, which thus would make chitosan less costly. The significance of the diversity and the applicability of the different forms of this remarkable biopolymer has yet to be determined. Thus, knowledge is sought about the nature of the exoskeletons of various insects and crustaceans, the cell walls of fungi and also of marine microorganisms. The optimum processing methods for these materials into valuable commercial chitin and chitosan products is needed. Moreover, processing conditions are specific to different sources and need optimisation and that is the gap in knowledge about BSF. Additionally, chitin and chitosan can unquestionably be promoted and marketed as a green product.

The electrospinning technology has proven to be a very versatile technique to fabricate highly porous nanofiber membranes from a very large selection of materials. A large number of research groups are dedicated to produce new and improved nanofibers, synthesising and modifying biocompatible materials, in particular using biological materials such as chitosan however very little is reported on BSF derived nanofibers. In this review, the preparation and

optimisation parameters of commercial chitosan electrospun nanofibers are discussed. Literature has reported that the electrospinning of chitosan into nanofibers is not that simple. Chitosan is hard to electrospin due to the high molecular weights and the stiff back bone making the polymer solution very viscous for the electric field to stretch. This obstacle can be overcome by the use of concentrated TFA as a solvent which was found to reduce the surface tension. It is clear that the selection of suitable materials and parameters during electrospinning, are critical to produce the appropriate nanofiber membrane system. Without question, electrospun nanofibrous membranes have already become an extremely promising platform for many different applications.

This study presents a new chitin and chitosan source from an insect widely used as an animal feed in agriculture and aquaculture. Since the biggest advantage of black soldier flies over other insects are their ability to convert waste into food and the large excessive amounts that could be harvested from BSF. This fly can thus be a potential raw material for production of chitosan and nanofibers. This newly manufactured chitosan can thus be used in future studies in various applications and also to fabricate nanofibers.

CHAPTER 3

MATERIALS & METHODS

Summary

This chapter discusses the chemicals and instrumentation used. It further presents detailed experimental procedures for the chemical extraction of chitin and chitosan through demineralisation, deproteinisation, decolouration and deacetylation methods. Chitosan nanofibers were fabricated via electrospinning by varying solution concentration, applied voltage, flow rate and distance between tip of the needle and collector. The optimised conditions were used to fabricate nanofiber mats. The description of the necessary sample preparations and parameters used for spectroscopic, microscopic and elemental analysis characterisation of the synthesised chitin, chitosan and fibrous mats are outlined. The details of how the molecular weight of the produced chitosans was determined are also described.

3.1 Sample collection, preparation and materials

Dead black soldier fly pupae shells and adult BSF flies were collected from AgriProtein farm (Philippi, Cape Town). Samples were then air-dried at room temperature for 24 h. Samples were ground into powder form with a mortar and pestle before the chitin extraction. Hydrochloric acid (HCl) (32%), sodium hydroxide (NaOH) (98%), sodium hypochlorite (NaClO) (12%), acetic acid (99%), sodium acetate (99%), and trifluoroacetic acid (TFA) (99%) were all purchased from Sigma-Aldrich (South Africa). Purified commercial powders of chitin and chitosan (MW=50 000-190 000 Da, DD=60-80%) isolated from shrimp shells were acquired from Sigma-Aldrich. All chemicals were of analytical reagent grade and were used without further purification. Deionised water ($18.2 \Omega^{-1}\text{cm}^2$) purified by a Milli-QTM system (Millipore) was used as reagent water for aqueous solution preparations.

3.2 Chitin isolation from black soldier flies

The chitin production conditions were optimised by defining the temperature of demineralisation (°C), demineralisation time (min), concentration of HCl (M), temperature of deproteinisation

(°C), deproteinisation time (h) and concentration of NaOH (M) as independent variables as shown in Table 3.1 and 3.2. Upon completion of the experiments, the chitin yields were calculated as the response variable. Finally, the optimum parameters for chitin production were determined.

i. Demineralisation

The pupae shells and adult BSF flies contain many inorganic components, of which calcium carbonate (CaCO₃) is the main (Erdogan & Kaya, 2016; Kaya *et al.*, 2015). 1 M HCl was used to remove calcium carbonate and to prevent the hydrolysis of chitin. Typically, 10 g of milled pupae shells or adult BSF were refluxed in 200 mL of 1 M HCl solution at 50 °C under constant stirring with a magnetic stirrer for 100 min. At the end of this step, the samples were filtered using 1 µM filter paper using a vacuum pump and then washed with distilled water until neutral pH was attained. The filtrate was then dried in an oven at 50 °C for 12 h.

Table 3.1: The chitin production conditions were optimised by varying temperature of demineralisation, demineralisation time and concentration of pupae shells and adult BSF as independent variables.

Sample code	Concentration HCl (M)	Time (min)	Temperature (°C)
MZ1	1	100	50
MZ2	2	100	50
MZ3	1	100	50
MZ4	1	120	50
MZ5	1	100	50
MZ6	1	100	70

ii. Deproteinisation

The acid-treated BSF samples were then refluxed with 200 mL of 1 M NaOH to remove proteins, at 85 °C for 10 h, using a heater magnetic stirrer system. After the 10 h treatment, the samples were filtered using 1 µM filter paper under vacuum and washed with distilled water until neutral pH was attained. The samples were then dried in an oven at 50 °C for 12 h.

Table 3.2: The chitin production conditions were optimised by varying temperature of deproteinisation, deproteinisation time and concentration of pupae shells and adult BSF as independent variables.

Sample code	Concentration NaOH (M)	Time (h)	Temperature (°C)
MZ7	1	10	85
MZ8	2	10	85
MZ9	1	10	85
MZ10	1	12	85
MZ11	1	10	85
MZ12	1	10	100

iii. Decolourisation

After deproteinisation, the samples were stirred in 100 mL of 3% NaClO at room temperature for 3 h. Once again, the samples were recovered by filtration and washed with distilled water (using 1 µM filter paper) until neutral pH was attained. Following this, the samples were put in an oven to dry at 50 °C for 12 h. The chitin contents of pupae shells and adult BSF flies were calculated using the dry weight of the obtained material.

3.3 Chitosan production

The optimised chitin produced in the previous experiments was used to optimise chitosan production. Again, chitosan was produced by considering three independent variables the deacetylation time (h), deacetylation temperature (°C) and concentration of NaOH (%) and the response variable was the maximum chitosan yield. Table 3.3 details the independent variables and values used to optimise chitosan production. Finally, the optimum parameters for chitosan production were determined.

3.3.1 Deacetylation

The conversion of chitin to chitosan involves deacetylation. The prepared chitins from the pupae shells and adult BSF flies isolated by the steps given in section 3.2 were refluxed in 100 mL of 70% NaOH solution for 5 h at 100 °C with constant stirring by using a magnetic stirrer. After 5 h

of reflux, the solid mass samples were filtered through 1 µM filter paper using a vacuum pump and washed with distilled water until the filtrate attained a neutral pH. Chitosan samples were dried in an oven at 50 °C for 12 h.

Table 3.3: The chitosan production conditions were optimised by varying temperature of deacetylation, deacetylation time and concentration of pupae shells-chitin and adult BSF-chitin as independent variables.

Sample code	Concentration NaOH (%)	Time (h)	Temperature (°C)
MZ14	50	5	100
MZ15	60	5	100
MZ16	70	5	100
MZ17	70	5	100
MZ18	70	7	100
MZ19	70	9	100
MZ20	70	5	60
MZ21	70	5	80
MZ22	70	5	100

3.4 Yield

The chitin yield was calculated based on the dry weight from the weight differences between the raw pupae shells or adult BSF waste and the obtained chitin after the chitin extraction procedure. The chitosan yield was calculated based on the dry weight from the weight difference between the obtained chitin and the obtained chitosan after the chitosan production procedure using the following equations:

$$\text{Chitin yield (\%)} = \frac{a}{b} \times 100 \quad \text{Equation 5}$$

where a is the obtained chitin weight (output) and b is the pupae shells/adult BSF waste weight (input).

$$\text{Chitosan yield (\%)} = \frac{c}{d} \times 100 \quad \text{Equation 6}$$

where c is the obtained chitosan weight (output) and d is the chitin weight (input).

3.5 Electrospinning of chitosan nanofibers

The commercial shrimp chitosan solutions were prepared at various concentrations (3, 5, 6 and 8 wt% (w:v)) by dissolving in a suitable mass in 90% (9:1, v/v) trifluoroacetic acid (TFA)/distilled water. The solutions were prepared at room temperature under vigorous stirring (100 rpm) for two days to obtain a homogeneous solution by using a magnetic stirrer. The prepared solutions were placed in a 5 mL plastic syringe fitted with a 21-gauge BD conventional needle. The syringe was placed in a syringe pump and the needle was connected to the high voltage supply, which generated a high voltage of up to 25 kV. In this study, the applied voltages were 20, 22 and 25 kV, the solution flow rates were 0.06, 0.08 and 0.1 mL/h and the distances between needle tip and collector were 7, 10 and 12 cm (Table 3.4). After electrospinning the nanofiber mats were removed from the aluminum foil used as collector, dried in ambient conditions and stored in a desiccator for further characterisations.

Table 3.4: Process parameters optimised for chitosan nanofiber fabrication.

Applied voltage (kV)	Flow rate (mL/h)	Tip-to-collector distance (cm)
20	0.1	12
22	0.1	12
25	0.1	12
25	0.06	12
25	0.08	12
25	0.1	12
25	0.1	7
25	0.1	10
25	0.1	12

3.6 Sample preparation for characterisation analysis

The dried synthesised chitin and chitosan samples were ground with a mortar and pestle to a powder form. The powdered chitins, chitosans and nanofibrous mat samples were studied with various characterisation techniques to verify the purity and composition of the synthesised and fabricated products in terms of morphology, stability, structural conformation and crystallinity.

This sub-section presents various characterisation techniques employed to attain the objectives of the study.

3.6.1 Elemental analysis

The dried chitin and chitosan samples extracted from the pupae shells and adults BSF of *H. illucens* were analysed for their nitrogen and carbon contents. The elemental analysis was done using a CHN Perkin-Elmer 2400 Elemental Analyser. The degree of acetylation (DA) of chitin and degree of deacetylation (DD) of chitosan was calculated according the following equations (Soon *et al.*, 2018):

$$DA = \left[\left(\frac{C}{N} - 5.14 \right) / 1.72 \right] \times 100 \quad \text{Equation 7}$$

$$DD = \left[\left(6.89 - \frac{C}{N} \right) / 1.72 \right] \times 100 \quad \text{Equation 8}$$

3.6.2 Fourier transform infrared spectroscopy (FTIR)

Fourier transform infrared (FTIR) spectroscopy was used to determine the presence of the functional groups thus to confirm the structural conformation, which are characteristic for chitin and chitosan. The FTIR spectra were obtained directly on the powder samples of chitin, chitosan, and the fabricated chitosan nanofibers. The FTIR spectra were taken on a Perkin Elmer Spectrum 100 FTIR Spectrometer fitted with a Universal ATR (attenuated total reflection). FTIR spectra of all samples were recorded in the range 4000-650 cm^{-1} with a resolution of 0.4 cm^{-1} in the absorbance mode for 4 scans at ambient temperature.

3.6.3 Thermogravimetric analysis (TGA)

Thermal stability of finely ground chitin, chitosan and the nanofibrous mats were examined by thermogravimetric experiments using a Perkin Elmer TGA 4000 Thermogravimetric Analyser instrument. Approximately 1-10 mg of the samples was placed inside the alumina crucibles. The

pre-weighed samples were then allowed to undergo the programmed heating in the temperature range 20-700 °C at a heating rate of 10 °C/min under nitrogen atmosphere purge of 20 mL/min.

3.6.4 X-ray diffraction (XRD)

The structure and crystallinity of the synthesised ground chitin and chitosan, and nanofibrous mats samples were analysed using a Bruker AXS (Germany) D8 Advance diffractometer. XRD patterns of the samples were recorded at 40 kV, 30 mA, and 2θ with a scan angle from 5° to 50° for chitin material and from 5° to 90° for chitosan material. The crystalline index (CrI) was calculated according to equation 1 in chapter 2, section 2.11.2 (Liu *et al.*, 2012).

3.6.5 Scanning electron microscopy (SEM)

The surface morphology of the chitin, chitosan and nanofibrous mat samples were evaluated with an EVOLS 10 ZEISS Auriga and Nova NanoSEM 230 Scanning Electron Microscope using the secondary electron mode with accelerating voltage of 25 kV to reveal the details of their micro and nano-structures at different magnifications. Prior to examination, chitin, chitosan and nanofibrous mat samples were coated with a carbon film to increase their conductivity by using a sputter coater under high vacuum conditions.

The nanofiber diameters were measured with the aid of image J software. The mean nanofiber diameter and distribution were determined from about 50 random measurements using micrographs representative of nanofiber morphology.

3.7 Viscosimetric determination of chitosan's molecular weight

The chitosan's molecular weight was measured by using an Ubbelohde viscometer. At six different concentrations, chitosan solutions were prepared using the solvent system 0.3 M acetic acid and 0.2 M sodium acetate (1:1, v/v). For each sample, measurements were repeated three times at 25 °C. The molecular weight of the chitosans were calculated from the values obtained using the Mark-Houwink equation (Erdogan & Kaya, 2016). The Mark-Houwink equation is as follows:

$$[\eta]=KM^a$$

Equation 9

where $[\eta]$ represents the intrinsic viscosity, M represents the viscosity-average molecular weight (g/mol or Da) of the polymer, K is a constant which is dependent on a given polymer type (mL/g) and a is a constant which depends on the chosen solvent. The following $K= 0.076$ mL/g and $a=0.76$ (Fai *et al.*, 2011) values are applicable for the polymer chitosan and the solvent system acetic acid and sodium acetate.

3.8 Summary of materials and methods

Chitin was optimally extracted from both the pupae shells and adult BSF through demineralisation, deproteinisation and decolouration processes. The extracted chitins were optimally converted to chitosan by deacetylation process. The commercial chitosan were electrospun into nanofibers by optimising the concentration, voltage, flow rate and tip-to-collector distance. The synthesised and fabricated products were characterised using different analytical techniques such as FTIR to examine the spectral patterns and peaks corresponding the stretching and vibrations of various functional groups, TGA to investigate the thermal stability, XRD to examine the crystalline structure and SEM to examine the morphology. Elemental analysis was carried out to determine the degree of acetylation and degree of deacetylation. The extracted chitosan samples molecular weight were measured by using an Ubbelohde viscometer. The commercial shrimp chitin and chitosan were compared to determine the purity of the extracted products. The electrospun chitosan nanofibers were compared to the bulk chitosan to determine how the structure, crystallinity and thermal stability had been altered after the electrospinning process.

CHAPTER 4

RESULTS & DISCUSSION

Summary

This chapter discusses the results obtained from the study of the extraction of chitin from pupae shells and adult BSF for the production of chitosan. The chapter specifically addresses the extractability, yield and purity of chitin and chitosan compared to the commercial products. The elemental, structural, morphological and thermal properties of these extracted products using analytical techniques such as SEM, FTIR, XRD, TGA and elemental analysis are discussed. The molecular weights of pupae-shells and adult BSF-based chitosan are also discussed. This chapter also discusses the electrospinning and optimisation of the electrospinning conditions (concentration, applied voltage, flow rate and collector distance) of the commercial shrimp chitosan. The optimised nanofibrous mats were compared to the pure chitosan by characterising with SEM, FTIR, XRD and TGA analysis.

4. Physiochemical characterisation of chitin and chitosan

This section presents the first attempt to characterise the physiochemical properties of chitin and chitosan extracted from pupae shells and adult BSF and determine its commercialisation value. The pupae shells and adult BSF were chemically extracted by adjusting the parameters, temperature, concentration and time, used for the extraction procedure in order to determine whether the extractability and yield of chitin and chitosan are dependent on these parameters. The several chemical treatments namely demineralisation, deproteinisation and deacetylation were taken into consideration to determine the effective concentration, time and temperature for yielding optimum chitin and chitosan output. The optimised products were further characterised to determine the effectiveness of the extraction process and the purity. The optimised products were characterised using the following different analytical techniques such as FTIR to examine the spectral patterns and peaks corresponding the stretching and vibration of various functional groups, XRD to examine the crystalline nature of the material, SEM to examine the morphology of the material, and TGA to investigate the thermal stability. Elemental analysis was carried out to calculate the degree of acetylation and degree of deacetylation from the carbon and nitrogen

content. The commercial shrimp chitin and chitosan were compared to determine the purity of the extracted products.

4.1 Yield of chitin

4.1.1 Demineralisation and Deproteinisation

The chitin production conditions were optimised by varying the temperature of demineralisation, demineralisation time, and concentration of HCl, temperature of deproteinisation, deproteinisation time and concentration of NaOH as independent variables (as shown in Tables 4.1 and 4.2) and the response variable was the maximum chitin yield (experimental details in chapter 3, section 3.2). The yield was calculated as a % of the mass input vs. output after the extraction procedure (equation 5 in chapter 3, section 3.4) on a dry weight basis. All the processes were done in duplicate.

Table 4.1: The % yield of extracted chitin from demineralisation with HCl.

Sample code	Concentration HCl (M)	Time (min)	Temperature (°C)	Pupae shells Yield (%)	Adult BSF Yield (%)
MZ1	1	100	50	78.3	68.1
MZ2	2	100	50	77.2	67.1
MZ3	1	100	50	79.5	68.5
MZ4	1	120	50	78.2	68.0
MZ5	1	100	50	78.5	69.9
MZ6	1	100	70	77.0	67.1

Table 4.2: The % yield of extracted chitin from deproteinisation with NaOH.

Sample code	Concentration NaOH (M)	Time (h)	Temperature (°C)	Pupae shells Yield (%)	Adult BSF Yield (%)
MZ7	1	10	85	12.7	5.3
MZ8	2	10	85	11.9	5.1
MZ9	1	10	85	13.3	4.9
MZ10	1	12	85	12.2	4.5
MZ11	1	10	85	12.5	5.4
MZ12	1	10	100	12.3	4.7

The % yield based on the dry weight for demineralisation and deproteinisation for both pupae shells and adult BSF was found to be the lowest with an increase in time, temperature and concentration (Table 4.1 and Table 4.2). This reveals that the extractability and yield were dependent on the time, temperature and concentration. Furthermore, the sequence of extraction (deproteinisation then demineralisation) has been reported to lead to a decrease in chitin yield. Deproteinisation before demineralisation erodes the protein layer that protects the material matrix, so the chitin becomes unprotected and completely exposed to acidic treatment, leading to the extensive removal of inorganic materials, with significant hydrolysis and loss of solid material in the chitin fraction, leading to the low yield of chitin (Lertsutthiwong *et al.*, 2002). However, in this study the pupae shells and adult BSF material was first subjected to demineralisation and then to deproteinisation. The best optimum conditions were obtained at 1 M HCl, 100 min and 50 °C for demineralisation and 1 M NaOH, 10 h and 85 °C for deproteinisation for both pupae shells-chitin (MZ3 & MZ9) and adult BSF-chitin (MZ5 & MZ11) respectively (Table 4.1 and 4.2). The final yield of the dry weight of chitin extracted from the adult BSF (MZ11) was 5%, while the dry weight of chitin extracted from the pupae shells (MZ9) was 13% (Table. 4.2). The results show that the percentage yield of chitin from pupae shells was higher than that of adult BSF.

The fully developed peritrophic matrix (PM) of the pupae shells in *H. illucens* may explain the lower chitin yield in the adult BSF because by the time of the adult stage the PM is completely ceased and degraded. *H. illucens* is a holometabolous insect which undergoes a complete metamorphosis. In holometabolous insects, morphological similarities between different metamorphosis stages are extremely low and these differences allow them to live in completely different habitats and feed on different food sources (Badenhorst, 2017). The fact that the adult BSF does not consume food may also be the reason responsible for the low adult BSF-chitin (MZ11) yield.

As shown in Table 4.2, the final yield in chitin content of pupae shells (MZ9) and adult BSF (MZ11) in this study favourably compares and competes with those of microcrustaceans and some insects, for example 3% - 7% in *Daphnia* (Ibitoye *et al.*, 2018), 5.3% - 8.9% in

grasshoppers (Kaya *et al.*, 2015), beetles (5%) (Marei *et al.*, 2016) and from spider species *Geolycosa vultuosa* (8% - 8.5%) and *Hogna radiate* (6.5% - 7%) (Kaya *et al.*, 2014; Kaya *et al.*, 2016; Waško *et al.*, 2016; Kaya *et al.*, 2015). The yield of chitin from pupae shells and adult BSF was also found to be higher than superworm (4.77% - 5.43%), larvae wasp (*Vespa crabro*) (2.1%) and pupae shells of *Musca domestica* (8.02%) (Kaya *et al.*, 2016; Kim *et al.*, 2016; Soon *et al.*, 2018). Kaya *et al.* (2014) found that the dry weight chitin yield of adult potato beetles (20%) was much higher than the larvae (7%). In addition, the dry weight of the grasshopper chitin yield of adult was 14% and for the nymph was 12% (Erdogan & Kaya, 2016). The results presented in this section showed a lower percentage chitin yield than that reported in literature of some commercial organisms (crab: 13% - 26%; shrimp: 14% - 42% and krill: 34% - 49%) (Synowiecki & Al-Khateeb, 2003; Tolaimate *et al.*, 2003). The chitin yield in this study is also lower compared to the results from other insects, like 8.5% in field crickets (Wang *et al.*, 2002), 18% - 21% in the *Daphia magna* resting eggs (Kaya *et al.*, 2013) and 15% in *Holotrichia parallela* (Liu *et al.*, 2012). This may be due to differences in source and extraction methods. Moreover, sex can dictate chitin yield in insects, as a *Decticus verrucirorus* male yields more chitin (11.84%) than the *Melanogryllus desertus* female (4.7%) (Kaya *et al.*, 2015), whereas the pupae shells and adult BSF used in this study were mixed sex.

Hence, pupae shells and adult BSF stand as a promising alternative chitin source among other insects.

4.2 Yield of chitosan

4.2.1 Deacetylation

The chitosan conditions were optimised by varying temperature of deacetylation, deacetylation time and concentration as independent variables (as shown in Table 4.3) and the response variable was the maximum chitosan yield (experimental details in chapter 3, section 3.3). The yield was calculated as a % of the mass input vs. output after the extraction procedure (equation 6 in chapter 3, section 3.4) on dry weight basis. The process was done in duplicate.

Table 4.3: The % yield of extracted chitosan from deacetylation with NaOH.

Sample code	Concentration NaOH (%)	Time (h)	Temperature (°C)	Pupae shells Yield (%)	Adult BSF Yield (%)
MZ14	50	5	100	10.1	1.5
MZ15	60	5	100	10.9	1.7
MZ16	70	5	100	11.4	2.2
MZ17	70	5	100	11.3	2.3
MZ18	70	7	100	11.1	2.1
MZ19	70	9	100	9.1	1.8
MZ20	70	5	60	10.3	1.1
MZ21	70	5	80	10.6	1.5
MZ22	70	5	100	11.3	2.4

The % yield for deacetylation for both pupae shells and adult BSF was found to be the highest with a decrease in temperature and concentration; however the yield was the lowest with an increase in time (Table 4.3). This reveals that the extractability and yield was dependent on the temperature and concentration. The best optimum conditions were obtained at 70% NaOH, 5 h and 100 °C for pupae shells-chitosan (MZ16) and adult BSF-chitosan (MZ22) (Table 4.3). The maximum chitosan yield obtained at optimum conditions were 2% for adult BSF-chitosan (MZ22) and 11% for pupae shells-chitosan (MZ16) (Table 4.3) on a dry weight basis. The results show that the percentage yield of chitosan from pupae shells was higher than that of adult BSF.

The chitosan yield of this study at 2% for adult BSF-chitosan (MZ22) and 11% for pupae shells-chitosan (MZ16) is higher in comparison to the chitosan yield of 0.24% from the American cockroach (*Periplaneta americananwere*) (Wanule *et al.*, 2014) and that of the pupae shells (5.87%) of *Musca domestica* (Kim *et al.*, 2016). In contrast, chitosan yielded from shrimp was 15.40% and 14% from krill (Hossain & Iqbal, 2014). Furthermore, the chitosan yield reported by Alimuniar and Zainuddin (1992) was 18.6% from prawn and No and Meyers (1989) reported approximately 23% from crawfish (Hossain & Iqbal, 2014; No & Meyers, 1989).

The difference in chitosan yield may be the result of different species of organisms being used. The relatively low chitosan yield may also be due to depolymerisation of the chitosan polymer,

loss of sample mass due to excessive removal of acetyl groups from the polymer during deacetylation and loss of chitosan particles during washing which may lead to partial yield loss. This study revealed that the chitin and chitosan yield varies depending on the insect species and also varies depending on the different cuticle and PM types at different development stages in the same insect. Thus the variation in the chitin yield of different species may be explained by the differences in the structures of insect cuticle and the PM. In particular, the large and anisotropic variations in the physiochemical properties of the insect cuticle derive from the ability of chitin to be arranged in unique ways and its potential to interact with a large assortment of proteins during the process of cuticle deposition. Considering the yield obtained from pupae shells and adult BSF it can be utilised as a potential source for chitin and chitosan owing to its commercial availability at low cost.

4.3 SEM Analysis

SEM analysis was performed to determine the differences between the surface morphologies of the chitin and chitosan from pupae shells and adult BSF after the optimum conditions, which were 1 M HCl, 100 min and 50 °C for demineralisation and 1 M NaOH, 10 h and 85 °C for deproteinisation, were obtained along with commercial shrimp chitin and chitosan. The morphology of pupae shells, adult BSF and commercial shrimp chitin and chitosan was examined by an EVOLS 10 ZEISS Auriga and Nova NanoSEM 230 scanning electron microscope. Prior to the SEM analysis, the chitin and chitosan samples were coated with carbon as given in the experimental details in chapter 3, section 3.6.5. The SEM micrographs of chitin extracted from pupae shells and adult BSF, along with the commercial shrimp chitin studied at different magnifications are presented in Figure 4.1.

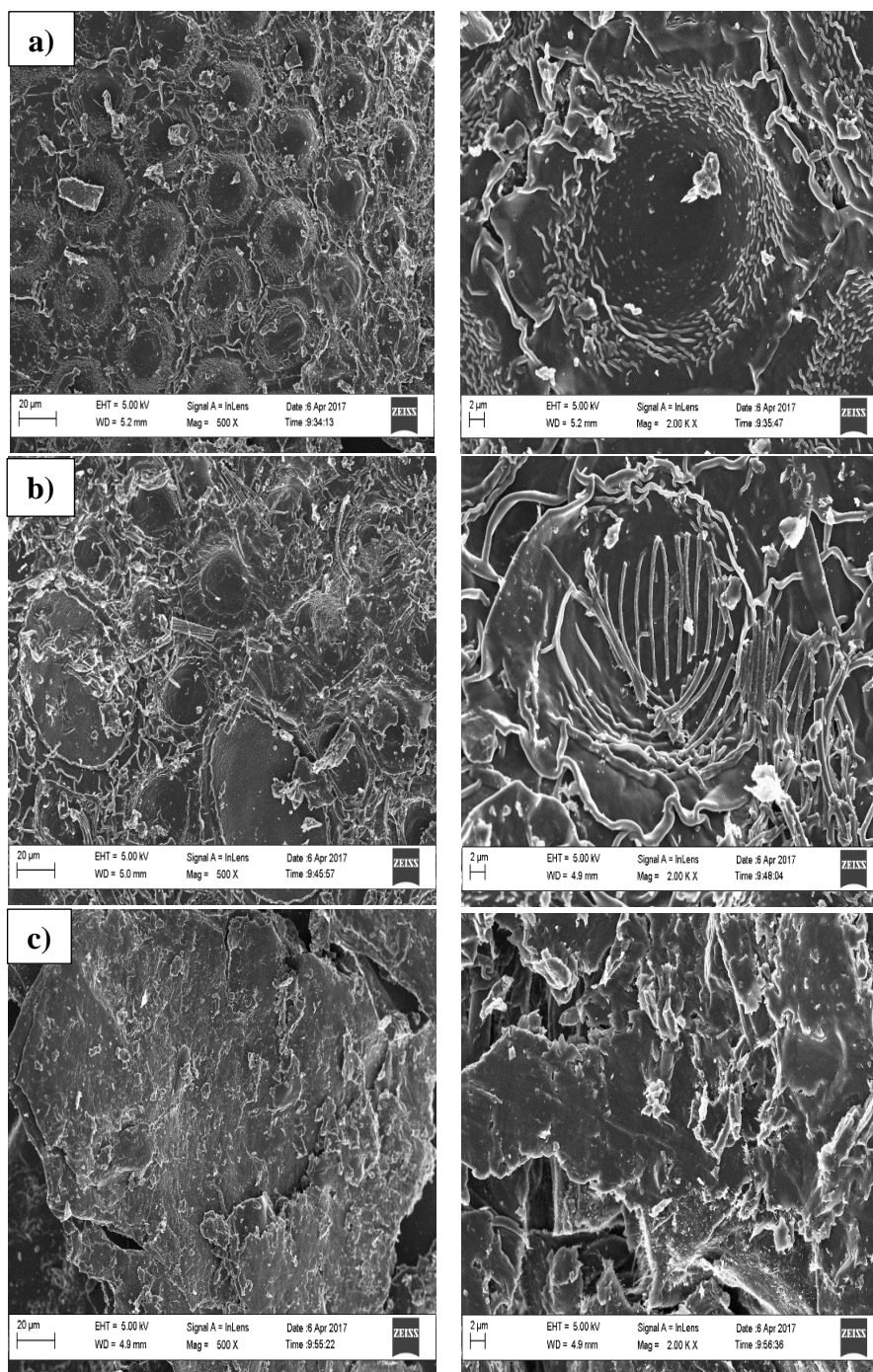


Figure 4.1: Scanning electron micrographs (SEM) of a) chitin from pupae shells, b) chitin from adult BSF and c) commercial shrimp chitin (Sigma Aldrich).

SEM analysis revealed the surface morphologies of pupae shells-chitin to be a tightly packed structure with repeating circular and hexagonal units in honeycomb-like arrangement (Figure 4.1a) while the adult BSF-chitin consists of loosely packed oval units separated by circular

shaped structures with repeating arrangements of fibers (Figure. 4.1b). Increase in magnification (2.00 KX) revealed that both chitins are fibrous in nature with no porosity observed. The average diameter of the fibrils was determined to be 694 nm and 502 nm for pupae shells and adult BSF-chitin respectively. In addition, the commercial shrimp chitin did not exhibit fibrillar structure nor pores but showed layers of crumbling flakes. Considering the different metamorphosis stages of the BSF insect (pupae and adult) it was found that both metamorphous stages exhibited different structure of chitin arrangement compared to that of commercial shrimp chitin.

In general, chitin can be grouped into four distinct forms based on its surface morphology. The first form is the smooth surface morphology without any nanofibers and pores, while the second form consists of nanofibers but no pores. The third form has nanofibers and pores together, and the fourth form has two types of pores in different sizes in combination with nanofibers. Based on the surface morphologies of the extracted chitin, the chitins extracted from adult BSF and pupae shells could be categorised into the second form characterised by nanofibers without any pores on the surface and the commercial shrimp chitin could be categorised into the first form. The presence of nanofibers in this study is in agreement with previous studies on chitin from crustaceans such as crab as well as from insects (Kaya *et al.*, 2014; Erdogan & Kaya, 2016). In contrast, chitins from *Holotrichia parallela* (Liu *et al.*, 2012), *Aliopus simulatrix* and *Duroniella latricornis* (Kaya *et al.*, 2015) consisted of nanopores and nanofibers. In addition, a study conducted on *Vespa crabro* showed that the chitins extracted from adult, pupae and larvae had both nanofibrils and pores, however a higher diversification in the surface morphology was observed for adult chitin than chitin obtained from larvae and pupae (Kaya *et al.*, 2016). Previous studies stated that cuticle morphology differs from region to region, even between individuals, as well as in different species. Additionally, Kaya *et al.* (2014) stated that chitins from the adults and larvae of potato beetle consisted of nanopores and nanofibers, and the number of pores in the adult chitin was much more than in the larval chitin. The surface morphology of chitin thus varies depending on the insect species and varies even in the same species at different metamorphosis stages probably due to the differences in the structure of cuticle and PM. In literature it is well recognised that chitins obtained from different sources display different surface morphologies, even at different metamorphosis stages of development, as also observed in this study.

Overall it was found that the surface morphology of the pupae shells-chitin and adult BSF-chitin was different from that of the commercial shrimp chitin. The reason may be due to the fact that chitin isolated from different parts of an insect's body and from different sexes has differing surface morphology. Surface morphology plays an effective role in determining the use of chitin and chitosan in different fields. Chitins with a porous structure are used in absorption of toxic metal ions, controlled drug delivery and tissue engineering, while the fibrillary structures are used in textiles (Kumar, 2000; Synowiecki & Al-Khateeb, 2003; Younes & Rinaudo, 2015).

The scanning electron micrographs of chitosan produced from pupae shells and adult BSF chitin after the optimum conditions which were 70% NaOH for 5 h at 100 °C was obtained and are presented alongside the commercial shrimp chitosan are depicted in Figure 4.2 (a,b &c).

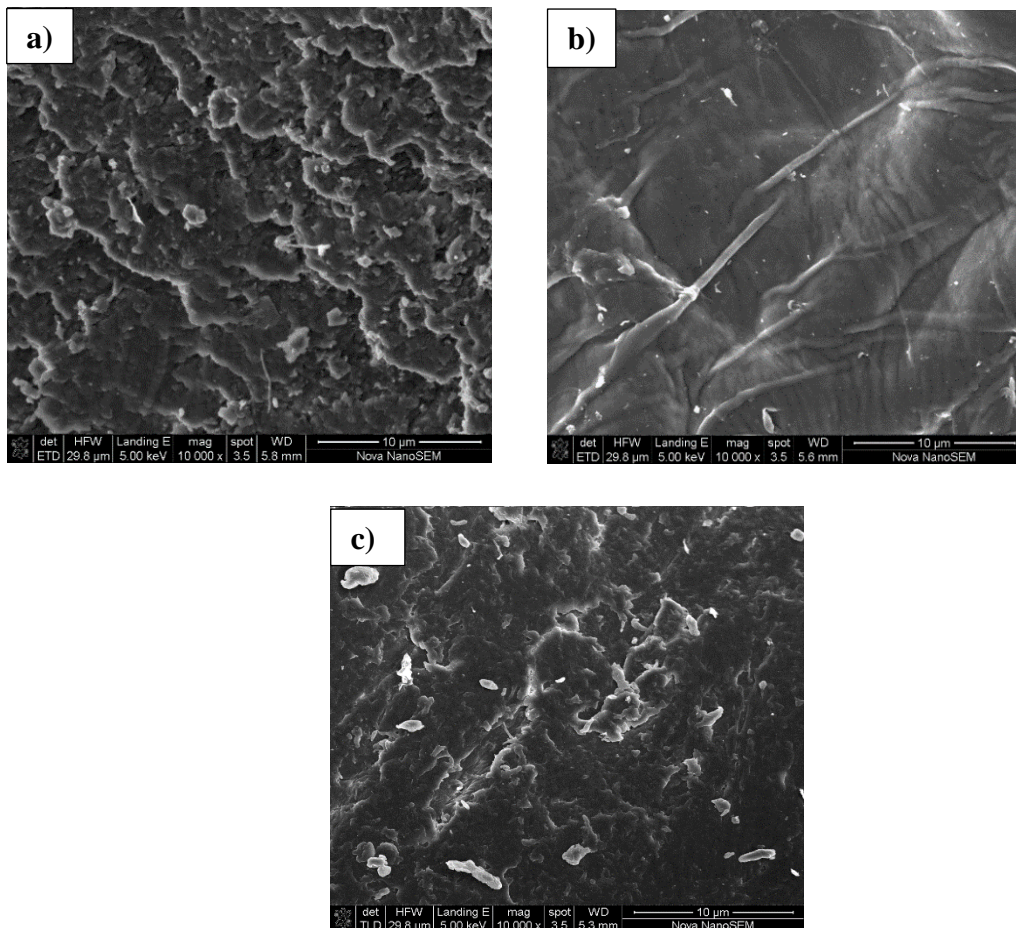


Figure 4.2: Scanning electron micrographs (SEM) of a) chitosan from pupae shell-chitin, b) chitosan from adult BSF-chitin and commercial chitosan (Sigma Aldrich).

The scanning electron micrographs revealed that the surface morphologies of pupae shells-chitosan were characterised by surface roughness and adult BSF-chitosan had a smooth surface, without any nanofibers and/or nanopores on both surfaces (Figure 4.2a&b). The commercially obtained chitosan from shrimp (Figure 4.2c) appeared slightly rougher than the adult BSF-chitosan.

The surface morphologies of the synthesised chitosans in this study were similar to that identified for two mushroom species (*Lactarius vellereus* and *Phyllophora ribis*) (Erdogan *et al.*, 2017; Masum *et al.*, 2011). Another finding similar to this study revealed that *Lentinula edodes* (shitake stipes) chitosans exhibited a firm structure without nanopores and nanofibers (Yen & Mau, 2007). In contrast, the chitosan obtained from the adults and larvae of potato beetle consisted of nanofibers (Kaya *et al.*, 2014). In another study the surface morphologies of chitosans from adult and nymph grasshoppers consisted of nanofibers with a highly porous structure, unlike the pupae shells and adult BSF chitosans (Erdogan & Kaya, 2016). As noted in this study compared with literature studies the surface morphologies of the chitosans thus vary depending upon the sources and the development stages.

Five different surface structures have been reported until now for chitin, and can also be used to define chitosan. They include (1) a hard and rough surface morphology with neither pores nor fibers, (2) surfaces with pores only, (3) a combination of fibers and pores, (4) surfaces with two types of pores with fibers, (5) and only fibers. However, these different reported morphologies depend on the magnification of the area being viewed. Therefore, in the present study as a general observation, i.e at lower magnification, a mixed type of surface morphology was observed for chitin and chitosan extracted from the pupae shells and adult BSF, which has not been previously reported i.e a combination of smooth, rough, flaky, and fibrous chitin surface morphology (Figure. 4.2a&b). The standard surface morphology of α -chitin and chitosan can be said not to have been established yet. This study reported that the pupae shells and adult BSF chitin and chitosan extracted exhibited different surface morphologies.

4.4 Elemental analysis

Various analysis techniques have been developed for the determination of the degree of acetylation (DA) and degree of deacetylation (DD). The chitin and chitosan obtained after the optimum conditions from the pupae shells and adult BSF, as well as that of commercial chitosan obtained from shrimp, were subjected to elemental analysis. The elemental analysis was conducted using an Elemental Analyzer Flash 2000, to determine the % carbon (C) and % nitrogen (N) content of the chitin and chitosan from both *H. illucens* (pupae shells and adult BSF) and commercial shrimp chitosan (experimental details in chapter 3, section 3.6.1). The % C and N results of obtained pupae shells-chitin, adult BSF-chitin and commercial shrimp chitin, and the corresponding chitosans are presented in Table 4.4. This study employed the elemental compositions of C and N, for the determination of the DA (equation 7 in chapter 3, section 3.6.1) and DD (equation 8 in chapter 3, section 3.6.1) of pupae shells, adult BSF and commercial shrimp chitin and chitosan as displayed in Table 4.4.

Table 4.4: Elemental analysis, DA and DD of chitin and chitosan from pupae shells and adult BSF compared to commercial shrimp chitin and chitosan.

Sample	% C	% N	% DA	% DD
Commercial chitin	42.8	6.3	96.4	N/A
Adult BSF-chitin	43.6	6.5	91.5	N/A
Pupae shells-chitin	44.1	6.2	115.1	N/A
Commercial chitosan	34.6	6.1	N/A	70
Adult BSF-chitosan	34.2	6.0	N/A	69
Pupae shells-chitosan	32.2	5.6	N/A	67

The results of the elemental analysis as tabulated in Table 4.4 showed that C and N content were 44.1% and 6.2% for pupae shells-chitin, 43.6% and 6.5% for adult BSF-chitin and 42.8% and 6.3% for commercial shrimp chitin, respectively. From this study, and as shown in Table 4.4, the percentage of N content present in adult BSF-chitin (6.5%) is higher than that of pupae shells-chitin (6.2%) and commercial shrimp chitin (6.3%) and both were observed to be lower than

6.89%, which is the reference N content typical for fully acetylated chitin (Liu *et al.*, 2012). The only slightly lower N content indicates that the amount of protein that was left in the pupae shells-chitin, adult BSF-chitin compared to the commercial shrimp chitin was similar which indicates an effective optimum deproteinisation (1 M NaOH for 10 h at 85 °C) process (Kaya *et al.*, 2015; Liu *et al.*, 2012). The corresponding DA of the extracted chitin value of adult BSF, pupae shells and commercial shrimp chitin were found to be 91.5%, 115.1% and 96.4%, respectively (Table. 4.4). The DA value of fully acetylated chitin is reported as 100% and this indicates the purity of chitin (Kaya *et al.*, 2017). In this study, the DA of the extracted chitins was slightly lower and higher than 100%, indicating a relatively high purity chitin extract. The leftover impurities could be mineral salts and protein residues (Kaya *et al.*, 2017).

From elemental analysis, this study reveals a % N of 6.5% and 6.2% for adult BSF-chitin and pupae shells-chitin respectively. The N content of chitin in this study is in agreement with that of earlier reports in other insects: 6.42% for *Geolycosa vultuosa*, 6.41 % for *Hogna radiate* (Kaya, *et al.*, 2014) and 6.3% for *Holotrichia parallela* (Liu *et al.*, 2012). The findings reported by Kaya *et al.* (2014) supports the results found in this study. Kaya *et al.* (2014) found the N content of chitins from *L. decemlineata* (potato beetle) were 6.6% for adult potato beetles and 5.2% for the larvae of potato beetles. In contrast, Erdogan & Kaya (2016) found that the N content of chitins from *D. maroccanus* (grasshopper) were 4.63% for the adult chitin and 5.66% for nymph chitin, respectively. The usual value (6.89%) obtained for fully acetylated chitin in previous studies was similar to the values of 6.5%, 6.2% and 6.3% obtained for pupae shells-chitin, adult BSF-chitin and commercial shrimp chitin respectively in the present study. A low amount of nitrogen signifies the minimum residual protein remaining in chitin; this is also a pointer to effective deproteinisation (1 M NaOH, 10 h, 85 °C). In addition, the N content of chitin is extremely important as it indicates the level of purity of the product. The N content of completely acetylated (pure) chitin is known to be 6.89% (Sajomsang & Gonil, 2010). At N levels above 6.89%, this suggests that there are protein remnants in the chitin sample, while below 6.89% this indicates the presence of mainly inorganic materials. It can therefore be said that the chitin extracted from pupae shells and adult BSF is not completely pure, but that adult BSF-chitin is purer than commercial chitin. Moreover, the pupae shells and adult BSF chitin contains a higher N level than fungi (2.96%). This is due to the fact that fungi possess chitin-glucan residues

(Ifuku *et al.*, 2011), which cannot be removed completely by chemical processes, impacting the N content of the fungi chitin.

One of the most important chemical properties that can determine the performance of chitin and chitosan is the degree of N-acetylation. In this study, it was recorded that the DA value of pupae shells-chitin was 115.1%, while the DA value of adult BSF-chitin and commercial shrimp chitin was 91.5% and 96.4% respectively (Table. 4.4). The DA of adult BSF and commercial shrimp chitin was similar to that previously reported for other shrimp (94.3%) and *Holotrichia parallela* (93.1%), as well as that from bumble bees (87.3%) and shrimp α -chitin (99.0%) calculated using a different formula (Majtán *et al.*, 2007). In addition, the DA result of pupae shells-chitin given in Table 4.4 is slightly higher than the adult BSF-chitin and commercial shrimp chitin when compared with other insects such as locusts (98%), honey bees (96%) and beetles (95%) (Marei *et al.*, 2016). These differences may be attributed to different methods of chitin isolation as well as differences in the sources. A DA greater than 100% is an indication that some inorganic materials are left in the polymer structure (Sajomsang & Gonil, 2010). In this study, results indicate that some inorganic materials may still be present in the pupae shell-chitin sample and this is further corroborated by the slightly lower percentage of N content in the pupae shells-chitin. Nevertheless, the extracted chitin from pupae shells and adult BSF in this study is still of acceptable purity and in some instances is purer when compared to that obtained in other studies. For instance, the DA is 101.02% in shrimps (Liu *et al.*, 2012), 132.5% in bumblebees (Majtán *et al.*, 2007), 151.7% in crude crabs (Yen *et al.*, 2009), 239.76% in *Letinula edodes*, 377.9% in *Grifola frondosa* and 560.9% in *Hypsizygus marmoreus* (Kaya *et al.*, 2014). In addition, DA values of adult and larval potato beetles chitins were calculated as 108% and 232%, respectively (Kaya *et al.*, 2014). Erdogan and Kaya (2016) found the DA values of chitins obtained from nymph chitin and adult chitin to be 187% and 232%, respectively.

As seen in Table 4.4 the DA varied depending on the chitin source and metamorphosis stage of development. Moreover, according to Hajji *et al.* (2014), DA of chitin affects the solubility, chemical reactivity and biodegradability in many industrial processes (Hajji *et al.*, 2014).

In Table 4.4 it is shown that the C and N content of BSF chitosans and commercial chitosan were measured as 34.19% and 6.0% for adult BSF-chitosan, as 32.15% and 5.6% for pupae shells-chitosan and 34.62% and 6.1% for commercial shrimp chitosan (Table. 4.4). In this study it was found that commercial chitosan had a higher percentage of N (6.1%) than pupae shells-chitosan (5.6%) and adult BSF-chitosan (6.0%). The C and N compositions in the pupae shells, adult BSF and commercial shrimp chitin were slightly higher than the pupae shells-chitosan, adult BSF-chitosan and commercial shrimp chitosan. The reason might be that during deacetylation, part of the acetyl chain in N-acetyl glucosamine was removed and converted to amine groups by forming new N-H bonds (Yeul & Rayalu, 2013). The removal of acetyl chains from chitin might have caused the reduction of C and N content in the chitosan. The DD values of the chitosans derived from *H. illucens* were calculated as 67% for the pupae shells-chitosan, 69% for the adult BSF-chitosan, and 70% for the commercial chitosan. The DD value of the chitosans was lower than 100% found for pure chitosan.

The N content of adult BSF-chitosan (6.0%), pupae shells-chitosan (5.6%) and commercial chitosan (6.1%) were lower than some other findings. Kaya et al. (2015) reported a higher N content for adult chitosan (7.2%) and for larval chitosan (6.9%) from potato beetles compared to the findings in this study. In addition, the N content of grasshopper chitosans were measured as 7.2% for the adult chitosan and as 6.45% for the nymph chitosan, respectively. It has been reported that the physiochemical and functional properties of chitosan are considerably affected by DD (Yen *et al.*, 2009). According to Kumari et al. (2017), the DD of chitosan depends on the species and the preparation methods, ranging from 56% to 99% with an average of 80%. The DD of pupae shells-chitosan, adult BSF-chitosan and commercial shrimp chitosan was lower than that previously reported for shrimp (92.19%) (Kucukgulmez *et al.*, 2011) and silkworm chrysalides (83%) (Paulino *et al.*, 2006). Furthermore, the DD value of chitosan from potato beetles was 82% for adult chitosan and 76% for larvae chitosan. However, these values are higher when compared with grasshoppers (64% for the adult chitosan and 22% for the nymph chitosan) (Erdogan & Kaya, 2016) and *Euphasia superba* (11.28%) (Wang *et al.*, 2013). The difference observed in DD could be due to the different concentration of alkali, temperature and duration used. According to No and Meyers (1997), the DD of chitosan ranges from 56% to 99%, therefore the chitosan produced from pupae shells and adult BSF is of acceptable purity.

DA and DD is an important factor affecting the properties of chitin and chitosan and the possible application areas of these materials. Literature stated that chitosan having a DD<80% can be used in gene delivery and enzyme immobilisation (Kaya *et al.*, 2017).

4.5 FTIR Analysis

FTIR spectroscopic analysis was used to determine the chemical structure and the spectral peaks corresponding to the stretching and vibration of various functional groups. IR characterisation of the chitin and chitosan was performed with Perkin Elmer Spectrum 100 FTIR spectrometer instrument with a frequency range of 4000 to 650 cm^{-1} (experimental details given in chapter 3, section 3.6.2). Figure 4.3 and Table 4.5 present the FTIR spectra and band assignments for chitin extracted after the optimum conditions was obtained from pupae shells and adult BSF and that of commercially extracted chitin from shrimp.

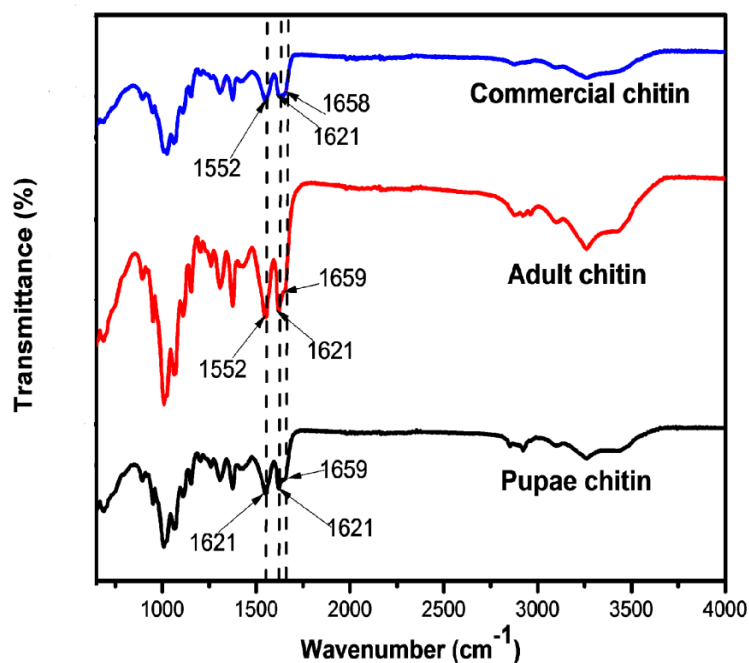


Figure 4.3: FTIR spectra of extracted chitins from adult BSF and pupae shells compared to commercial shrimp chitin (Sigma Aldrich).

Table 4.5: The FTIR assignment bands (cm^{-1}) of chitin isolated from pupae shells and adult BSF, *H. illucens*.

Functional group and vibration modes	Classification	Pupae shells-chitin	Adult BSF-chitin	Commercial shrimp chitin	Other commercial chitin
O-H stretching		3454	3453	3453	3437
N-H stretching		3257-3094	3257-3087	3264-3087	3101-3259
CH ₃ symmetrical stretch and CH ₂ asymmetric stretch	Aliphatic compounds	2923	2925		2937
CH ₃ symmetrical stretch	Aliphatic compound	2853	2860	2872	2867
C-O secondary amide stretch	Amide I	1659	1659	1658	1654
C-O secondary amide stretch	Amide I	1621	1621	1621	1620
N-H bend, C-N stretch	Amide II	1552	1552	1552	1553
CH ₂ ending and CH ₃ deformation		1425	1425	1426	1430
CH bends CH ₃ symmetrical deformation		1372	1374	1374	1376
CH ₂ wagging	Amide II, components of proteins	1314	1312	1312	1318
Asymmetric bridge oxygen stretching		1160	1160	1166	1155
Asymmetric in-phase ring stretching mode		1116	1116	1116	1114
C-O-C asymmetric stretch in phase ring	Saccharide rings	1071	1071	1078	1068
C-O asymmetric stretch in phase ring		1008	1008	1021	1024
CH ₃ wagging	Along chain	957	957	945	952
CH ring stretching	Saccharide rings	888	888	894	896
Reference		Current study	Current study	Current study	Kaya et al. (2015)

The characteristic chitin bands amide I, which correspond to the C=O secondary amide stretch, and amide II, which correspond to the N-H bend and C-N stretch, were detected in the three chitin samples (Figure 4.3). The amide I band displayed two peaks; a weak intensity peak at approximately 1659-1658 cm^{-1} and a strong and well defined intensity peak at approximately 1621 cm^{-1} wavenumbers. The amide II band was displayed at a wavenumber of 1552 cm^{-1} (Figure 4.3 and Table 4.5).

Alpha chitin can be distinguished from beta chitin by FTIR spectroscopy. In the α -chitin spectrum, the amide I band splits into two components at approximately 1660 and 1625 cm^{-1} , whereas a single band is observed in the β -chitin at approximately 1656 cm^{-1} (Lavall *et al.*, 2007; Kaya *et al.*, 2015). The splitting of the amide I band at approximately 1660 cm^{-1} and 1625 cm^{-1} in the α -chitin spectrum is attributed to the two types of H-bonds formed by amide groups in the antiparallel alignment present in the crystalline regions of α -chitin. The study revealed that the chitin extracted from pupae shells and adult BSF is of α -form and is very similar to that of commercial shrimp chitin. Moreover, there were no bands at 1540 cm^{-1} in the spectral evaluation of pupae shells-chitin, adult BSF-chitin and commercial shrimp chitin, which suggests no protein residues were present in the chitins (Morin & Dufresne, 2002). This also shows that the deproteinisation (1 M NaOH for 10 h at 85 °C) process during chitin isolation was sufficient. Other major bands detected in FTIR spectra were as follows: 3434-3423 cm^{-1} (O-H stretching), 3267-3262 cm^{-1} (asymmetric N-H stretching), 3105-3097 cm^{-1} (symmetric N-H stretching), 2923-2922 cm^{-1} (asymmetric C-H stretching), 2878-2845 cm^{-1} (symmetric C-H stretching), 1376-1375 cm^{-1} (CH bend, CH₃ symmetric deformation), 1154-1153 cm^{-1} (C-O-C asymmetric stretching) and 1115-1111 cm^{-1} and 1022-1009 cm^{-1} (C-O-C symmetric stretching) (Kaya *et al.*, 2015; Kaya *et al.*, 2017; Waško *et al.*, 2016) (Table 4.5). The β -glycosidic bond which is known for standard α -chitin was recorded at 897-896 cm^{-1} (Wysocki *et al.*, 2013).

Considering the results of FTIR, these explain that the 3442, 3267-3105, 1660, 1550 and 1310 cm^{-1} characteristic bands for chitin are attributed to O-H stretching, N-H stretching and amides I, II and III, respectively. In this study, all these characteristic bands are present and similar in the chitin extraction from pupae shells, adult BSF and those obtained for commercial shrimp chitin. Chitin isolated from pupae shells, adult BSF (Figure 4.3 and Table 4.5) possess peaks at 3454, 3257-3094, 1659, 1621, 1552 and 1314 cm^{-1} and 3453, 3257-3087, 1659, 1621, 1552 and 1312 cm^{-1} respectively, which was similar to that of the findings published recently by Waško *et al.* (2016), and that for other organisms, such as crab, shrimp, potato beetle and grasshopper (Erdogan & Kaya, 2016; Suneeta *et al.*, 2016; Yen *et al.*, 2009; Kaya *et al.*, 2015, 2016), as well as to that obtained from commercial shrimp evaluated in this study (3453, 3264-3087, 1658, 1621, and 1312 cm^{-1}). Also, in agreement with some previous reports (Liu *et al.*, 2012; Simionato *et al.*, 2014), the amide I band of pupae shells, adult BSF and commercial shrimp

chitin splits into two bands appearing at 1659/1658 and 1621 cm^{-1} (Figure 4.3), indicating that the chitin isolated from the pupae shells and adult BSF in this study and that commercially obtained from shrimp is in the α -crystal form (Erdogan & Kaya, 2016; Kaya *et al.*, 2014; Liu *et al.*, 2012). For pupae shells, adult BSF and commercial shrimp chitin, some other strong and broad bands were also respectively observed at 3454, 3453, and 3453 cm^{-1} (O-H stretching), 3257-3094, 3257-3087 and 3264-3087 cm^{-1} (N-H stretching), 2923 and 2925 (CH_3 symmetrical stretching and CH_2 asymmetric stretching) 2853, 2860 and 2872 cm^{-1} (aliphatic compounds), 1621-1659, 1621-1659 and 1621-1658 cm^{-1} (amide I), 1552. 1552 and 1552 cm^{-1} (amide II), 1425, 1425 and 1426 cm^{-1} (CH_2 bending and CH_3 deformation), 1372, 1374 and 1374 cm^{-1} (CH bend, CH_3 symmetrical deformation), 1312, 1312 and 1312 cm^{-1} (CH_2 wagging), 1160, 1160 and 1166 cm^{-1} (asymmetric bridge oxygen stretching), 1116, 1116 and 1116 cm^{-1} (asymmetric in-phase ring stretching mode), 1071, 1071 and 1078 cm^{-1} (saccharide rings), 1008, 1008 and 1021 cm^{-1} (C-O assymetrical stretching in-phase ring), 957, 957 and 945 cm^{-1} (along chain) and 888, 888 and 894 cm^{-1} (saccharide rings) and they agreed with other reports (Erdogan & Kaya, 2016; Kaya *et al.*, 2014; Yen *et al.*, 2009). It was also observed that the 1540 cm^{-1} absorption band, which is attributed to protein, was totally absent in adult BSF, pupae shells and commercial shrimp chitin, hence confirming the effectiveness of the deproteinisation process (1 M NaOH for 85 °C at 10 h) conditions (Majtán *et al.*, 2007).

The FTIR analysis has confirmed the successful extraction of α -chitin from pupae shells and adult BSF. From the FTIR results, it can be concluded that there is a very close similarity between the chemical composition and bonding of chitin from the pupae shells, adult BSF and shrimp chitin obtained commercially as well as from other insects and commercial chitin. Hence, pupae shells and adult BSF chitin can be used in place of commercial shrimp chitin.

The infrared spectra of the pupae shells, adult BSF and commercial shrimp chitosan samples are shown in Figure 4.4 with band assignments shown in Table 4.6.

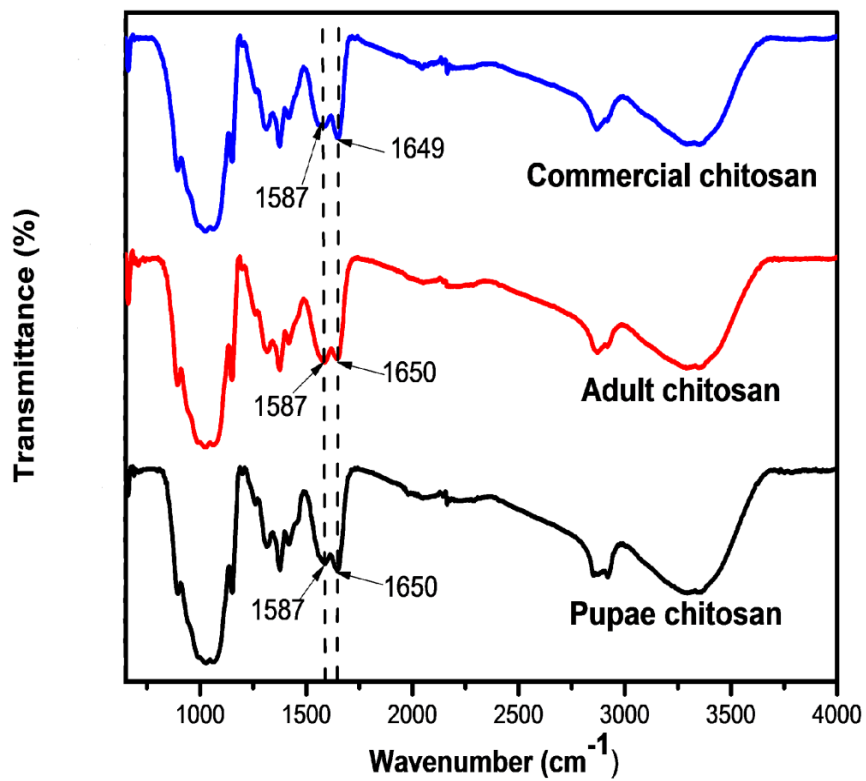


Figure 4.4: FTIR spectra of extracted adult BSF and pupae shells chitosan compared to the commercial shrimp chitosan (Sigma Aldrich).

Table 4.6: The FTIR assignments of bands (cm^{-1}) of chitosan isolated from the pupae shells and adult BSF, *H. illucens*.

Functional group and vibration modes	Pupae shells-chitosan	Adult BSF-chitosan	Commercial shrimp chitosan	Other commercial chitosan
ν (NH_2) associated with primary amines and OH associated with pyranose ring	3358	3352	3358	3356
ν_{as} (CH_2) in CH_2OH group	2916	2923	2929	2921
ν (C-H) in pyranose ring	2860	2860	2872	2871
ν (C=O) in NHCOCH_3 group (amide I band)	1650	1650	1649	1652
ν (NH_2) in NHCOCH_3 group (amide II band)	1587	1587	1587	1586
δ (CH_2) in CH_2OH group	1425	1425	1425	1420
δ_s (CH_3) in NHCOCH_3 group	1374	1374	1374	1375
δ (C-H) in pyranose ring	1306	1306	1305	1317
Complex vibrations of NHCO group (amide II band)	1255	1255	1253	1258
ν_s (C-O-C) (glycosidic linkage)	1153	1153	1160	1149
ν_{as} (C-O-C) (glycosidic linkage)	1082	1082	1082	1062
ν (C-O) in secondary OH group	1027	1027	1021	1021
ν (C-O) in primary OH group	-	-	-	985
Pyranose ring skeletal vibrations	894	894	888	895
Reference	Current study	Current study	Current study	Kaya et al. (2013)

To verify the presence of the characteristic peaks, FTIR spectra of chitosan samples obtained from the pupae shell-chitin and adult BSF-chitin were examined, along with the commercial shrimp chitosan (Table 4.6). The characteristic bands were recorded at 1650 cm^{-1} and 1587 cm^{-1} for the chitosan from adult BSF, 1650 cm^{-1} and 1587 cm^{-1} for the pupae shells-chitosan and at 1649 cm^{-1} and 1587 cm^{-1} for commercial chitosan (Figure 4.4). In literature it is known that the peaks at approximately $1650\text{-}1655 \text{ cm}^{-1}$ and $1583\text{-}1590 \text{ cm}^{-1}$, which correspond to (C=O) in the NHCOCH_3 group (amide I band) and (NH_2) in the NHCOCH_3 group (amide II band), are characteristic for chitosan (Table. 4.6) (Krishnaveni & Ragunathan, 2015; Erdogan & Kaya, 2016). The band of amide I has a higher intensity than the band of amide II, which suggests an efficient deacetylation (70% NaOH for 5 h at $100 \text{ }^\circ\text{C}$). When the deacetylation of chitin occurs, the absorption band assigned to amide II decreases, while the increase of the intensity of the

amide I band indicates the formation of NH₂ groups (Erdogan & Kaya, 2016). The FTIR spectra showed that chitosan extracted from pupae shells and adult BSF was very similar to that of commercial shrimp chitosan.

Further absorption bands (Table. 4.6) that were observed in the region of 3000-3500 cm⁻¹ are attributed to symmetric stretching vibrations of NH₂ and OH groups. The absorption peaks at approximately 2860 cm⁻¹ and 2916/2923 cm⁻¹ are attributed to the asymmetric and symmetric stretching vibrations of C-H groups. The vibration bands at approximately 1650 cm⁻¹ in the spectrum of chitosans indicated the presence of amide I while the vibration band at approximately 1587 cm⁻¹ corresponds to the amide II. The absorption peaks at 1374 and 1255 cm⁻¹ are attributed to N-H bending vibration of primary amides and C-O-C stretching, respectively (Chatterjee *et al.*, 2005; Kaya *et al.*, 2013). The absorption band at 1153 cm⁻¹ showed the spectral β(1-4) glycosidic bond in the polysaccharide unit, and the band at 1082 cm⁻¹ was assigned to the stretching of C-O-C in the glucose ring (Moussout *et al.*, 2016).

Chitosan from the pupae shells and adult BSF exhibited a broad band at 3358 and 3352 cm⁻¹ (Figure 4.4), and at 3358 cm⁻¹ in shrimp chitosan, respectively corresponding to the stretching vibration of N-H and O-H, the extension vibration of N-H and the intermolecular hydrogen bonds of polysaccharide. The absorption bands at 2916 and 2860 cm⁻¹ for pupae shells, 2923 and 2860 cm⁻¹ for adult BSF chitosan and 2929 and 2872 cm⁻¹ for commercial shrimp chitosan were assigned to the asymmetric and symmetric C-H stretching vibration, respectively. As expected, an evident absence of the split amide I band was observed in pupae shells, adult BSF and commercial chitosan (Figure 4.4) with a prominent characteristic band at 1587 cm⁻¹ revealing the success of N-deacetylation in all three sources of chitosan. The absorption at 1425 and 1374 cm⁻¹, 1425 and 1374 cm⁻¹ and 1425 and 1374 cm⁻¹ for pupae shells, adult BSF and commercial chitosan, respectively, was assigned to the C-N stretching vibrations. The band at 1306 (pupae shells-chitosan and adult BSF-chitosan) and 1305 cm⁻¹ (commercial chitosan) were attributed to the O-H bending vibration. The C-O stretching vibration in the secondary alcohol was respectively evaluated for pupae shells-chitosan, adult BSF-chitosan and commercial shrimp chitosan at a wavenumber of 1153, 1153 and 1160 cm⁻¹. Nevertheless, a C-O stretching vibration in the alcohol was seen at 1027 cm⁻¹ (pupae shells-chitosan) and adult BSF-chitosan) and 1026

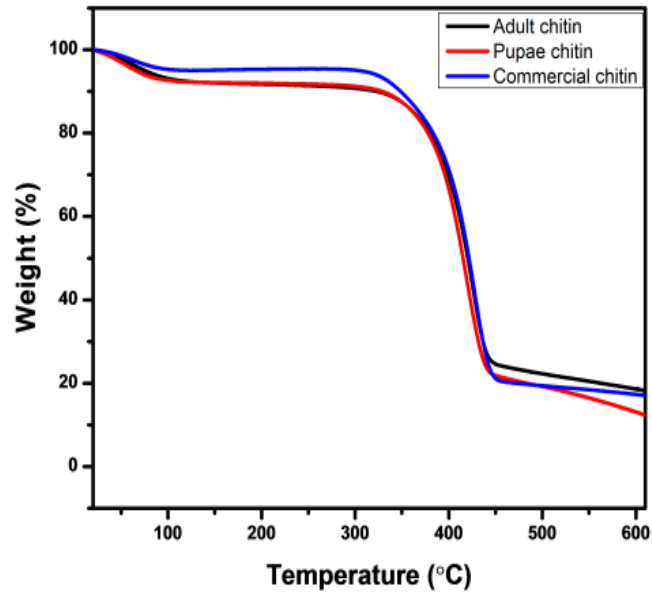
cm⁻¹ (commercial shrimp chitosan). Also, absorption at 894 cm⁻¹ and 888 cm⁻¹ was ascribed to the C-H out-of-plane vibration of the ring of monosaccharides.

The FTIR results showed that the chitins extracted were successfully transformed into chitosan via deacetylation. From the FTIR results it can suggest that the similarity between the chemical composition and bonding types of chitosan in the pupae shells, adult BSF and commercial shrimp chitosan are very close, and can therefore be substituted for each other during utilisation. The spectra of pupae shells-chitosan and adult BSF-chitosan were similar to those of commercial shrimp chitosan, and chitosan extracts from insects such as grasshoppers, potato beetle, silkworm crysalides and two orthoptera species (Paulino *et al.*, 2006; Kaya *et al.*, 2014, Kaya *et al.*, 2015; Erdogan & Kaya, 2016).

4.6 TGA analysis

The thermal degradation behaviour of chitin and chitosan obtained after applying the optimum demineralisation, deproteinisation and deacetylation conditions respectively to pupae shells and adult BSF were determined with thermogravimetric analysis. Weight loss with respect to the temperature was quantified from the thermograms by monitoring the thermal degradation profiles of the samples. The thermal stability was obtained using a Perkin Elemer TGA 4000 Thermogravimetric Analyser instrument in a temperature range between 20-600 °C under N₂ (experimental details in chapter 3, section 3.6.3). TGA (A) and DTG (B) thermograms of chitin from pupae shells, adult BSF and commercial shrimp chitin are presented in Figure 4.5 and Table 4.7.

A



B

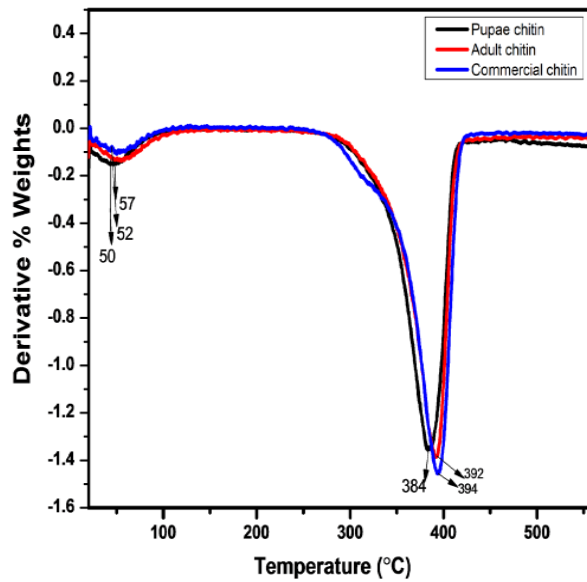


Figure 4.5: TGA (A) and DTG (B) thermograms of the extracted adult BSF-chitin and pupae shells-chitin compared to the commercial shrimp chitin (Sigma Aldrich).

Table 4.7: Thermogravimetric results of commercial shrimp chitin and chitin extracted from pupae shells and adult BSF.

	Pupae shells-chitin		Adult BSF-chitin		Commercial chitin	
First mass loss (%)	3.38	22-105 °C	3.45	27-90 °C	3.78	21-120 °C
Second mass loss (%)	65.4	250-450 °C	60.8	285-425 °C	73.4	250-430 °C
Total mass loss (%)	68.7		64.2		77.1	
DTG _{max} (°C)	384		392		394	
Residue (%)	25		22		21	

In this study it was found that the pupae shells-chitin, adult BSF-chitin and commercial shrimp chitin displayed weight loss in two steps (Figure 4.5 and Table 4.7). The commercial shrimp chitin revealed the highest loss in total mass (77%); this was followed by the pupae shell-chitin (68%) and adult BSF-chitin (64%). The first stage of decomposition for commercial shrimp chitin occurred at 52 °C (started at 21 °C to 120 °C), for pupae shells-chitin it occurred at 50 °C (started at 22 °C to 105 °C) and for adult BSF-chitin it occurred at 57 °C (started at 27 °C to 90 °C). This was accompanied by a weight loss of 3.78%, 3.38% and 3.45%, respectively. The weight loss observed in the first phase stems from the evaporation of water absorbed in the chitin (Paulino *et al.*, 2006). It is evident that the pupae shells-chitin lost more water than the commercial chitin before equilibrating, similar to the adult BSF-chitin. From the derivative thermal graphs it was observed that all the chitin samples were stable up to 270 °C and then all three chitin samples started degrading at 270 °C up to 430 °C however, the commercial shrimp chitin showed a slight 10 °C increase in thermal stability. Hence, the second decomposition phase started at 250 °C and attained a maximum value at 430 °C with a weight loss of 73.4% for commercial shrimp chitin. For pupae shell-chitin it started at 250 °C and attained a maximum value at 450 °C with a weight loss of 65.4% and for adult BSF-chitin it started at 285 °C and attained a maximum value at 425 °C with a weight loss of 60.8%. The mass loss observed in the second phase was due to the thermal degradation in N₂ of chitin (Paulino *et al.*, 2006; Gonil & Sajomsang, 2012). The maximum thermal degradation temperature (DTG_{max}) values was

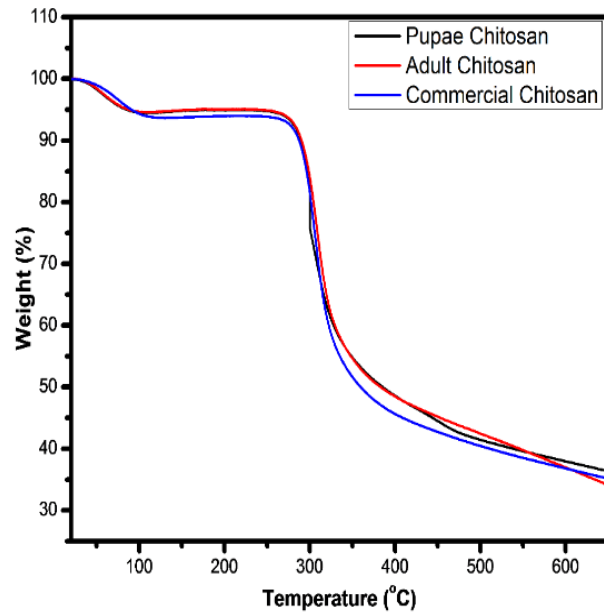
observed to be 394 °C for the commercial shrimp chitin, 392 °C for the adult BSF-chitin and 384 °C for the pupae shells-chitin (Figure 4.5), indicative of alpha chitin.

The profile of high weight loss above 250 °C and a sharp gradient decrease indicates the loss of organic matter with the remaining weight being the residue comprising mainly of carbon. The residue left in the case of commercial shrimp chitin was 21% and for pupae shells-chitin it was 22% (Table 4.7). The adult BSF-chitin had about 25% residue remaining, which was about 3% more than the pupae shells-chitin and the commercial shrimp chitin. (Table 4.7). The difference might be due to the additional components present in the adult BSF-chitin (legs, wings and antenna) which contain carbon (Kaya *et al.*, 2016) and this is in agreement with elemental analysis results or it could be due to residual inorganic components.

Similar findings revealed weight losses in chitins isolated from organisms such as crab, krill, shrimp, crayfish, grasshopper and potato beetle in two major steps in the range of 30-650 °C, which is consistent with this study (Kaya *et al.*, 2016; Waśko *et al.*, 2016; Kaya *et al.*, 2017). Moreover, previous studies showed that the DTG_{max} values of α -chitins ranged between 350 and 390 °C (Sajomsang & Gonil, 2010; Kaya *et al.*, 2016; Waśko *et al.*, 2016) and beta chitin value is approximately 270-300 °C (Kaya *et al.*, 2017), this is due to its antiparallel alignment with the adjacent polymer chains that are able to form more hydrogen bonds. The DTG_{max} values of the chitin from the commercial shrimp, pupae shells and adult BSF thus reveal that they are in the alpha form and this is in agreement with the FTIR and XRD analysis. The commercial chitin was slightly more thermally stable followed by the adult BSF-chitin and pupae shells-chitin. The adult BSF-chitin had a slight higher DTG_{max} value than the pupae shells-chitin, indicating that the adult BSF-chitin is slightly more thermally stable than the pupae shells-chitin. Similar results was reported by Kaya *et al.* (2014), where it was noted that the thermal stability of chitin from adult potato beetle (DTG_{max}: 379 °C) was much higher than that of the chitin from larvae (DTG_{max}: 307 °C). Sclerotisation is the major factor affecting the mechanical properties and stability of insect cuticles (Andersen, 2010). The difference in thermal stability between adult BSF-chitin and pupae shells-chitin in terms of thermal stability can be explained by the increased degree of cross linking depending on the higher degree of sclerotisation in the cuticle of adults. This study found that the thermal stability of adult BSF-chitin and pupae shell-chitin differs marginally between development stages of the *H. illucens* insect.

The TGA (A) and DTG (B) thermograms of chitosan obtained at optimum conditions from pupae shells, adult BSF, and commercial chitosan are presented in Figure 4.6 and Table 4.8.

A



B

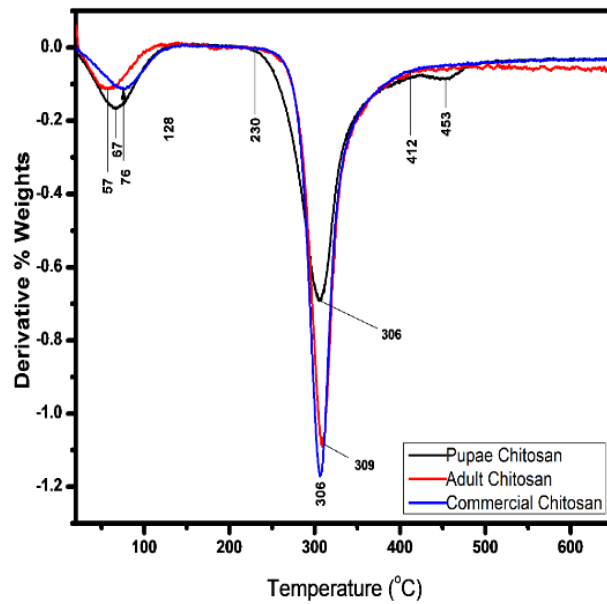


Figure 4.6: TGA (A) and DTG (B) thermograms of the extracted pupae shells-chitosan and adult BSF-chitosan compared to the commercial shrimp chitosan (Sigma Aldrich).

Table 4.8: Thermogravimetric results of commercial shrimp chitosan and chitosan extracted from pupae shells and adult BSF.

	Pupae shell-chitosan		Adult BSF-chitosan		Commercial chitosan	
First mass loss (%)	9	20-130 °C	5.7	20-130°C	6.8	20-130 °C
Second mass loss (%)	45.5	220-490 °C	44.8	220-490°C	50.3	220-490°C
Third mass loss (%)	4	453 °C	N/A		N/A	
Total mass loss (%)	54.5		50.5		57.1	
DTGmax(°C)	306		309		306	
Residue (%)	37		35		34	

In this study it was found that adult BSF-chitosan and commercial shrimp chitosan displayed two degradation steps (Figure 4.6 and Table 4.8). Meanwhile, the pupae shells-chitosan showed three degradation steps. The first degradation occurred in the range of 20 – 130 °C and is recognised as the evaporation of water molecules followed by the second stage of decomposition between 220 – 490 °C resulting in the degradation of saccharide structure of the chitosan molecules. In this study it was observed that commercial chitosan shows very similar degradation to pupae shells-chitosan and adult BSF-chitosan. The water loss in the first step was 9% for pupae shells-chitosan and 5.7% for adult BSF-chitosan, whereas it was 6.8% for the commercial chitosan. From the thermograph, it was evident that the pupae shells-chitosan contains more water within its structure hence the some what higher weight loss observed. Chitosan being a hygroscopic compound, absorbs moisture from the atmosphere when exposed hence the need for proper storage. This difference might have been due to incomplete drying of the processed sample before the characterisation. The second decomposition stage involves the determination of the thermal stability of the chitosan samples. From the derivative thermal graphs, it was observed that all the chitosan samples were stable up to 220 °C. In the second stage, the mass losses of the pupae shells-chitosan, adult BSF-chitosan and commercial chitosan were 45.5%, 44.8% and 50.3% respectively. The profile of weight loss and a sharp gradient decrease indicates the loss of organic matter from the thermal degradation in N₂ of the polymer structure.

In this study, the DTG_{max} values of pupae shells-chitosan and commercial chitosan were determined to be 306 °C, while the adult BSF-chitosan was 309 °C (Table. 4.8). Furthermore, the pupae shells-chitosan DTG curve displayed a third small peak at 453 °C with a mass loss of 4%. Similar results were reported with silkworm chrysalides and *Z. morio* (Paulino *et al.*, 2006; Soon *et al.*, 2018). Previous studies claimed that the third mass loss observed in pupae shells-chitosan corresponds to the residual cross-linked degradation of chitosan (Georgieva *et al.*, 2012) or also could be due to the degradation of D-glucosamine and N-acetyl glucosamine (Soon *et al.*, 2018). The pupae shells-chitosan had about 37% residue remaining, whereas adult BSF-chitosan and commercial chitosan had about 34% and 35%, respectively. The thermal stabilities of chitosans from pupae shells and adult BSF were similar to each other in this study.

Erdogan and Kaya (2016) reported that the mass loss in the second step, of chitosan *Dociostaurus maroccanus* nymph and adults, was 59% and 62% and the DTG_{max} value was 308 °C and 302 °C respectively. Likewise, the DTG_{max} value of chitosan from *Daphnia longispina* resting eggs was determined to be 303 °C (Kaya *et al.*, 2014). The DTG_{max} values found in this study were similar to those given in the literature. It was reported that the thermal stability of adult potato beetle chitosan (DTG_{max}: 289 °C) was slightly lower than that of larvae (DTG_{max}: 292 °C) (Kaya *et al.*, 2014).

Considering the results of this study it was found the thermal degradation temperature of chitosan was lower than that of chitin due to its amine group which has a lower polarity than chitin's amide group with comparatively higher polarity. The reason that the thermal stability of the chitosan is lower than chitin could also be because the deacetylated chitosan molecule is easier to decompose. The chitins and chitosans from pupae shells and adult BSF differ slightly in terms of their TGA analysis. Thermostability of chitin and chitosan is one of the most important properties because thermostable polymers have application in extreme biomimetics (Wysokowski *et al.*, 2015).

4.7 XRD analysis

XRD analysis was applied to detect the crystallinity of chitin and chitosan from pupae shells and adult BSF obtained at optimum conditions was compared to commercial shrimp chitin and chitosan. The x-ray diffraction patterns was obtained on a Bruker AXS D8 Advance diffractometer and were recorded at 40 kV, 30 mA and 2θ (experimental details in chapter 3, section 3.6.4). The x-ray diffraction patterns of the obtained pupae shells-chitin; adult BSF-chitin and commercial shrimp chitin are present in Figure 4.7 and Table 4.9.

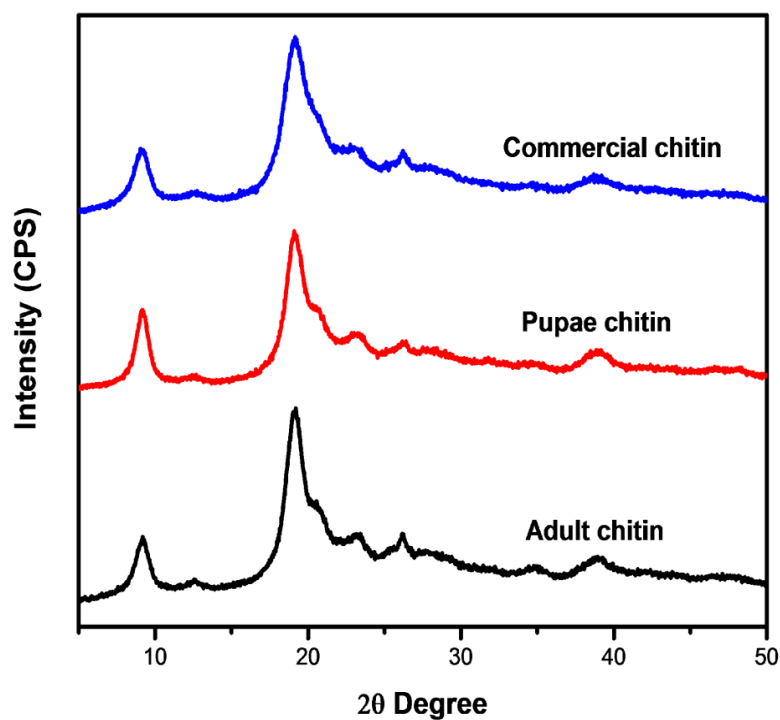


Figure 4.7: X-ray Diffractograms of the extracted adult BSF-chitin and pupae shells-chitin compared to the commercial shrimp chitin (Sigma Aldrich).

Table 4.9: X-ray diffraction data of commercial shrimp chitin and chitins isolated from pupae shells and adult BFS.

Sample	XRD peaks at 2 θ	CrI (%)
Pupae shells-chitin	9.2, 19.2, 23.0, 26.3, and 38.3 $^{\circ}$	50.3
Adult BSF-chitin	9.2, 19.2, 23.4, 26.2, and 38.4 $^{\circ}$	49.6
Commercial chitin	9.2, 19.3, 23.1, 26.4, and 38.5 $^{\circ}$	60.1

The results of the XRD of chitin extracted from the pupae shells and adult BSF with the commercial chitin, scanned at 2 θ , and between 5 and 50 $^{\circ}$ shows a total of five crystalline peaks at 9.2, 19.3, 23.1, 26.4 and 38.5 $^{\circ}$ for pupae shells-chitin, 9.2, 19.2, 23.4, 26.2, and 38.4 $^{\circ}$ for adult BSF-chitin and 9.2, 19.2, 23.0, 26.3, and 38.3 $^{\circ}$ for commercial shrimp chitin (Figure 4.7 and Table 4.9).

Two sharp peaks at approximately 9.2 $^{\circ}$ and 19.3 $^{\circ}$ (pupae shells-chitin, 9.2 $^{\circ}$ and 19.2 $^{\circ}$ (adult BSF-chitin) and, 9.2 $^{\circ}$ and 19.2 $^{\circ}$ (commercial shrimp chitin) were observed and three broad but less intense peaks at approximately 23.1 $^{\circ}$, 26.4 $^{\circ}$ and 38.5 $^{\circ}$ (pupae shells-chitin), 23.4 $^{\circ}$, 26.2 $^{\circ}$ and 38.4 $^{\circ}$ (adult BSF-chitin) and, 23.0 $^{\circ}$, 26.3 $^{\circ}$ and 38.3 $^{\circ}$ (commercial shrimp chitin) were observed (Figure 4.7 and Table. 4.9). It has been revealed in previous studies that the crystallinity index (CrI) values of chitin vary between 47% and 91%, depending on the species, the method of isolation and calculation (Liu *et al.*, 2012). In this study, the chitin from pupae shells and adult BSF shows a CrI (equation 1 in chapter 2, section 2.11.2) value of 50.3% and 49.6%, while commercial shrimp chitin has a CrI of 60.1% (Table 4.9).

Consistent with this study, previous studies reported that α -chitin has two characteristic sharp peaks at 9 $^{\circ}$ and 19 $^{\circ}$ (Erdogan *et al.*, 2017), while four other weak peaks were observed at 12 $^{\circ}$, 21 $^{\circ}$, 23 $^{\circ}$ and 26 $^{\circ}$ (Liu *et al.*, 2012; Sajomsang & Gonil, 2010). The peaks observed in this study are suggestive of α -chitin also produced from shrimp, crab, potato beetle and grasshopper (Kaya *et al.*, 2014; Kaya *et al.*, 2015; Erdogan & Kaya, 2016; Kaya *et al.*, 2017). The peaks at 9.2 $^{\circ}$ -38.5 $^{\circ}$ observed for pupae shells-chitin, adult BSF-chitin and commercial shrimp chitin were

similar to the report of Kaya et al. (2017). The CrI values of chitin and its derivatives play a major role in the determination and effectiveness of their application (Aranaz *et al.*, 2009). In this study, the CrI of commercial chitin (60.1%) differed to adult BSF-chitin (49.6%) and pupae shells-chitin (50.3%). The findings in this study are consistent with crystallinity obtained in chitin from larvae cuticles (54%) and silkworm pupae exuviae (*Bombyx mori*) (Zhang *et al.*, 2000). Furthermore, Abdou et al. (2008) measured the CrI values for chitins extracted from brown shrimp, pink shrimp, crab and crayfish as 64%, 66.6%, 59.86% and 56.94%, respectively (Abdou *et al.*, 2008). However, this is inconsistent with other insects: *Holotrichia parallela* (89.05%) and cicada sloughs (89.7%) (Liu *et al.*, 2012). In addition, the CrI values of chitins extracted from grasshopper were reported as 71% for adult and 74% for nymph (Erdogan & Kaya, 2016). This may be as a result of the difference in species, the method of chitin extraction and the purity of the chitin used. It has been speculated that the high MW compound catechol that is left in the cricket chitin may be responsible for the high crystallinity (Liu *et al.*, 2012). In this study, the fairly low CrI values of pupae shells-chitin and adult BSF-chitin were similar to those reported by Waśko et al. (2016), which is advantageous in adsorption studies. Aranaz et al. (2009) reported that chitin with low crystallinity is desirable in toxic metal removal by providing low diffusion resistance in adsorption applications (Aranaz *et al.*, 2009).

The x-ray diffraction patterns of the chitosan synthesised from pupae shells and adult BSF obtained from optimum conditions compared to commercial shrimp chitosan are depicted in Figure 4.8.

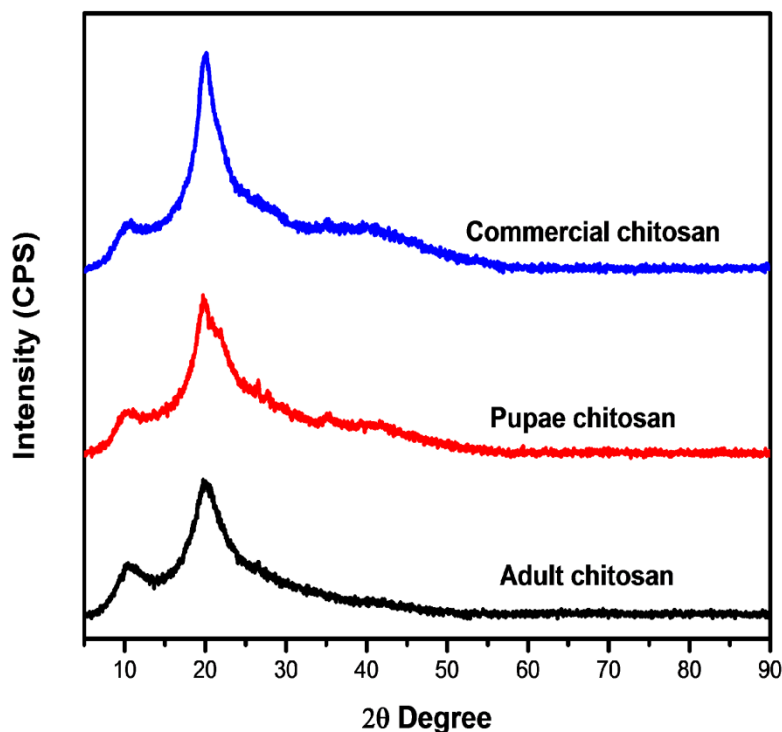


Figure 4.8: X-ray Diffractograms of the extracted adult BSF-chitosan and pupae shells-chitosan compared to the commercial shrimp chitosan (Sigma Aldrich).

The XRD spectra of chitosan extracted from the pupae shells and adult BSF scanned at 2θ , and between 5 and 90° show a total of two strong peaks. These peaks were approximately at 10.4° and 20.3° 2θ for adult BSF-chitosan, 10.2° and 20.2° 2θ for chitosan from pupae shells and around 10.3° and 20.2° 2θ for commercial chitosan (Figure. 4.8). The first peak is assigned to N-acetyl-D-glucosamine sequences (Glc-NAc) and the second peak to the sequences N-glucosamine (GlcN) in the polymer chain, respectively. In this study, the chitosan from pupae shells and adult BSF showed a CrI (equation 1 in chapter 2, section 2.11.2) value of 69% and 52%, while commercial shrimp chitosan had a CrI of 73%.

Two sharp peaks characteristic of chitosan at approximately 9° - 11° and 19° - 21° are consistent with this current study and this is in agreement with the reports of Yen et al. (2009); Kaya, (2015); Kaya et al. (2015); Ahing & Wid (2016). The findings of Erdogan and Kaya (2016) who reported the two peaks at around 10.76° and 20.30° for nymph chitosan and around 10.96° and

20.14° for adult chitosan were similar to this study. This does, however, differ from the work of Zaku et al. (2011) which showed that the XRD of chitosan from fish had crystalline reflections at 14.4°, 20.0°, 26.7°, 37.3° and 54.3°. The CrI values found in this study were inconsistent with the reported values of commercial chitosan, shrimp, crab and fish chitosan that were found to be 96, 82, 88 and 84% respectively (Kumari *et al.*, 2017). Kaya et al. (2014) and Liu et al. (2012) have estimated the CrI values of chitosan isolated from sources such as crab and insects to be in the range of 54 and 91% (Kaya *et al.*, 2014; Liu *et al.*, 2012).

Considering the results found in this study both pupae shells and adult BSF chitin and chitosan samples are crystalline in nature. When also considering the results of these studies, it can be concluded that the crystallinity of α -chitins and chitosan does not change significantly between different developmental stages such as the pupae shells and adult BSF. The results of this study suggested that N-deacetylation and purification did not alter the natural crystallinity of pupae shells and adult BSF chitosan.

4.8 Determination of the optimum chitosan's molecular weight

The chitosan's molecular weight obtained at optimum conditions was measured by using an Ubbelohde viscometer at 25 °C (experimental details in chapter 3, section 3.7). The molecular weight of the chitosan samples was determined using the Mark-Houwink equation (equation 9 in chapter 3, section 3.7). Intrinsic viscosity of chitosan is the function of the degree of ionisation as well as ionic strength (Hossain & Iqbal, 2014). The average molecular weight (MW), intrinsic viscosity and Mark-Houwink constants are shown in Table 4.10.

Table 4.10: Intrinsic viscosity, Mark-Houwink constants and average molecular weight of pupae shells-chitosan, adult BSF-chitosan and commercial shrimp-chitosan.

Sample	$[\eta]$ (mL/g)	K (mL/g)	a	MW (Da)
Pupae shells-chitosan	865	0.076	0.76	217 324
Adult BSF-chitosan	860	0.076	0.76	215 673
Commercial shrimp-chitosan	790	0.076	0.76	192 877

K= is a constant which is dependent on a given polymer type; a= is a constant which depends on the chosen solvent.

The MW of chitosan can range from 100 kDa to thousands of kDa, depending on the degradation of the chain that occurs during the production process (Lemma *et al.*, 2016). In this study, the 217 324 Da/217 kDa of pupae shells-chitosan and 215 673 Da/216 kDa of adult BSF-chitosan exhibited a higher average MW than commercial shrimp chitosan (192 877 Da/193 kDa) (Table 4.10). This finding can be explained by the use of a 70% NaOH concentration and the long reaction time of 5 h needed during the deacetylation process, which causes chain degradation and results in the chitosan having lower MW. In contrast, Weska *et al.* (2007) observed that optimum conditions for the deacetylation stage were 130 °C, 90 min, and a 45% NaOH, which yielded a low MW of 150 kDa. Yen *et al.* (2009) reported that crab chitin treated with 40% NaOH at 105 °C for 60, 90 and 120 min resulted in an average MW of chitosan of 526, 513 and 483 kDa, respectively that decreased as the deacetylation time was prolonged. In comparison the best optimum conditions obtained in this study was 70% NaOH, for 5 h at 100 °C. It is however clear that the average MW of chitosan varied according to different applied process conditions.

Results presented in this section showed a lower MW than that reported for some crustacean groups, such as *Artemia* and crab shells (450-570 kDa and 483-526 kDa), although the results were in agreement with the honeybee chitosan (200-250 kDa) (Nemtsev *et al.*, 2004; Tajik *et al.*, 2008; Yen *et al.*, 2009). Some products were found to have lower MW, such as shrimp (2.20 kDa), grasshoppers (7.2 kDa for the adults and 5.6 kDa for the nymphs) and potato beetles

(2.722 kDa for adult and 2.676 kDa for larvae) (Erdogan & Kaya, 2016; Kaya *et al.*, 2014; Kucukgulmez *et al.*, 2011). Previous studies agreed that a low MW is between 50 000 and 190 000 Da, a medium MW is between 190 000 and 310 000 Da and a high MW is between 310 000 and 375 000 Da. Regarding the results of this study, it can be concluded that the chitosans extracted from pupae shells and adult BSF had a medium MW (Mishra, n.d.).

The MW is one of the important factors affecting the physiochemical and functional properties of chitosan and it determines the application areas of chitosan. According to Erdogan & Kaya (2016) chitosan with low MW was useful in medical and agricultural applications. Moreover, in another review study it was reported that low MW chitosan was also commonly used in areas such as gene transfer, wound healing and food protection (Aranaz *et al.*, 2009). In addition, chitosan having a medium MW turned out to have higher anti-cholesterol activity than that of high MW chitosan (Kumari *et al.*, 2017). This study revealed that the chitosans are of a medium MW and thus can be evaluated for use in those application areas. Considering the results found in this study compared with the results found in literature the average MW of chitosan varies according to the chitosan source and the chitosan preparation method.

This is the first study to explain the differences in the physiochemical properties of chitin and chitosan obtained from pupae shells and adult BSF. The physiochemical properties of chitin and chitosan biopolymers are the most important factors determining their use in various fields and according to the results found in this study there were only small differences in physiochemical properties between the different metamorphous development stages of pupae shells and adult BSF. Hence, it is possible to extract chitin from such sources and determine its physiochemical properties to expand the use of chitin and chitosan in different application areas.

4.9 Electrospinning of chitosan nanofibers

The following parameters were examined in this study: determination of electrospinnability of the fibers by optimising the chitosan concentration including various process parameters. Electrospinning of the commercial shrimp chitosan at 3, 5, 6 and 8 wt% solution in 90% TFA solution was optimised for the fabrication of fibers by varying the applied voltage (between 20,

22 and 25 kV), flow rate (between 0.06, 0.08 and 0.1 mL/h) and collection distance (between 7, 10 and 12 cm) (experimental details in chapter 3, section 3.5). A number of experiments were carried out to determine the optimum processing conditions in order to fabricate nanofibrous mats. Determination of morphology and size of fibers was obtained using SEM, determination of structural interaction was obtained using FTIR, determination of crystallinity of fibers was obtained using XRD and determination of thermal degradation of obtained fibers was performed using TGA analysis.

4.9.1 The optimisation of chitosan nanofibers

In this study, different concentrations of the commercial shrimp chitosan were optimised including the applied voltage, flow rate and tip to collector distance to control the fabrication, formation, morphology and diameter of chitosan nanofibers. The optimisation of the electrospun chitosan nanofiber mats were observed using a Nova NanoSEM 230 and EVOLS 10 ZEISS Auriga scanning electron microscope (experimental details in chapter 3, section 3.6.5).

4.9.1.1 Effect of applied voltage and flow rate

SEM images of Figure 4.9 show the effect of electrical field voltage on the structure of electrospun nanofibers prepared from commercial shrimp chitosan at different voltages under the following applied conditions of 5 wt% of commercial chitosan in TFA, a flow rate of 0.1 mL/h and 10 cm tip to collector distance.

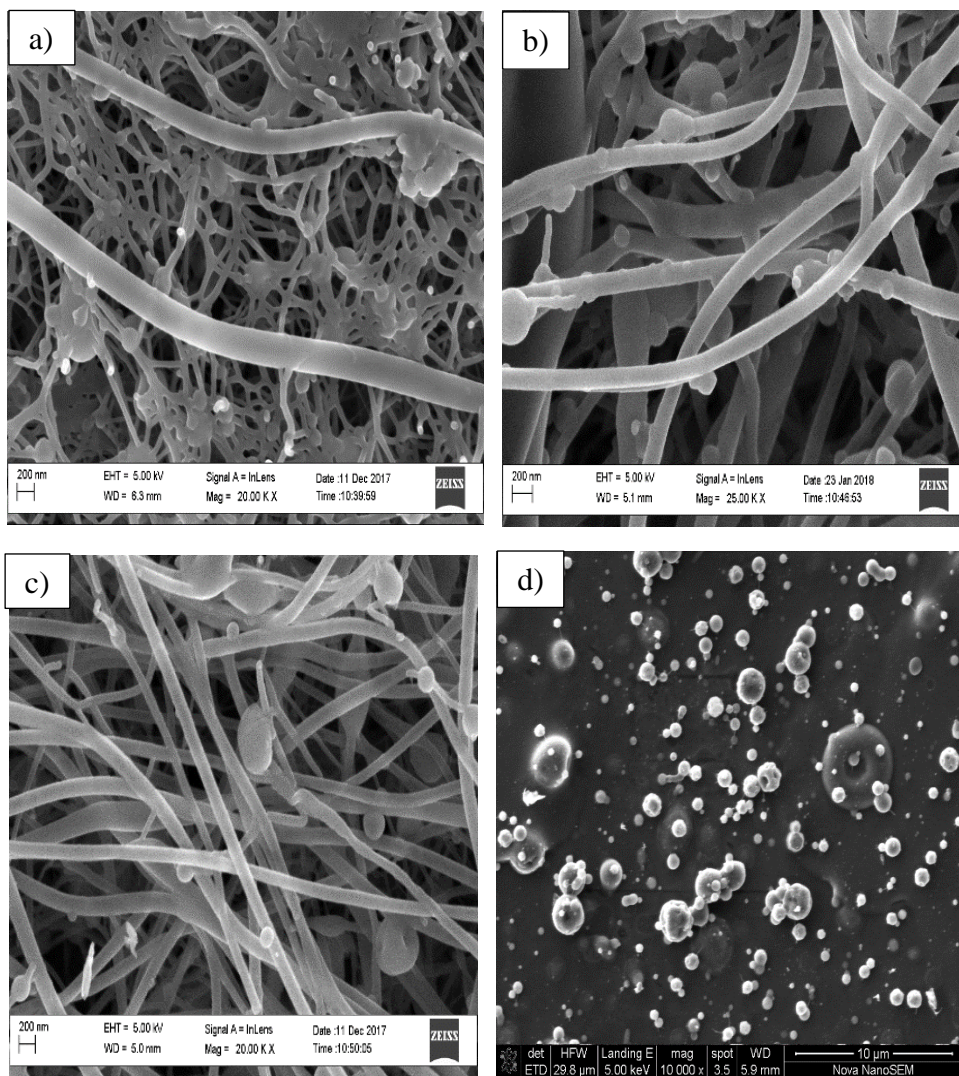


Figure 4.9: SEM micrographic images depicting the differences in voltage of commercial chitosan nanofibers: 20 kV (a), 22 kV (b), 25 kV (c) and >25 kV (d). In all experiments 5 wt% of commercial chitosan in TFA, a flow rate of 0.1 mL/h and 10 cm tip to collector distance were used.

In this study it was noticed that an increase in the applied voltage ($20\text{ kV} < 22\text{ kV} < 25\text{ kV}$) resulted in a reduction of the formation of beads and a finer nanofiber diameter (Figure 4.9a-c).

An increase in voltage resulted in a reduction of beads and microspheres with the formation of non-uniform nanofibers for commercial chitosan nanofibers (Figure 4.9). The voltage at 25 kV (Figure 4.9c) led to greater stretching of the solution due to the greater coulombic forces in the jet as well as due to the stronger electric field (Homayoni *et al.*, 2009; Mazoochi & Jabbari,

2011; Pakravan *et al.*, 2012). Given the increased stretching of the jet due to the higher voltage, there was less bead formation observed for commercial chitosan nanofiber. The decrease in number and size of beads and microspheres with increase in the voltage might be referred to the surface tension of polymer solutions; higher voltage overcome the surface tension of the polymer solution and initiated jet formation.

SEM images of Figure 4.10 show the effect of flow rate on the structure of electrospun nanofibers prepared from commercial shrimp chitosan at different flow rates under the following applied conditions of 5 wt% of commercial chitosan in TFA, a voltage of 25 kV and 10 cm tip to collector distance.

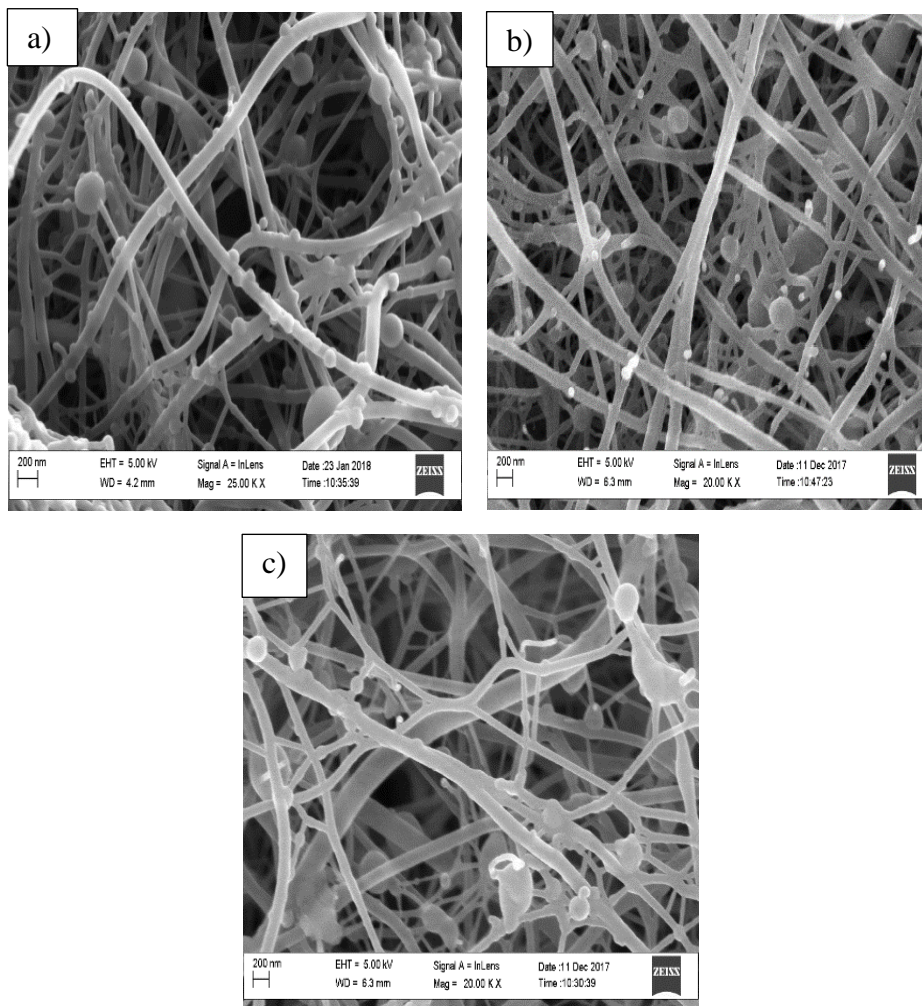


Figure 4.10: SEM micrographic images depicting the differences in electrospinning flow rate of commercial chitosan nanofibers: 0.06 mL/h (a), 0.08 mL/h (b) and 0.1 mL/h (c). In all experiments 5 wt% of commercial chitosan in TFA, a voltage of 25 kV and 10 cm tip to collector distance were used.

A slow flow rate of 0.06 mL/h (Figure 4.10a) and 0.08 mL/h (Figure 4.10b) resulted in the formation of the Taylor's cone and an unsteady jet resulting in the formation of fibers, beads and microspheres because the rate of passage of the solution through the tip of the needle was very low, however, at a higher speed of 0.1 mL/h (Figure 4.10c) more uniform fibers with less formation of microspheres and beads were obtained.

The SEM results obtained in this study showed that the uniformity of the chitosan nanofibers improved and less bead and microspheres formation was visible at an increased voltage (25 kV)

and flow rate (0.1 mL/h) (see Figure 4.9c and Figure 4.10c). As shown in these figures, increasing the applied voltage and flow rate not only decreased and refined nanofibers diameters, but also improved the quality of electrospun nanofibers. These results are consistent with results in other studies on chitosan from shrimp using a high flow rate and high voltage (Bhardwaj & Kundu, 2010; Pakravan *et al.*, 2012).

Regarding the applied voltages studied, it should be mentioned that chitosan is difficult to electrospin into a fibrous structure due to its polycationic character in an acidic aqueous solution and to the numerous amino groups in its backbone. The protonation of commercial chitosan amine groups greatly contributes to its partial solubility. Its polycationic nature thus excessively increased the surface tension of the solution resulting in a viscous solution. High electrical force was thus required to produce chitosan nanofibers, however small droplets that became particles were formed easily for commercial chitosan, which resulted from the electrospaying process (at >25 kV) (Figure 4.9d), likely due to the repulsive forces between ionic groups in the chitosan backbone in the acidic solution.

4.9.1.2 Effect of tip-to-collector distance

The SEM images of Figure 4.11 show the effect of tip-to-collector distance on the structure of electrospun nanofibers prepared from commercial shrimp chitosan at different tip to collector distance under the following applied conditions of 5 wt% of commercial chitosan in TFA, a flow rate of 0.1 mL/h and a voltage of 25 kV.

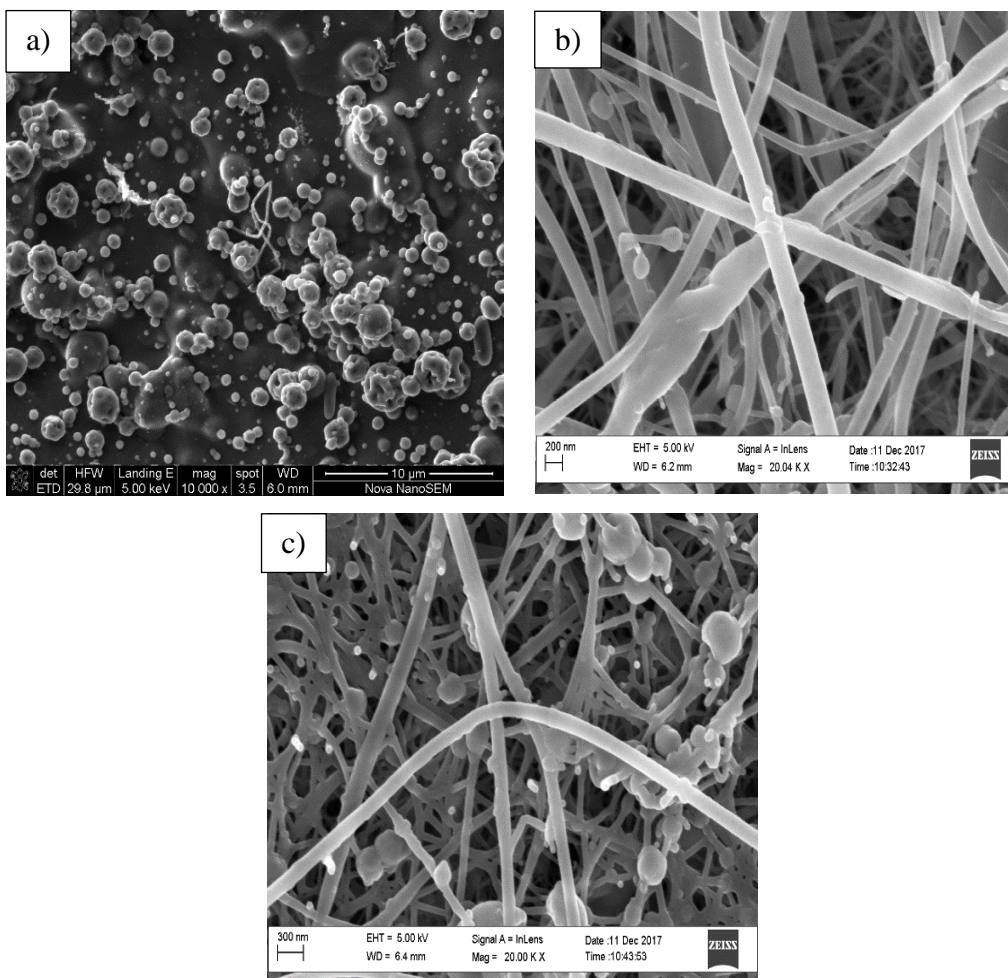


Figure 4.11: SEM micrographic images depicting the differences in tip-to-collector distance during electrospinning of commercial chitosan nanofibers: 7 cm (a), 10 cm (b) and 12 cm (c). In all experiments 5 wt% of commercial chitosan in TFA, a voltage of 25 kV and a flow rate of 0.1 mL/h were used.

When the collector distance was 7 cm (Figure 4.11a), the distance between the tip of the needle to the collector was too short and the instability of the jet increased and the spinning solution could not be fully stretched, resulting in the formations of droplets and the formation of microspheres and beads. At 10 cm (Figure 4.11b) nanofibers were obtained with formation of fewer beads and microspheres. However, when the tip to collector distance was 12 cm (Figure 4.11c), the strength of the electric field became too weak so that the fiber diameter decreased and formation of beads increased. When the distance was 10 cm (Figure 4.11b), the distance was large enough to allow evaporation of the solvent during the course of the travel of the solution

which resulted in less formation of microspheres and less beads. This result was consistent with results found in other studies (Mazoochi & Jabbari, 2011; Sangsanoh & Supaphol, 2006).

4.9.1.3 Effect of concentration on chitosan nanofibers

After the optimum voltage, flow rate and tip to collector distance were obtained, the optimum concentration of commercial chitosan in TFA as solvent was examined at 3, 5, 6 and 8 wt% (Figure 4.12) prepared under the following applied conditions of a voltage of 25 kV, a flow rate of 0.1 mL/h and 10 cm tip to collector distance (the experimental details are in chapter 3 of section 3.5).

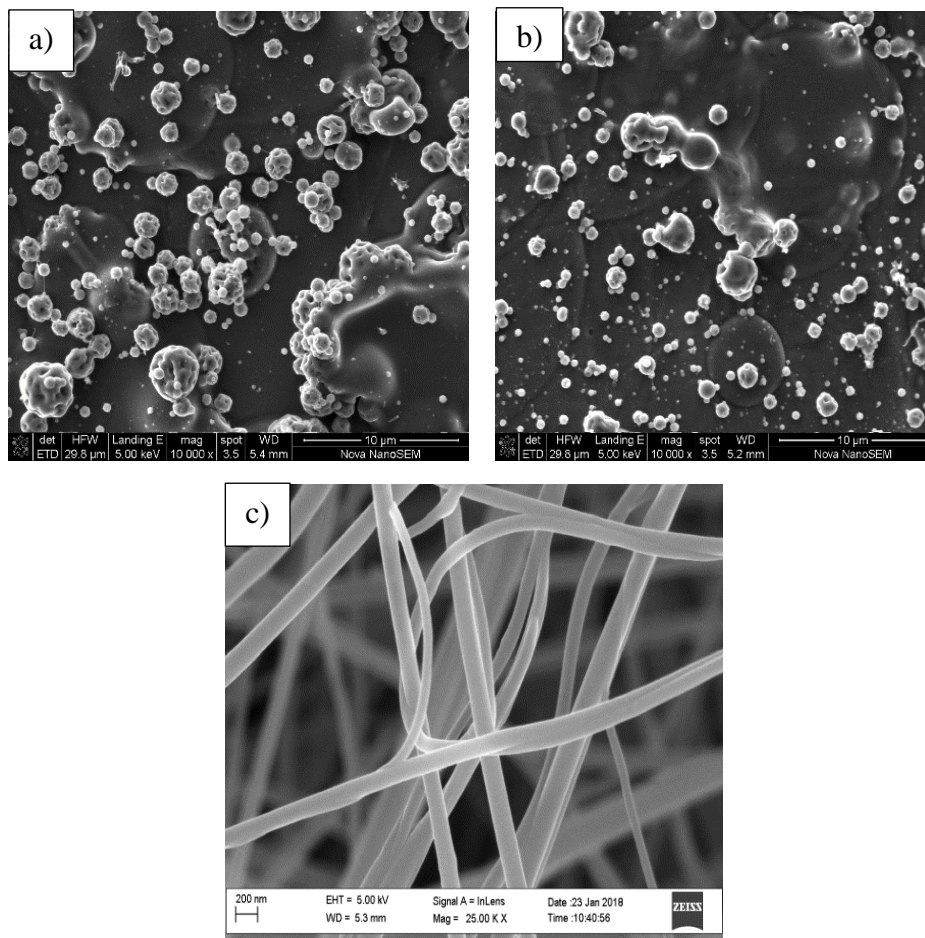


Figure 4.12: SEM micrographic images depicting the differences in solution concentration used to prepare commercial chitosan nanofibers: 3 wt% (a), 5 wt% (b) and 6 wt% (c). In all experiments a voltage of 25 kV, a flow rate of 0.1 mL/h and 10 cm tip to collector distance were used.

In the case of 3 wt% (Figure 4.12a) and 5 wt% (Figure 4.12b) of commercial shrimp chitosan concentrations in TFA, the SEM micrographs of the commercial shrimp chitosan obtained after spinning showed no electrospun nanofibers with only the formation of beads and microspheres with the average particle sizes in the range 0.3-10 μM . The presence of microspheres and beads might be attributed to the low chitosan concentration in TFA and this resulted in the electrospinning process under the applied conditions. The concentration was too low to initiate a high degree of entanglement during solvent evaporation in the jet. This entanglement is needed for fiber formation and locally the charge density increased due to solvent evaporation. However, the decrease in the number and size of beads and microspheres were observed with an increase in concentration which caused the concentration to overcome the surface tension of the chitosan solutions and the higher concentration allowed jet formation. Bead free electrospun nanofibers were obtained when the solution concentration was increased to 6 wt% (Figure 4.12c). The increase in the polymer concentration increased the viscosity of the solution to a critical value, therefore, eliminating the beads completely in the commercial nanofibrous mats. At 8 wt% concentration, no electrospinning was observed as the solution was too viscous which resulted in the drying of the drop at the needle tip.

The electrospinning parameters such as collector distance, applied voltage and flow rate optimised in this study had significantly affected the electrospinnability and the quality of the nanofibrous mats. The electrospinning process is initiated at the point at which the electrostatic force in a solution overcomes the surface tension of the solution. This required high concentration of 6 wt% chitosan (Figure 4.12c) in TFA and a high voltage of 25 kV (Figure 4.9c)), specifically, needing a strong electrical charge to accelerate the jet extension and cause a greater volume of solution to be drawn from the needle. Bead free electrospun nanofibers were obtained when the solution concentration was increased to 6 wt% and a high voltage of 25 kV, which might be attributed to the increased solution viscosity. Increase in the polymer concentration has increased the viscosity of the solution to a critical value, therefore, eliminating the beads completely. However the viscosity became too viscous at a higher chitosan to TFA concentration (8 wt%) which solution could not be electrospun. The higher voltage at 25 kV (Figure 4.9c) led to a greater stretching of the 6 wt% (Figure 4.12c) solution and directly affected

the electrospinnability and morphology of the electrospun chitosan nanofibers by a decrease in the formation of beads and microspheres. An increase in flow rate of 0.1 mL/h (Figure 4.10c) in turn increased nanofiber formation and lessened the formation of beads. Tip to collector distance of 10 cm (Figure 4.11b) had a direct influence on the jet flight time and electric field strength. A decrease in this distance shortened flight times and solvent evaporation times, and increased the electric field strength, which resulted in less bead and microspheres formation and a complete beadless network of nanofibers for commercial chitosan.

4.9.2 Characterisation of optimum chitosan nanofibers

Characterisation of the optimum chitosan nanofibrous mats made in this study was undertaken primarily to correlate test measurements of the useful properties of these materials and also to ensure consistent high quality of the product during manufacture. In general, there are a large number of different characterisation techniques that can be used for understanding the properties of nanofibers. In the following sections, selected characterisation tests based on several common expected uses of nanofiber materials are presented. The analysis of fiber chemical and physical structures, and stability of electrospun chitosan nanofibrous mats are the most important properties in several application areas.

The nanofibers obtained at optimal conditions using a concentration of 6 wt% commercial chitosan in TFA, an applied voltage of 25 kV with a polymeric flow rate of 0.1 mL/h and tip to collector distance of 10 cm were further characterised.

4.9.2.1 Morphology and size distribution of optimised chitosan nanofibers

SEM analysis was performed on the optimised fibers to determine the surface morphologies of the electrospun commercial shrimp chitosan nanofibrous mats. The morphology of nanofibrous mats were examined by a scanning electron microscope. Prior to the SEM analysis, the nanofibrous mat samples were coated with carbon (experimental details in chapter 3, section 3.6.5). From the SEM micrographs for each sample, approximately 50 individual diameters obtained to calculate the average fiber diameters. The SEM micrographs and corresponding

histogram of the electrospun nanofiber at optimised conditions (6 wt%, 25 kV, 0.1 mL/h and 10 cm) are displayed in Figure 4.13 at different magnifications.

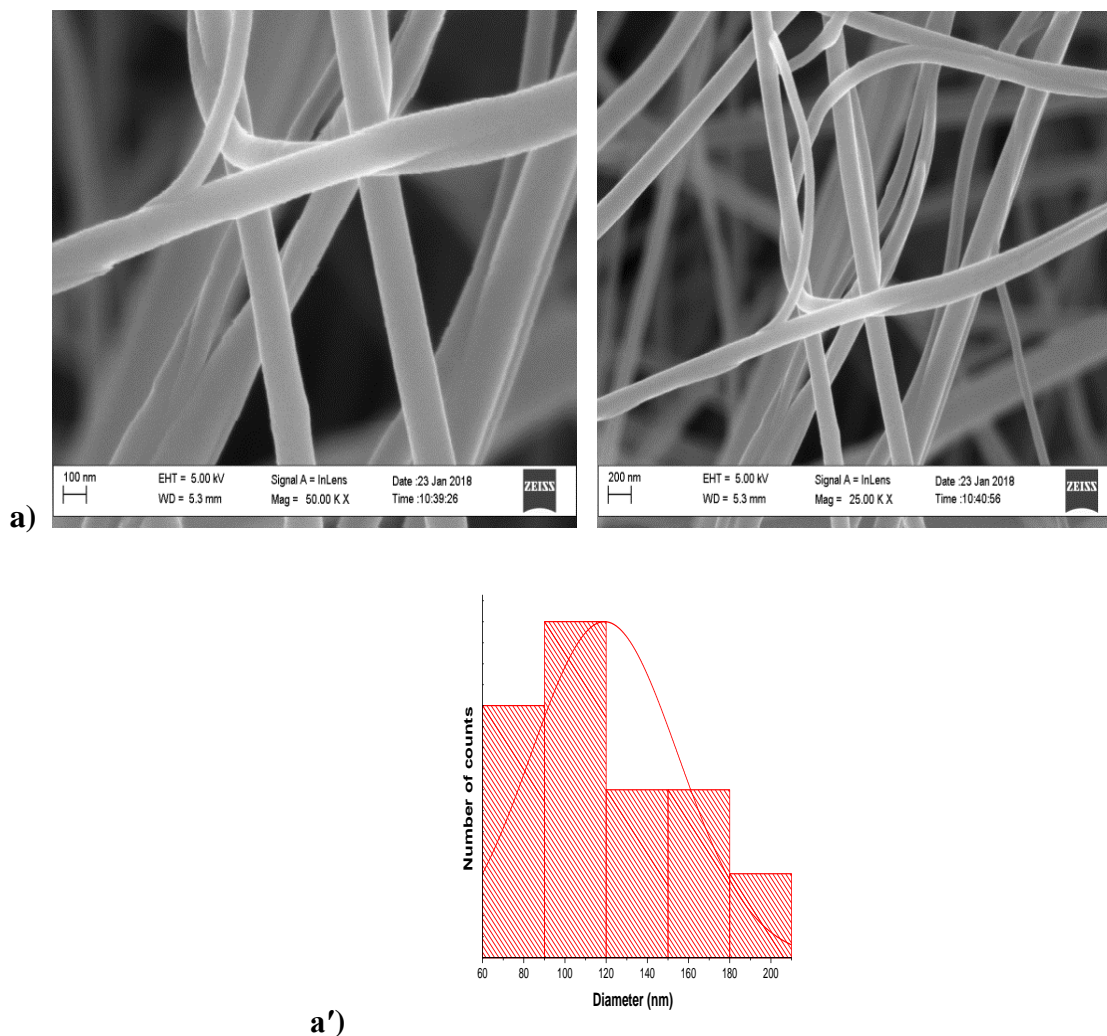


Figure 4.13: SEM micrographs (a) and the corresponding histogram (a') of the commercial chitosan nanofibers at optimised electrospinning conditions (6 wt% commercial chitosan in TFA, a voltage of 25 kV, a flow rate of 0.1 mL/h and 10 cm tip to collector distance).

As shown in the SEM micrographs (a) and the corresponding histogram (a') (Figure 4.13), fiber morphology for commercial chitosan nanofibers had a regular morphology, thus the fibers had a more uniform cross-section, with some small variations in fiber diameter (Figure 4.13a&a'). As shown in Figure 4.13, at the optimum conditions, not only was there a decrease in the formation of beads and nanofibers diameters, but also an improved quality of the electrospun nanofiber. In

addition, as the chitosan concentration increased, it was found that viscosity increased by visual appearance, fiber stretching became more difficult, and as a consequence, thick fibers were produced with broader fiber diameter distribution. One likely explanation is that a balance must be achieved between solution viscosity and the fiber-forming forces of the chitosan that are derived from the velocity of solution exiting the nozzle in order to produce nanofibers with regular cross-sections. For higher viscosity polymer solutions, nanofiber stretching became more difficult, less efficient and unstable giving rise to broader nanofiber diameter distribution and formation of beads. Visual inspection at 6 wt% chitosan in TFA compared to 8 wt% showed a less viscous consistency that could be attributed to the amino groups that caused stronger interchain interaction in 8 wt% solution and poor electrospinnability (Oliveira *et al.*, 2013). As observed in the histogram the diameters of the optimum nanofibers obtained at 6 wt% were in a range of 60-200 nm (average 130 nm) (Figure 4.13a'), whereas 8 wt% was too viscous to spin. The decrease in the average diameter of the nanofibers might be due to the larger electrostatic stretching force, which resulted in the jet acceleration and stretching in the electric field, thereby favouring thinner fiber formation.

The wt% concentration of chitosan in TFA and the applied voltage were found to be the parameters that most influenced the properties of commercial chitosan solution which subsequently affected the viscosity, surface tension and spinnability during the electrospinning process. This indicates that the repulsive forces between ionic groups in the chitosan backbone obstructed the formation of continuous nanofibers during the electrospinning process. Therefore, the electrospinnability, morphology and diameter of the electrospun commercial chitosan nanofibrous mats were significantly affected by the viscosity and surface tension of the solution.

In contrast, De Vrieze *et al.* (2007) obtained good-quality beadless chitosan (shrimp) nanofibers at voltage of 20 kV, a distance between capillary tip and collector of 10 cm and a flow rate of 0.3 mL/h. Kaya *et al.* (2016) on the other hand successfully produced nanofibers with an average diameter of 40 ± 12.35 nm electrospun from *Drosophila melanogaster* at their conditions of 80% acetic acid, a voltage of 24 kV, 16 cm tip to collector distance and a flow rate of 0.3 mL/h. Slightly lower diameter nanofibers were obtained from commercial shrimp chitosan in this study (60-200 nm) compared to the nanofibers (330-610 nm) produced by Ohkawa *et al.* (2004). In

addition, a study reported lower diameters for nanofibers produced from shrimp chitosan of 74 ± 28.77 nm at a voltage of 26 kV, a flow rate of 1.2 mL/h and 6.4 cm tip to collector distance (Schiffman & Schauer, 2007a).

Production of regular electrospun nanofibers from pure chitosan solutions is known to be challenging. Due to this, chitosan blends were used by others for example blends with synthetic polymers to enhance the spinnability of different MW chitosans in a common solvent. The chitosan MW from which nanofibers have been obtained varies from 85 kDa (Pakravan *et al.*, 2012) up to 570 kDa (Rieger *et al.*, 2016; Sangsanoh & Supaphol, 2006), however the optimum MW is often difficult to obtain precisely due to the presence of aggregates (Lemma *et al.*, 2016). The concentration used for electrospinning is directly related to the chitosan MW which determines the solution viscosity. It has been demonstrated that low MW (30 kDa) or higher MW (398 kDa) are not able to give good fibers in 90% acetic acid (Sun & Li, 2011). However, the low MW of 193 kDa of the commercial shrimp chitosan in this study was suitable to obtain beadless chitosan nanofibrous mats (see results in chapter 4 of section 4.8).

Overall, the results confirm that the optimal electrospinning process parameters had a significant effect on reducing the diameter of the fibers and also encouraged faster solvent evaporation to yield drier fibers with less bead formation. However, these results indicate that optimum electrospinning conditions to obtain beadless chitosan nanofibers largely depend on the properties of the polymer solutions and the process parameters.

These electrospun nanofibers produced in optimum conditions of 6 wt% of commercial chitosan in TFA, 25 kV applied voltage, 0.1 mL/h solution flow rate and 10 cm tip to collector distance were used to perform further physiochemical analyses.

4.9.2.2 Structural analysis of optimised chitosan nanofibers

FTIR spectroscopic analysis was used to evaluate the structural and compositional homogeneity and the spectral peaks corresponding to the stretching and vibration of various functional groups of the bulk commercial chitosan and electrospun chitosan nanofiber. FTIR spectra for bulk commercial chitosan and electrospun chitosan nanofibrous mat were measured using Perkin

Elmer Spectrum 100 FTIR spectrometer instrument. All spectra were taken in the spectral range of 4000 to 650 cm^{-1} by accumulation of 4 scans (experimental details given in chapter 3, section 3.6.2). FTIR spectroscopy was used to investigate changes of the functional groups that occur during the chitosan nanofibers via electrospinning. Figure 4.14 and Table 4.11 present the FTIR spectrum and band assignments of electrospun chitosan nanofiber made from bulk commercial shrimp chitosan and the bulk chitosan.

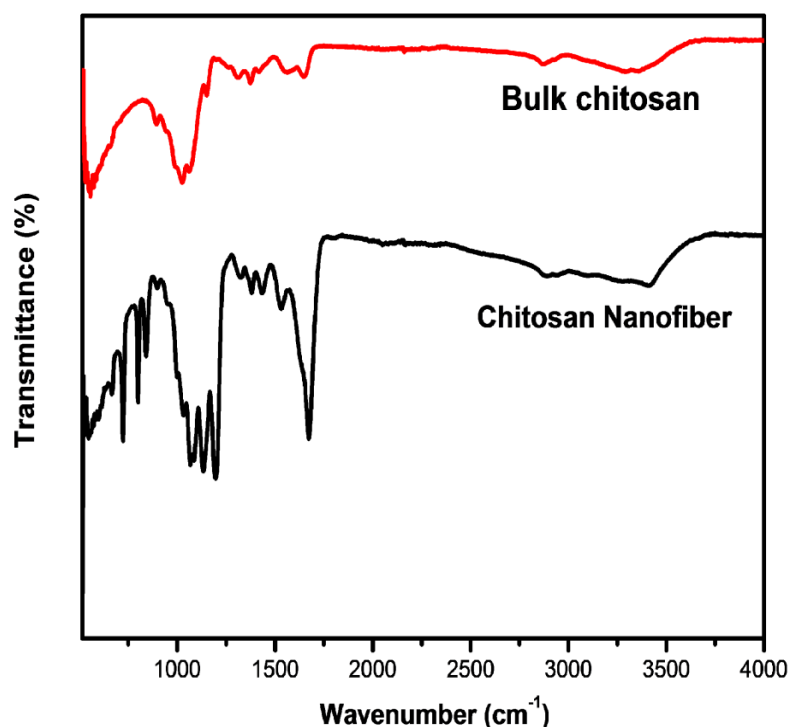


Figure 4.14: FTIR spectra of the nanofibrous mat fabricated from commercial chitosan at optimum conditions (6 wt% of commercial chitosan in TFA, 25 kV applied voltage, a flow rate of 0.1 mL/h and 10 cm tip to collector distance) compared to bulk commercial chitosan.

Table 4.11: The FTIR assignments of bands (cm^{-1}) of the commercial shrimp chitosan nanofibrous mat and bulk commercial chitosan.

Functional group and vibration modes	Commercial chitosan nanofiber	Chitosan
ν (NH_2) associated with primary amines and OH associated with pyranose ring	3412	3372
ν_{as} (CH_2) in CH_2OH group	-	3292
ν (C-H) in pyranose ring	2881	2881
ν (C=O) in NHCOCH_3 group (amide I band)	1677	1657
ν (NH_2) in NHCOCH_3 group (amide II band)	1526	1556
δ (CH_2) in CH_2OH group	1436	1426
δ_s (CH_3) in NHCOCH_3 group	1376	1376
δ (C-H) in pyranose ring	1326	1305
Complex vibrations of NHCO group (amide II band)	-	-
ν_s (C-O-C) (glycosidic linkage)	1195	1155
ν_{as} (C-O-C) (glycosidic linkage)	1135	1075
ν (C-O) in secondary OH group	1065	1025
ν (C-O) in primary OH group	-	-
Pyranose ring skeletal vibrations	894-724	894

For comparison, the measured FTIR spectrum of the bulk chitosan is shown in Figure 4.14 and Table 4.11. The commercial shrimp chitosan nanofibers exhibited a number of transmittance peaks at 1526 cm^{-1} , C-H stretching band at 2881 cm^{-1} , the bridge oxygen stretching band at 1376 cm^{-1} , and the C-O stretching bands at 1065 cm^{-1} (Nirmala *et al.*, 2011). The broad peak between 3500 and 3200 cm^{-1} corresponds to a stretching of OH group (Table 4.11). The intensity of amide I is larger than that of the amide II which is attributed to the resonance between the carbonyl stretching and the electric field of the incoming IR beam (Nirmala *et al.*, 2011). For the bulk commercial chitosan, the broad absorption in the range approximately at 3600 cm^{-1} to 3000 cm^{-1} was assigned to O-H and N-H stretching vibrations. The absorptions at 1657 cm^{-1} and 1556 cm^{-1} were attributed, respectively, to the amide I (C=O stretching) and amide II (C-N stretching and C-N-H bending vibrations) of amide functional groups in the solid state (Ibitoye *et al.*, 2018). A weaker amino characteristic peak at 1305 cm^{-1} is associated with C-H bending vibration and the peak at 1075 cm^{-1} is assigned to C-O-C stretching. The absorption band at 894

cm^{-1} is assigned to the saccharide structure (Ibitoye *et al.*, 2018). The electrospun commercial shrimp chitosan nanofibers can be divided into two main different groups of bands associated with N-H stretching, including NH_4^+ (bands at 1677 and 1526 cm^{-1}) and the C-O stretching of $\text{C}_2\text{F}_3\text{O}_2^-$ (bands at 1195, 1135, 1065, and 894 cm^{-1}) (Torres-Giner *et al.*, 2008). In addition, the electrospun nanofiber did not display a peak at 1790 cm^{-1} and 1786 cm^{-1} caused by TFA, indicating the absence of carboxylic acid, which indicates a complete evaporation of the TFA solvent. Additionally, the protonated amine groups remained constant in the electrospun chitosan nanofibers indicating a high degree of conformance between the bulk commercial chitosan and chitosan nanofiber. In the electrospinning process, there exists a rapid solvent evaporation as well as phase separation as the polymer solution jet is thinned (Schiffman & Schauer, 2007b). However, it is possible that, if the solvent utilised is not volatile enough for the chosen process parameters, some solvent will remain in the nanofibers post-electrospinning as observed by Schiffman and Schauer (2007b).

Overall, the results confirm that after the bulk commercial shrimp chitosan was electrospun into nanofibers, the chitosan fibers structure still exhibited the active NH_4^+ and $\text{C}_2\text{F}_3\text{O}_2^-$ groups. The findings in this study are in agreement with the results obtained by Torres *et al.* (2008), Mazoochi and Jabbari (2011) and Nirmala *et al.* (2011). In addition, Torres *et al.* (2008) also verified that the protonated groups and properties were successfully retained in the chitosan from crab shells after the electrospinning to nanofibers which still exhibited a very strong antimicrobial activity. In contrast, Schiffman and Schauer (2007b) observed that the bulk chitosan and electrospun chitosan nanofibers displayed a peak at 1790 cm^{-1} and 1786 cm^{-1} respectively, showing retention of TFA.

The results of the FTIR spectra of the commercial chitosan nanofiber compared to the bulk chitosan indicates the existence of the relevant functional groups of chitosan in the nanofibers. These results suggest that bulk chitosan was successfully configured into nanofibers. FTIR spectroscopy of the electrospun chitosan nanofiber also shows that the TFA solvent did not affect the chemical nature of the polymer during the electrospinning process; however it slightly intensified some absorption peaks.

4.9.2.3 Crystalline structure of the optimised chitosan nanofibers

XRD analysis was applied to detect the crystalline structure of the electrospun nanofiber made from bulk commercial shrimp chitosan compared to the bulk commercial chitosan. The x-ray diffraction patterns were obtained on a Bruker AXS D8 diffractometer and were recorded at 40kV, 30mA and 2θ (5-90) (experimental details in chapter 3, section 3.6.4). The diffractograms of the electrospun commercial chitosan nanofiber and the bulk commercial chitosan are depicted in Figure 4.15.

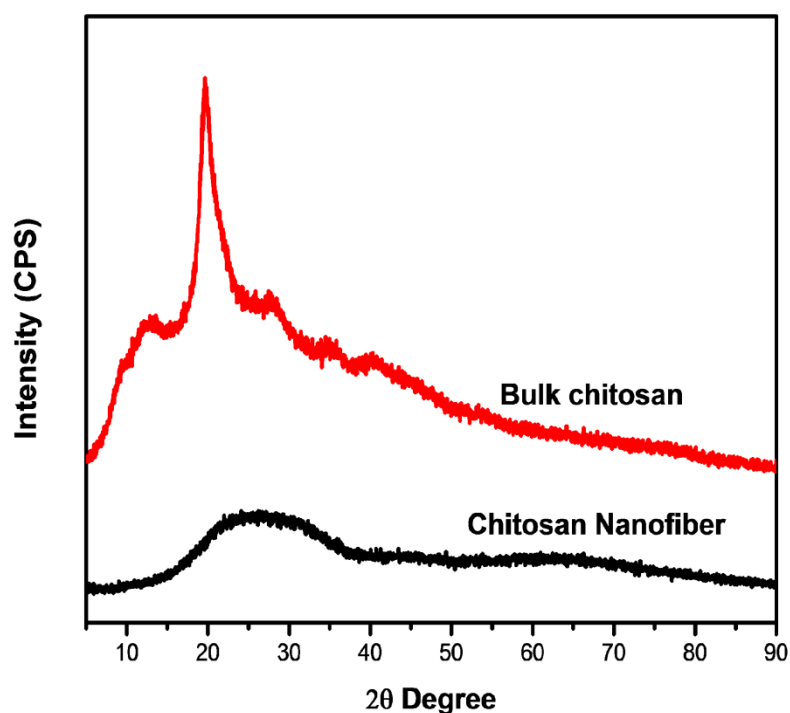


Figure 4.15: X-ray Diffractograms of the nanofibrous mats fabricated from commercial chitosan at optimum conditions (6 wt% of commercial chitosan in TFA, 25 kV applied voltage, a flow rate of 0.1 mL/h and 10 cm tip to collector distance) compared to the bulk commercial chitosan.

For bulk commercial chitosan, the diffractogram showed two peaks, one sharp feature peak and one weak peak around $2\theta=20.1^\circ$ and $2\theta=10.5^\circ$, respectively (Figure 4.15). The peak appearing around $2\theta=20.1^\circ$ has a much higher intensity than the peak around $2\theta=10.5^\circ$ and this is characteristic of chitosan as was discussed in section 4.6. A broad and less intense peak at about 20° - 33° was exhibited in the electrospun nanofiber mat which corresponds to the characteristic

diffraction pattern for the commercial chitosan polymer (Figure 4.15). This diffraction peak appears to be very broad due to the nanostructured nature of the electrospun chitosan nanofiber thus, the lower long range ordering and nano domain ordering nature of chitosan nanofibers can be deduced through the broadening of the peak (Nirmala *et al.*, 2011; Schiffman *et al.*, 2009).

The difference between the intensity of the main peak in bulk commercial chitosan as compared to the electrospun counterpart may be related to the orientation of the chitosan crystals according to the strong elongational field in the electrospinning process, and possibly also to fewer crystals formed (Pakravan *et al.*, 2012). The difference might probably also be due to the fast evaporation of the TFA solvent during the electrospinning process that may prevent the crystals to form completely. The findings of this study are in agreement with Nirmala *et al.* (2011) and Schiffman *et al.* (2009), however, Nirmala *et al.* (2011) obtained a broad peak at about 19° in the electrospun chitosan nanofibers.

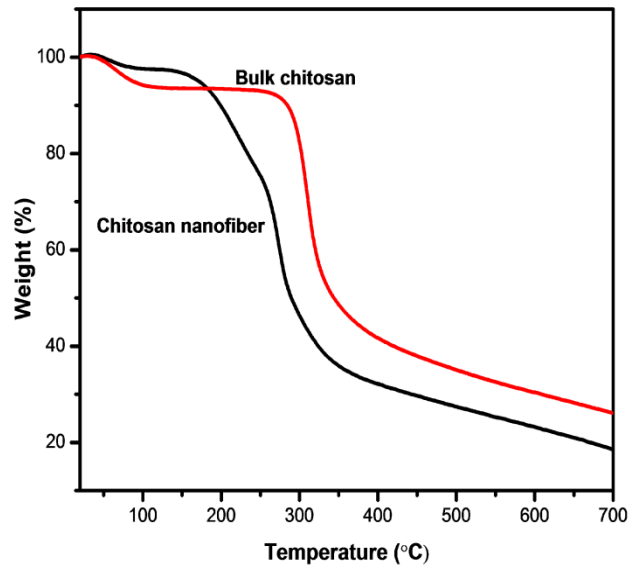
Overall, the results confirm that the electrospun chitosan nanofiber samples exhibited a decrease in the crystallinity due to randomly distributed disruptions of the functional NH₂ and OH groups during the electrospinning process, which diminishes the regularity of the extended chitosan crystal structure, resulting in a more amorphous structure (Cooper *et al.*, 2011). The results confirm that the regular long range order of the crystalline structure of chitosan was altered by the electrospinning process.

4.9.2.4 Thermal degradation behaviour of the optimised chitosan nanofibers

Thermogravimetric analyses were carried out to determine the thermal stability of the electrospun commercial chitosan nanofiber compared to bulk commercial chitosan under nitrogen atmosphere with a flow rate of 20 mL/min. Weight loss with respect to the temperature was quantified from the thermograms by monitoring the thermal degradation profiles of the samples. The thermal stability was obtained using a Perkin Elemer TGA 4000 Thermogravimetric Analyser instrument in a temperature range between 20 to 700 °C at a rate of 10 °C/min under nitrogen atmosphere (experimental details in chapter 3, section 3.6.3). TGA

thermograms (A) and corresponding DTG (B) curves of the electrospun commercial chitosan nanofiber, compared with bulk commercial chitosan, are depicted in Figure 4.16.

A



B

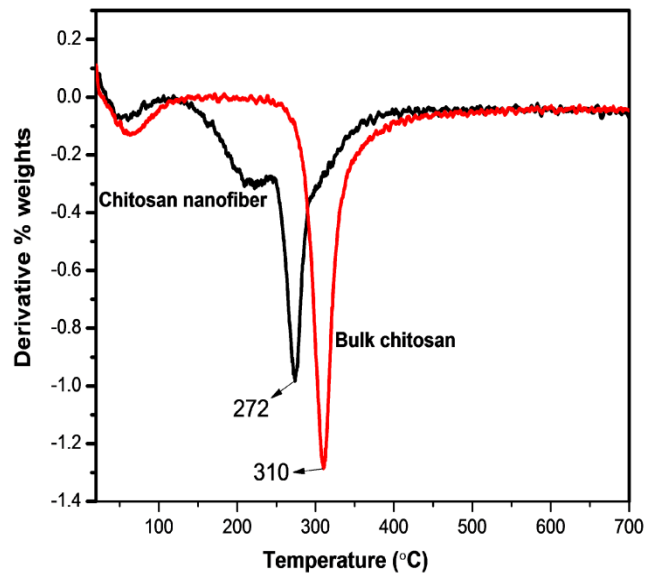


Figure 4.16: TGA (A) and DTG (B) thermograms of the electrospun commercial chitosan nanofiber fabricated from commercial chitosan at optimum conditions (6 wt% of commercial chitosan in TFA, 25 kV applied voltage, a flow rate of 0.1 mL/h solution and 10 cm tip to collector distance) compared with the bulk commercial chitosan.

There are two stages of degradation in the TGA curves for bulk chitosan, the first mass loss occurred in the region 30-130 °C with mass loss of 6.8%, which is attributed to evaporation of moisture that is physically absorbed and strongly hydrogen bonded to the chitosan and the second mass loss occurred in the region 220-490 °C with a mass loss of 50% due to the degradation of the polysaccharide chains and dehydration of deacetylated units of chitosan (Figure 4.16A) (Grząbka-Zasadzińska *et al.*, 2017). The electrospun commercial chitosan nanofibers were decomposed in the region of 120-480 °C and the mass loss was 75% (Figure 4.16A). This increased mass loss might be due to the presence of TFA (Haider *et al.*, 2012), which induced thermal degradation. The thermal degradation peak for bulk commercial chitosan was approximately 310 °C, whereas the thermal degradation peak for the electrospun commercial chitosan nanofiber was approximately 272 °C (Figure 4.16B). These results shows that the bulk chitosan was thermally more stable compared to the electrospun commercial chitosan nanofibers which is usual for nanomaterial. The results of this study are in agreement with Cooper *et al.* (2011), Choo *et al.* (2016) and Mazoochi and Jabbari (2011) studies.

Overall, the thermal properties of chitosan were slightly altered during the electrospinning process. Chitosan nanofiber have lower decomposition temperatures than bulk chitosan due to the higher surface area of the nanofibers and the decrease in thermal stability caused by decreased N-acetyl content and crystallinity (Sik *et al.*, 2009). This result is in good agreement with XRD data. Bulk and nanofiber chitosan does have a level of heat resistance, however, the thermal properties of electrospun chitosan nanofibers could possibly be modified by blending them with other more thermally stable polymers.

4.10 Summary of results and discussion

The best optimum conditions obtained at 1 M HCl, 100 min and 50 °C for demineralisation and 1 M NaOH, 10 h and 85 °C for deproteinisation yielded the highest final dry weight yield of 13% and 5% for pupae shells and adult BSF chitin respectively. The best optimum conditions obtained at 70% NaOH, 5 h and 100 °C for deacetylation yielded the highest final dry weight yield of 11% and 2% for pupae shells and adult BSF chitosan respectively. Both chitins extracted proved to be fibrous in nature with no porosity, whereas the pupae shells and adult BSF chitosan were characterised without any nanofibers and/or nanopores. The elemental analysis results

revealed that both chitins with a degree of acetylation of 115.1% for pupae shells and 91.5% for adult BSF are of acceptable purity. In addition, both chitosans with a degree of deacetylation of 67% for pupae shells and 69% for adult BSF are of acceptable purity. FTIR, TGA and XRD analysis results demonstrated that the chitins from both pupae shells and adult BSF were in the α -form. The FTIR results showed that the extracted chitins were successfully transformed into chitosan. The thermal degradation temperature of chitosan (pupae shells: 306 °C and adult BSF: 309 °C) was lower than that of chitin (pupae shells: 384 °C and adult BSF: 392 °C). Both pupae shells and adult BSF chitin and chitosan samples are crystalline in nature. The MW of the chitosan samples were 217 kDa for pupae shells and 216 kDa for adult BSF. The optimum conditions of the electrospun commercial chitosan nanofibers were obtained at 6 wt% commercial chitosan in TFA, an applied voltage of 25 kV, a tip to collector distance of 10 cm and a flow rate of 0.1 mL/h. The morphology of the optimised commercial chitosan nanofibers had a regular smooth morphology with some small variations in fiber diameter in a bead free network with an average diameter of 130 nm in a range of 60 nm to 200 nm. FTIR analysis revealed that the chemical nature of the polymer during the electrospinning process was not altered. The XRD analysis revealed that the electrospun nanofibers are amorphous and TGA showed that the bulk chitosan (310 °C) was more thermally stable than the electrospun commercial chitosan nanofibers (272 °C).

CHAPTER 5

CONCLUSION AND FUTURE RECOMMENDATIONS

Summary

This chapter gives a brief overview of the results obtained via the conceptual framework of the research and reviews the specific objectives of the study to validate whether the aims of this study were achieved or not. The success, challenges encountered and shortcomings of the study are further discussed. Also outlined here, are the perspectives on future developments for enhancing the electrospinnability of the chitosan nanofibers based on the electrospinning process.

5.1 Conclusion

This study has investigated the extraction of chitin from pupae shells and adult BSF by using a chemical method. This present study is the first finding providing the physiochemical changes of chitin and chitosan extracted from BSF pupae shells and adult BSF. The best optimum conditions obtained for pupae shells and adult BSF for demineralisation process provided the highest yield with decrease in time from 120 to 100 min, temperature from 70 to 50 °C and concentration from 2 to 1 M. Furthermore, the best optimum conditions obtained for pupae shells and adult BSF for deproteinisation process provided the highest yield with decrease in time from 12 to 10 h, temperature from 100 to 85 °C and concentration from 2 to 1 M. This study revealed that the chitin yield was dependent on the time, concentration and temperature. Hence, the following best optimum conditions was obtained for demineralisation at 1 M HCl for 100 min at 50 °C and for deproteinisation at 1 M NaOH for 10 h at 85 °C with the highest final chitin yield of 13% and 5% for pupae shells and adult BSF respectively. The yield of pupae shells and adult BSF chitosan during deacetylation optimisation was found to be the highest with an increase in temperature from 60 to 100 °C and concentration from 50 to 70%; however the yield of chitosan was the lowest with an increase in time from 5 to 9 h. This revealed that the yield of chitosan was dependent on the temperature and concentration. Hence, the following best optimum conditions for deacetylation was obtained at 70% NaOH for 5 h at 100 °C with the highest

chitosan yield of 11% and 2% for pupae shells and adult BSF respectively. In addition, the low amount of nitrogen content shown by elemental analysis, indicated that the amount of proteins that was left in the pupae shells-chitin (6.2%) and adult BSF-chitin (6.5%) was low, which indicates an effective optimum deproteinisation (1 M NaOH, 85 °C, 10 h) method. Furthermore, in the FTIR spectra of pupae shells-chitin and adult BSF-chitin the absorption band 1540 cm⁻¹ which is attributed to protein was found to be absent, hence confirming the effectiveness of the optimum deproteinisation conditions (1 M NaOH, 85 °C, 10 h) method.

According to the elemental analysis both extracted chitins (degree of acetylation: 115.1% (pupae shells) and 91.5% (adult BSF)) and chitosans (degree of deacetylation: 67% pupae shells and 69% (adult BSF)) are of acceptable purity. Both chitins extracted from pupae shells and adult BSF were fibrous in nature with no porosity. After deacetylation, the pupae shells-chitosan was characterised by surface roughness and adult BSF-chitosan mainly had a smooth surface, both without any nanofibers and/or nanopores. The FTIR analysis confirmed the successful extraction of α -chitin from pupae shells and adult BSF. In addition, the FTIR results further showed that the extracted chitins were successfully transformed into chitosan by deacetylation at 70% NaOH for 5 h at 100 °C conditions. The chemical composition and bonding types of chitin and chitosan from adult BSF and pupae shells were very close to a commercially obtained shrimp chitosan product as well as literature. The DTG_{max} values of the chitin from the pupae shells (384 °C) and adult BSF (392 °C) thus also confirmed that the chitins extracted were in the alpha form. The commercial chitin (394 °C) was slightly more thermally stable followed by the adult BSF-chitin (392 °C) and pupae shells-chitin (384 °C). Considering the results of this study it was noted that the thermal degradation temperature of chitosan (306 °C (pupae shells) and 309 °C (adult BSF)) under nitrogen gas was lower than chitins (384 °C (pupae shells) and 392 °C (adult BSF)) due to its amine group which has lower polarity than the chitin amide group with comparatively higher polarity. Both chitin and chitosan samples from pupae shells and adult BSF were crystalline in nature. The MW of the chitosan samples determined by using Mark-Houwink equation was of medium MW (217 kDa (pupae shells) and 216 kDa (adult BSF)). It can thus be concluded overall, that the pupae shells and adult BSF chitins and chitosans were extractable with similar properties to commercial shrimp chitin and chitosan and that there were only small differences in

the physiochemical properties of chitin and chitosan extracted from the different metamorphous development stages of pupae shells and adult BSF.

The characteristics of the chitin and chitosan from pupae shells and adult BSF were similar to those of commercial chitin and chitosan extracted from shrimp, as evaluated by elemental analysis, infrared spectroscopy, x-ray diffraction, scanning electron microscopy and thermogravimetric analysis. Therefore, pupae shells and adult BSF are a suitable alternative source of chitin and chitosan. In addition, chitin and chitosan extracted from pupae shells and adult BSF can generally be said to be of similar quality and purity to commercially produced chitin and chitosan from shrimp, making it an alternative in terms of utilisation and applications. Moreover, due to the fact that BSF populations are large; the adults and pupae shells of this commercially available animal feed species should be collected and transformed into important materials, such as chitin and chitosan, instead of being discarded as waste material.

The electrospinning of bulk commercial shrimp chitosan was difficult to achieve due to its polycationic arrangement and high viscosity. The electrospinning parameters including the collector distance, applied voltage, flow rate and chitosan concentration in TFA optimised in this study had significantly affected the electrospinnability and the quality of the nanofibrous mats. The voltage at 25 kV led to greater stretching of the solution due to the greater coulombic forces in the jet, giving the increased stretching of the jet due to the higher voltage, there was less bead formation observed for commercial chitosan nanofiber. In addition the voltage at 25 kV overcame the surface tension of the polymer solution and therefore initiated jet formation. At an increased flow rate of 0.1 mL/h the uniformity of the chitosan nanofibers improved and less bead and microspheres formation was visible. At the tip to collector distance of 10 cm the distance was large enough to allow evaporation of the solvent during the course of the travel of the solution which resulted in less formation of microspheres and less beads. Bead free electrospun nanofibers were obtained when the solution concentration was increased from 5 wt% to 6 wt% at the optimum conditions of an applied voltage of 25 kV, a flow rate of 0.1 mL/h and a tip to collector distance of 10 cm. The increase in the polymer concentration increased the viscosity of the solution to a critical value, therefore, eliminating the beads completely in the commercial

nanofibrous mats. However the solution became too viscous at a higher chitosan/TFA concentration (8 wt%) which could not be electrospun.

At the optimum conditions of 6 wt% commercial chitosan in TFA, an applied voltage of 25 kV, a flow rate of 0.1 mL/h and a tip to collector distance of 10 cm the morphology for commercial chitosan nanofibers had a regular smooth morphology with some small variations in fiber diameter. In addition, with an increase in the chitosan concentration, it was found that viscosity increased by visual appearance, fiber stretching became more difficult, and as a consequence, thick fibers were produced with broader fiber diameter distribution. The diameters of the optimum nanofibers obtained were in a range of 60 nm to 200 nm.

Overall, the results showed that chitosan nanofiber diameter decreased as applied voltage and flow rate increased, and for tip to collector distance, inverse results were found. The optimum conditions of 6 wt% commercial chitosan in TFA, an applied voltage of 25 kV, a tip to collector distance of 10 cm and a flow rate of 0.1 mL/h resulted in stable, high-quality regular nanofibers of an average diameter of 130 nm for commercial chitosan in a bead free network.

FTIR characterisation of the electrospun chitosan nanofiber made from bulk shrimp chitosan revealed that the amide groups endowed chitosan nanofibers with a stable structure. The electrospun commercial chitosan was found to be of an amorphous nature with less crystallinity than the bulk chitosan due to its nanostructure. The thermal degradation peak for bulk commercial chitosan and electrospun commercial chitosan nanofibers was approximately 310 °C and 272 °C respectively. These results shows that the bulk chitosan was thermally more stable compared to the electrospun commercial chitosan nanofibers which is usual for nanomaterial.

The significance of this study is finding the optimum conditions to extract chitin and chitosan from the promising new alternative source derived from the BSF biomass waste material, owing to its commercial availability at low cost.

5.2 Future work and recommendations

Future developments of the produced chitin and chitosan materials would be by investigating particular applications in different fields. More environmental-friendly solvents than TFA should be investigated to meet the mass production need to prepare chitin and chitosan from these BSF biological sources.

Future investigations should also include the electrospinning of pupae shells and adult BSF chitosan. The high viscosity found at a solution concentration of 8 wt% should be investigated through the application of an alkali treatment of the commercial bulk chitosan which further hydrolyses chitosan chains in order to decrease the MW and in turn reduce its viscosity. The polycationic nature of chitosan excessively increased the surface tension of the solution resulting in a viscous solution therefore surfactants that could lower surface tension of the spinning solution to help reduce the viscosity and electrospinning to occur at a lower electric field should be included in future studies. Regarding the environmental and cost issues with TFA, future studies should include decreasing the solvent concentration or changing the type of solvent used to fabricate nanofibrous mats. In addition, mass production using a solvent such as acetic acid is difficult as the electrospinning rate yield for these solutions is relatively low. In addition, future work should include using a solvent that has less of an environmental impact and a relatively high output. The neutralisation of the obtained nanofibers, with a base or basic salt solution or chemical crosslinking with glutaraldehyde to stabilise the chitosan nanofibers in aqueous media must also be investigated in the future for water stability of the electrospun chitosan nanofibers. The chitosan nanofibers that are stable in an aqueous environment would thus have the potential to be used in biomedical applications. An electrospinning approach generating chitosan-based nanofibers with a substantially-high yield suitable for scale-up production should be the ultimate goal to push electrospun nanofibers from the laboratory to industry.

References

- Abdou, E. S., Nagy, K. S. A., & Elsabee, M. Z. (2008). Extraction and characterization of chitin and chitosan from local sources. *Bioresource Technology*, 99(5), 1359–1367.
- Ahing, F. A., & Wid, N. (2016). Extraction and characterization of chitosan from shrimp shell waste in sabah. *Transactions on Science and Technology*, 3(12), 227–237.
- Alfonso, C., Nuero, O. M., Santamarfa, F., & Reyes, F. (1995). Current Microbiology Purification of a heat-stable chitin deacetylase from *Aspergillus niduans* and its role in cell wall degradation. *Current Microbiology*, 30, 49–54.
- Alooh, A. O. (2015). Quantifying food plate waste : case study of a university dining facility. March 2015. Retrieved from <http://scholar.sun.ac.za/handle/10019.1/96611>
- Andersen, S. O. (2010). Insect cuticular sclerotization: a review. *Insect Biochemistry and Molecular Biology*, 40(3), 166–178.
- Araki, Y., & Ito, E. (1974). A pathway of chitosan formation in *mucor rouxii*: enzymatic deacetylation of chitin. *Biochemical and Biophysical Research Communications*, 56(3), 669–675.
- Aranaz, I., Mengibar, M., Harris, R., Paños, I., Miralles, B., Acosta, N., & Heras, Á. (2009). Functional characterization of chitin and chitosan. *Current Chemical Biology*, 3, 203–230.
- Badenhorst, R. (2017). Genetic diversity in a commercial black soldier fly, *Hermetia illucens* (Diptera: Stratiomyidae), population. March 2017. Retrieved from http://ir.nrf.ac.za/bitstream/handle/10907/1278/badenhorst_genetic_2017.pdf?sequence=1&isAllowed=y
- Bae, M. J., Shin, H. S., Kim, E. K., Kim, J., & Shon, D. H. (2013). Oral administration of chitin and chitosan prevents peanut-induced anaphylaxis in a murine food allergy model. *International Journal of Biological Macromolecules*, 61, 164–168.
- Benelli, G., Canale, A., Raspi, A., & Fornaciari, G. (2014). The death scenario of an Italian Renaissance princess can shed light on a zoological dilemma: did the black soldier fly reach Europe with Columbus? *Journal of Archaeological Science*, 49, 203–205.

- Bhardwaj, N., & Kundu, S. C. (2010). Electrospinning: A fascinating fiber fabrication technique. *Biotechnology Advances*, 28(3), 325–347.
- Boarin Alcalde, L., & Graciano Fonseca, G. (2016). Alkali process for chitin extraction and chitosan production from Nile tilapia (*Oreochromis niloticus*) scales. *Latin American Journal of Aquatic Research*, 44(4), 683–688.
- Bondari, K., & Sheppard, D. C. (1981). Soldier fly larvae as feed in commercial fish production. *Aquaculture*, 24, 103–109.
- Brits, D. (2017). Improving feeding efficiencies of black soldier fly larvae, *Hermetia illucens* (L., 1758) (Diptera: Stratiomyidae: Hermetiinae) through manipulation of feeding conditions for industrial mass rearing. March 2017. Retrieved from <http://ir.nrf.ac.za/handle/10907/1248>
- Cárdenas, G., Cabrera, G., Taboada, E., & Miranda, S. P. (2004). Chitin characterization by SEM, FTIR, XRD, and ¹³C cross polarization/mass angle spinning NMR. *Journal of Applied Polymer Science*, 93(4), 1876–1885.
- Casper, C. L., Stephens, J. S., Tassi, N. G., Chase, D. B., & Rabolt, J. F. (2003). Controlling surface morphology of electrospun polystyrene fibers: effect of humidity and molecular weight in the electrospinning process. *Macromolecules*, 37, 573-578.
- Chen, J. P., Chang, G. Y., & Chen, J. K. (2008). Electrospun collagen/chitosan nanofibrous membrane as wound dressing. *Colloids and Surfaces A: Physicochemical and Engineering Aspects*, 313–314, 183–188.
- Choi, W. H., Yun, J. H., Chu, J. P., & Chu, K. B. (2012). Antibacterial effect of extracts of *Hermetia illucens* (Diptera: Stratiomyidae) larvae against Gram-negative bacteria. *Entomological Research*, 42(5), 219–226.
- Choorit, W., Patthanamane, W., & Manurakchinakorn, S. (2008). Use of response surface method for the determination of demineralization efficiency in fermented shrimp shells. *Bioresource Technology*, 99(14), 6168–6173.

- Cooper, A., Bhattarai, N., Kievit, F. M., Rossol, M., & Zhang, M. (2011). Electrospinning of chitosan derivative nanofibers with structural stability in an aqueous environment. *Physical Chemistry Chemical Physics*, 13(21), 9969.
- Cooper, A., Oldinski, R., Ma, H., Bryers, J. D., & Zhang, M. (2013). Chitosan-based nanofibrous membranes for antibacterial filter applications. *Carbohydrate Polymers*, 92(1), 254–259.
- Cummins, V. C., Rawles, S. D., Thompson, K. R., Velasquez, A., Kobayashi, Y., Hager, J., & Webster, C. D. (2017). Evaluation of black soldier fly (*Hermetia illucens*) larvae meal as partial or total replacement of marine fish meal in practical diets for Pacific white shrimp (*Litopenaeus vannamei*). *Aquaculture*, 473, 337–344.
- Daraghmeh, N. H., Chowdhry, B. Z., Leharne, S. A., Al Omari, M. M., & Badwan, A. A. (2011). Chitin. *In profiles of drug substances, excipients, and related methodology*, 36, 35–10.
- Dash, M., Chiellini, F., Ottenbrite, R. M., & Chiellini, E. (2011). Chitosan-A versatile semi-synthetic polymer in biomedical applications. *Progress in Polymer Science*, 36(8), 981-1014.
- De Groot, M., & Veenvliet, P. (2011). *Hermetia illucens* L. (Diptera, Stratiomyidae), a new alien invasive species in Slovenia. *Acta Entomologica Slovenica*, 19(2), 195-198.
- De Vrieze, S., Westbroek, P., Van Camp, T., & Van Langenhove, L. (2007). Electrospinning of chitosan nanofibrous structures: feasibility study. *Journal of Materials Science*, 42(19), 8029–8034.
- Diener, S., Zurbrügg, C., & Tockner, K. (2009). Conversion of organic material by black soldier fly larvae: establishing optimal feeding rates. *Waste Management & Research*, 27(6), 603–610.
- Ding, F., Deng, H., Du, Y., Shi, X., & Wang, Q. (2014). Emerging chitin and chitosan nanofibrous materials for biomedical applications. *Nanoscale*, 6, 9477–9493.
- Ehrlich, H. (2010). Chitin and collagen as universal and alternative templates in biomineralization. *International Geology Review*, 52(7–8), 661–699.

- Elieh-Ali-Komi, D., & Hamblin, M. R. (2016). Chitin and chitosan: production and application of versatile biomedical nanomaterials. *International Journal of Advanced Research*, 4(3), 411–427.
- Elsabee, M. Z., Naguib, H. F., & Morsi, R. E. (2012). Chitosan based nanofibers, review. *Materials Science and Engineering C*, 32(7), 1711–1726.
- Erdogan, S., & Kaya, M. (2016). High similarity in physicochemical properties of chitin and chitosan from nymphs and adults of a grasshopper. *International Journal of Biological Macromolecules*, 89, 118–126.
- Erdogan, S., Kaya, M., & Akata, I. (2017). Chitin extraction and chitosan production from cell wall of two mushroom species (*Lactarius vellereus* and *Phyllophora ribis*). *AIP Conference Proceedings*, 1809, 020012.
- Fai, A.E.C., Stamford, T.C.M., Stamford-Arnaud, T.M., Santa-Cruz, P.D.A., Freitas da Silva, M.C., Campos-Takaki, G.M., & Stamford, T.L.M. (2011). Physicochemical characteristics and functional properties of chitin and chitosan produced by *Mucor circinelloides* using yam bean as substrate. *Molecules*, 16, 7143-7154.
- Gabler, F., Lalander, C., & Vinnerås, B. (2014). Using black soldier fly for waste recycling and effective *Salmonella* spp. reduction. *Agronomy for sustainable development*, 35, 261-271.
- Gao, X. D., Katsumoto, T., & Onodera, K. (1995). Purification and characterization of chitin deacetylase from *Absidia coerulea*. *Journal of Biochemistry*, 117, 257–263.
- Geng, X., Kwon, O. H., & Jang, J. (2005). Electrospinning of chitosan dissolved in concentrated acetic acid solution. *Biomaterials*, 26(27), 5427–5432.
- Georgieva, V., Zvezdova, D., & Vlaev, L. (2012). Non-isothermal kinetics of thermal degradation of chitosan. *Chemistry Central Journal*, 6(1), 81.
- Gonil, P., & Sajomsang, W. (2012). Applications of magnetic resonance spectroscopy to chitin from insect cuticles. *International Journal of Biological Macromolecules*, 51(4), 514–522.
- Green, T. R., & Popa, R. (2012). Enhanced ammonia content in compost Leachate processed by black soldier fly larvae. *Applied Biochemistry and Biotechnology*, 166(6), 1381–1387.

- Grzabka-Zasadzińska, A., Amietszajew, T., & Borysiak, S. (2017). Thermal and mechanical properties of chitosan nanocomposites with cellulose modified in ionic liquids. *Journal of Thermal Analysis and Calorimetry*, 130(1), 143–154.
- Haghi, A. K., & Akbari, M. (2007). Trends in electrospinning of natural nanofibers. *Physica Status Solidi (A)*, 204(6), 1830–1834.
- Haider, S., & Park, S. Y. (2009). Preparation of the electrospun chitosan nanofibers and their applications to the adsorption of Cu(II) and Pb(II) ions from an aqueous solution. *Journal of Membrane Science*, 328(1–2), 90–96.
- Haider, S., Al-Zeghayer, Y., Al-Masry, W.A & Ali, F. A. A. (2012). Fabrication of chitosan nanofibers membrane with improved stability and britility. *Advanced science letters*, 17, 217-223.
- Hajji, S., Younes, I., Ghorbel-Bellaaj, O., Hajji, R., Rinaudo, M., Nasri, M., & Jellouli, K. (2014). Structural differences between chitin and chitosan extracted from three different marine sources. *International Journal of Biological Macromolecules*, 65, 298–306.
- Hayati, I., Bailey, A., & Tadros, T. (1987). Investigations into the mechanisms of electrohydrodynamic spraying of liquids: I. effect of electric field and the environment on pendant drops and factors affecting the formation of stable jets and atomization. *Journal of Colloid and Interface Science*, 117(1), 205–221.
- Heo, C. C., Mohamad, A. M., Ahmad, F. M. S., Jeffery, J., Kurahashi, H., & Omar, B. (2008). Study of insect succession and rate of decomposition on a partially burned pig carcass in an oil palm plantation in Malaysia. *Tropical Biomedicine*, 25(3), 202–8.
- Hirano, S. (1996). Chitin biotechnology applications. *Biotechnology Annual Review*, 2, 237–258.
- Holmes, L. A., VanLaerhoven, S. L., & Tomberlin, J. K. (2016). Lower temperature threshold of black soldier fly (Diptera: Stratiomyidae) development. *Journal of Insects as Food and Feed*, 2(4), 255–262.
- Homayoni, H., Ravandi, S. A. H., & Valizadeh, M. (2009). Electrospinning of chitosan nanofibers: processing optimization. *Carbohydrate Polymers*, 77(3), 656–661.

- Hossain, M. S., & Iqbal, A. (2014). Production and characterization of chitosan from shrimp waste. *Journal of the Bangladesh Agricultural University*, *12*(1), 153–160.
- Ibitoye, E. B., Lokman, I. H., Hezmee, M. N. M., Goh, Y. M., Zuki, A. B. Z., & Jimoh, A. A. (2018). Extraction and physicochemical characterization of chitin and chitosan isolated from house cricket. *Biomedical Materials (Bristol)*, *13*(2).
- Ifuku, S., Nomura, R., Morimoto, M., & Saimoto, H. (2011). Preparation of chitin nanofibers from mushrooms. *Materials*, *4*(8), 1417–1425.
- Ioelovich, M. (2014). Crystallinity and hydrophilicity of chitin and chitosan. *Journal of Chemistry*, *3*(3), 7–14.
- Jayakumar, R., Nwe, N., Tokura, S., & Tamura, H. (2007). Sulfated chitin and chitosan as novel biomaterials. *International Journal of Biological Macromolecules*, *40*(3), 175–181.
- Karapanagiotidis, I. T., Daskalopoulou, E., Vogiatzis, I., Rumbos, C., Mente, E., & Athanassiou, C. G. (2014). Substitution of fishmeal by fly *Hermetia illucens* prepupae meal in the diet of Gilthead Seabream (*Sparus aurata*). *HydroMedit*, *2014*, 110–114.
- Kardas, I., Struszczyk, M. H., Kucharska, M., van den Broek, L. A. M., van Dam, J. E. G., & Ciechańska, D. (2012). Chitin and chitosan as functional biopolymers for industrial applications. *The European Polysaccharide Network of Excellence (EPNOE)* (pp. 329–373). Vienna: Springer Vienna. Retrieved from https://doi.org/10.1007/978-3-7091-0421-7_11
- Kaya, M., Akyuz, B., Bulut, E., Sargin, I., Eroglu, F., & Tan, G. (2016). Chitosan nanofiber production from *Drosophila* by electrospinning. *International Journal of Biological Macromolecules*, *92*, 49–55.
- Kaya, M., Baran, T., Asan-Ozusaglam, M., Cakmak, Y. S., Tozak, K. O., Mol, A., & Sezen, G. (2015). Extraction and characterization of chitin and chitosan with antimicrobial and antioxidant activities from cosmopolitan Orthoptera species (Insecta). *Biotechnology and Bioprocess Engineering*, *20*(1), 168–179.

- Kaya, M., Baran, T., Erdolan, S., Menteş, A., Aşan Özusađlam, M., & Çakmak, Y. S. (2014). Physicochemical comparison of chitin and chitosan obtained from larvae and adult Colorado potato beetle (*Leptinotarsa decemlineata*). *Materials Science and Engineering C*, *45*, 72–81.
- Kaya, M., Baran, T., & Karaarslan, M. (2015). A new method for fast chitin extraction from shells of crab, crayfish and shrimp. *Natural Product Research*, *29*(15), 1477–1480.
- Kaya, M., Baublys, V., Can, E., Šatkauskiene, I., Bitim, B., Tubelyte, V., & Baran, T. (2014). Comparison of physicochemical properties of chitins isolated from an insect (*Melolontha melolontha*) and a crustacean species (*Oniscus asellus*). *Zoomorphology*, *133*(3), 285–293.
- Kaya, M., Baublys, V., Šatkauskiene, I., Akyuz, B., Bulut, E., & Tubelyte, V. (2015). First chitin extraction from *Plumatella repens* (Bryozoa) with comparison to chitins of insect and fungal origin. *International Journal of Biological Macromolecules*, *79*, 126–132.
- Kaya, M., Cakmak, Y. S., Baran, T., Asan-Ozusaglam, M., Menten, A., & Tozak, K. O. (2014). New chitin, chitosan, and O-carboxymethyl chitosan sources from resting eggs of *Daphnia longispina* (Crustacea); with physicochemical characterization, and antimicrobial and antioxidant activities. *Biotechnology and Bioprocess Engineering*, *19*, 58–69.
- Kaya, M., Erdogan, S., Mol, A., & Baran, T. (2015). Comparison of chitin structures isolated from seven Orthoptera species. *International Journal of Biological Macromolecules*, *72*, 797–805.
- Kaya, M., Lelešius, E., Nagrockaitė, R., Sargin, I., Arslan, G., Mol, A., & Bitim, B. (2015). Differentiations of chitin content and surface morphologies of chitins extracted from male and female grasshopper species. *Peer-reviewed open access scientific journal*, *10*(1), e0115531.
- Kaya, M., Mujtaba, M., Ehrlich, H., Salaberria, A. M., Baran, T., Amemiya, C. T., & Labidi, J. (2017). On chemistry of γ -chitin. *Carbohydrate Polymers*, *176*(July), 177–186.
- Kaya, M., Sargin, I., Tozak, K. Ö., Baran, T., Erdogan, S., & Sezen, G. (2013). Chitin extraction and characterization from *Daphnia magna* resting eggs. *International Journal of Biological Macromolecules*, *61*, 459–464.

- Kaya, M., Seyyar, O., Baran, T., Erdoğan, S., & Kar, M. (2014). A physicochemical characterization of fully acetylated chitin structure isolated from two spider species: with new surface morphology. *International Journal of Biological Macromolecules*, *65*, 553–558.
- Kaya, M., Seyyar, O., Baran, T., & Turkes, T. (2014). Bat guano as new and attractive chitin and chitosan source. *Frontiers in Zoology*, *11*(1), 59.
- Kaya, M., Sofi, K., Sargin, I., & Mujtaba, M. (2016). Changes in physicochemical properties of chitin at developmental stages (larvae, pupa and adult) of *Vespa crabro* (wasp). *Carbohydrate Polymers*, *145*, 64–70.
- Ki, C. S., Baek, D. H., Gang, K. D., Lee, K. H., Um, I. C., & Park, Y. H. (2005). Characterization of gelatin nanofiber prepared from gelatin–formic acid solution. *Polymer*, *46*(14), 5094–5102.
- Kim, M. W., Han, Y. S., Jo, Y. H., Choi, M. H., Kang, S. H., Kim, S. A., & Jung, W. J. (2016). Extraction of chitin and chitosan from housefly, *Musca domestica*, pupa shells. *Entomological Research*, *46*(5), 324–328.
- Kim, W., Bae, S., Park, K., Lee, S., Choi, Y., Han, S., & Koh, Y. (2011). Biochemical characterization of digestive enzymes in the black soldier fly, *Hermetia illucens* (Diptera: Stratiomyidae). *Journal of Asia-Pacific Entomology*, *14*(1), 11–14.
- Krishnaveni, B., & Ragnathan, R. (2015). Extraction and characterization of chitin and chitosan from *Aspergillus terreus* sps, synthesis of their bionanocomposites and study of their productive applications. *Journal of Chemical and Pharmaceutical Research*, *7*(2), 115–132.
- Kucukgulmez, A., Celik, M., Yanar, Y., Sen, D., Polat, H., & Kadak, A. E. (2011). Physicochemical characterization of chitosan extracted from *Metapenaeus stebbingi* shells. *Food Chemistry*, *126*(3), 1144–1148.
- Kumari, S., Kumar Annamareddy, S. H., Abanti, S., & Kumar Rath, P. (2017). Physicochemical properties and characterization of chitosan synthesized from fish scales, crab and shrimp shells. *International Journal of Biological Macromolecules*, *104*, 1697–1705.

- Kumari, S., & Rath, P. K. (2014). Extraction and characterization of chitin and chitosan from (Labeo rohita) Fish Scales. *Procedia Materials Science*, 6, 482–489.
- Lavall, R. L., Assis, O. B. G., & Campana-Filho, S. P. (2007). β -Chitin from the pens of *Loligo* sp.: extraction and characterization. *Bioresource Technology*, 98(13), 2465–2472.
- Lee, S. B., Kim, Y. S., Ham, S.-K., Lim, H. J., Choi, Y. C., & Park, K. H. (2013). Effect of soldier fly casts mixed soil on change of soil properties in root zone and growth of *Zoysiagrass*. *Weed & Turfgrass Science*, 2(3), 298–305.
- Lehane, M. J. (1997). Peritrophic matrix structure and function. *Annual Review of Entomology*, 42, 525–50.
- Lemma, S. M., Bossard, F., & Rinaudo, M. (2016). Preparation of pure and stable chitosan nanofibers by electrospinning in the presence of poly(ethylene oxide). *International Journal of Molecular Sciences*, 17(11).
- Leong, S. Y., Kutty, S. R. M., Malakahmad, A., & Tan, C. K. (2016). Feasibility study of biodiesel production using lipids of *Hermetia illucens* larva fed with organic waste. *Waste Management*, 47, 84–90.
- Leong, S. Y., Kutty, S. R. M., Tan, C. K., & Tey, L. H. (2015). Comparative study on the effect on organic waste on lauric acid produced by *Hermetia illucens* larvae via bioconversion. *Journal of Engineering Science and Technology Special Issue on ACEE Conference August*, 8. 52-63.
- Lertsutthiwong, P., How, N. C., & Chandkrachang, S. (2002). Effect of chemical treatment on the characteristics of shrimp chitosan. *Journal of Metals Materials and Minerals*, 12(1), 11–18.
- Li, Q., Zheng, L., Cai, H., Garza, E., Yu, Z., & Zhou, S. (2011). From organic waste to biodiesel: black soldier fly, *Hermetia illucens*, makes it feasible. *Fuel*, 90(4), 1545–1548.
- Liu, S., Sun, J., Yu, L., Zhang, C., Bi, J., Zhu, F., & Yang, Q. (2012). Extraction and characterization of chitin from the beetle *Holotrichia parallela* motschulsky. *Molecules*, 17(4), 4604–4611.

- Ma, G., Fang, D., Liu, Y., Zhu, X., & Nie, J. (2012). Electrospun sodium alginate/poly(ethylene oxide) core-shell nanofibers scaffolds potential for tissue engineering applications. *Carbohydrate Polymers*, 87(1), 737–743.
- Magalhães, R., Sánchez-López, A., Leal, R. S., Martínez-Llorens, S., Oliva-Teles, A., & Peres, H. (2017). Black soldier fly (*Hermetia illucens*) pre-pupae meal as a fish meal replacement in diets for European seabass (*Dicentrarchus labrax*). *Aquaculture*, 476, 79–85.
- Majtán, J., Bíliková, K., Markovič, O., Gróf, J., Kogan, G., & Šimúth, J. (2007). Isolation and characterization of chitin from bumblebee (*Bombus terrestris*). *International Journal of Biological Macromolecules*, 40(3), 237–241.
- Marei, N. H., El-Samie, E. A., Salah, T., Saad, G. R., & Elwahy, A. H. M. (2016). Isolation and characterization of chitosan from different local insects in Egypt. *International Journal of Biological Macromolecules*, 82, 871–877.
- Marreco, P. R., Moreira, P. da L., Genari, S. C., & Moraes, A. M. (2004). Effects of different sterilization methods on the morphology, mechanical properties, and cytotoxicity of chitosan membranes used as wound dressings. *Journal of Biomedical Materials Research*, 71B(2), 268–277.
- Mati-Baouche, N., Elchinger, P.-H., de Baynast, H., Pierre, G., Delattre, C., & Michaud, P. (2014). Chitosan as an adhesive. *European Polymer Journal*, 60, 198–212.
- McKee, M.G., Wilkes, G.L., Colby, R.H & Long. T.E. (2004). Correlations of solution rheology with electrospun fiber formation of linear and branched polyesters. *Macromolecules*, 37(5), 1760-1767.
- Mazoochi, T., & Jabbari, V. (2011). Chitosan nanofibrous scaffold fabricated via electrospinning: the effect of processing parameters on the nanofiber morphology. *International Journal of Polymer Analysis and Characterization*, 16(5), 277–289.
- Merzendorfer, H. (2003). Chitin metabolism in insects: structure, function and regulation of chitin synthases and chitinases. *Journal of Experimental Biology*, 206(24), 4393–4412.

- Mishra, M. K. (n.d.). *Handbook of encapsulation and controlled release*. Retrieved from https://books.google.co.in/books?id=pY7wCgAAQBAJ&pg=PA278&lpg=PA278&dq=Classification+of+chitosan+based+on+molecular+weight+low,+medium+and+high&source=bl&ots=OolMBfn7w&sig=hg7bToa_PN0UbKJIopN0m4skPzA&hl=en&sa=X&ved=0ahUK EwjgZ_S7djKAhWHGY4KHfBKCxMQ6AEILjAC#v=onepage&q=Classification of chitosan based on molecular weight low%2C medium and high&f=false
- Mit-uppatham, C., Nithitanakul, M., & Supaphol, P. (2004). Ultrafine electrospun polyamide-6 fibers: effect of solution conditions on morphology and average fiber diameter. *Macromolecular Chemistry and Physics*, 205(17), 2327–2338.
- Mohammedi, Z. (2017). Chitosan and chitosan oligosaccharides: applications in medicine, agriculture and biotechnology. *International Journal of Bioorganic Chemistry*, 2(3), 102–106.
- Monarul Islam, M., Md Masum, S., Mahbubur Rahman, M., Ashraful Islam Molla, M., Shaikh, A. A., & Roy, S. (2011). Preparation of chitosan from shrimp shell and investigation of its properties. *International Journal of Basic & Applied Sciences IJBAS-IJENS*, 11, 1–77.
- Morin, A., & Dufresne, A. (2002). Nanocomposites of chitin whiskers from *Riftia* tubes and poly(caprolactone). *Macromolecules*, 35(6), 2190–2199.
- Moussout, H., Ahlafi, H., Aazza, M., & Bourakhouadar, M. (2016). Kinetics and mechanism of the thermal degradation of biopolymers chitin and chitosan using thermogravimetric analysis. *Polymer Degradation and Stability*, 130, 1–9.
- Ndueze, O. U., Okiwelu, S. N., Umeozor, O. C., & Noutcha, M. A. E. (2013). Arthropod succession on wildlife carcasses in lowland rainforest, Rivers State, Nigeria. *European Journal of Experimental Biology*, 3(5), 106–110.
- Nemtsev, S. V., Zueva, O. Y., Khismatullin, M. R., Albulov, A. I., & Varlamov, V. P. (2004). Isolation of chitin and chitosan from honeybees. *Applied Biochemistry and Microbiology*, 40(1), 39–43.

- Newton, L., Sheppard, C., Watson, D. W., & Burtle, G. (2005). Using the black soldier fly, *Hermetia illucens*, as a value-added tool for the management of swine manure executive summary. Animal and poultry waste management center, North Carolina State University, Raleigh, NC. USA. Retrieved from http://www.organicvaluerecovery.com/studies/studies_htm_files/bsf_value_added.pdf
- Nguyen, D. T., Bouguet, V., Spranghers, T., Vangansbeke, D., & De Clercq, P. (2015). Beneficial effect of supplementing an artificial diet for *Amblyseius swirskii* with *Hermetia illucens* haemolymph. *Journal of Applied Entomology*, *139*(5), 342–351.
- Nguyen, T. T. X., Tomberlin, J. K., & Vanlaerhoven, S. (2015). Ability of black soldier fly (Diptera: Stratiomyidae) larvae to recycle food waste. *Environmental Entomology*, *44*(2), 406–410.
- Nirmala, R., Il, B. W., Navamathavan, R., El-Newehy, M. H., & Kim, H. Y. (2011). Preparation and characterizations of anisotropic chitosan nanofibers via electrospinning. *Macromolecular Research*, *19*(4), 345–350.
- No, H. K., & Meyers, S. P. (1989). Crawfish chitosan as a coagulant in recovery of organic compounds from seafood processing streams. *Journal of Agricultural and Food Chemistry*, *37*(3), 580–583.
- Ofem, M. I., Anyandi, A. J., Ene, E. B., Iver, C. R. R., & Of, U. N. I. V. (2017). Properties of chitin reinforces composites: a review, *Nigerian Journal of Technology*, *36*(1), 57–71.
- Oliveira, J. E., Mattoso, L. H. C., Orts, W. J., & Medeiros, E. S. (2013). Structural and morphological characterization of micro and nanofibers produced by electrospinning and solution blow spinning : a comparative study, *Advances in Materials Science and Engineering*, *2013*, 1-14
- Pakravan, M., Heuzey, M. C., & Ajji, A. (2012). Core-shell structured PEO-chitosan nanofibers by coaxial electrospinning. *Biomacromolecules*, *13*(2), 412–421.

- Park, K. H., Choi, Y. C., Nam, S. H., Kim, W. T., Kim, A. Y., & Kim, S. Y. (2012). Recombinant expression and enzyme activity of chymotrypsin-like protease from black soldier fly, *Hermetia illucens* (Diptera: Stratiomyidae). *International Journal of Industrial Entomology*, 25(2), 181–185.
- Paulino, A. T., Simionato, J. I., Garcia, J. C., & Nozaki, J. (2006). Characterization of chitosan and chitin produced from silkworm crysalides. *Carbohydrate Polymers*, 64(1), 98–103.
- Pham, Q. P., Sharma, U., & Mikos, A. G. (2006). Electrospun poly(ϵ -caprolactone) microfiber and multilayer nanofiber/microfiber scaffolds: characterization of scaffolds and measurement of cellular infiltration. *Biomacromolecules*, 7(10), 2796–2805.
- Philibert, T., Lee, B. H., & Fabien, N. (2017). Current status and new perspectives on chitin and chitosan as functional biopolymers. *Applied Biochemistry and Biotechnology*, 181(4), 1314–1337.
- Prabaharan, M., & Jayakumar, R. (2009). Chitosan-graft- β -cyclodextrin scaffolds with controlled drug release capability for tissue engineering applications. *International Journal of Biological Macromolecules*, 44(4), 320–325.
- Pujol-Luz, J. R., Francez, P. A. da C., Ururahy-Rodrigues, A., & Constantino, R. (2008). The black soldier-fly, *Hermetia illucens* (Diptera, Stratiomyidae), used to estimate the postmortem interval in a case in Amapá State, Brazil. *Journal of Forensic Sciences*, 53(2), 476–478.
- Ravi Kumar, M. N. (2000). A review of chitin and chitosan applications. *Reactive and Functional Polymers*, 46(1), 1–27.
- Rawda M. B., & Hadeer I. M. (2015). Chitin extration, composition of different six insect species and their comparable characteristics with that of the shrimp. *Journal of American Science*, 11(6), 127–134.
- Renault, F., Sancey, B., Charles, J., Morin-Crini, N., Badot, P. M., Winterton, P., & Crini, G. (2009). Chitosan flocculation of cardboard-mill secondary biological wastewater. *Chemical Engineering Journal*, 155(3), 775–783.

- Rieger, K. A., Birch, N. P., & Schiffman, J. D. (2016). Electrospinning chitosan/poly(ethylene oxide) solutions with essential oils: correlating solution rheology to nanofiber formation. *Carbohydrate Polymers*, *139*, 131–138.
- Sajomsang, W., & Gonil, P. (2010). Preparation and characterization of α -chitin from cicada sloughs. *Materials Science and Engineering C*, *30*(3), 357–363.
- Salomone, R., Saija, G., Mondello, G., Giannetto, A., Fasulo, S., & Savastano, D. (2017). Environmental impact of food waste bioconversion by insects: application of life cycle assessment to process using *Hermetia illucens*. *Journal of Cleaner Production*, *140*, 890–905.
- Sangsanoh, P., & Supaphol, P. (2006). Stability improvement of electrospun chitosan nanofibrous membranes in neutral or weak basic aqueous solutions. *Biomacromolecules*, *7*(10), 2710–2714.
- Schiffman, J. D., & Schauer, C. L. (2007a). Cross-linking chitosan nanofibers. *Biomacromolecules*, *8*(2), 594-601.
- Schiffman, J. D., & Schauer, C. L. (2007b). One-step electrospinning of cross-linked chitosan fibers. *Biomacromolecules*, *8*(9), 2665-2667.
- Schiffman, J. D., Stulga, L. A., & Schauer, C. L. (2009). Chitin and chitosan: transformations due to the electrospinning process. *Polymer Engineering & Science*, *49*(10), 1918-1920.
- Shanmuga Priya, D., Suriyaprabha, R., Yuvakkumar, R., & Rajendran, V. (2014). Chitosan-incorporated different nanocomposite HPMC films for food preservation. *Journal of Nanoparticle Research*, *16*(2), 2248.
- Shao, L., Devenport, M., & Jacobs-Lorena, M. (2001). The peritrophic matrix of hematophagous insects. *Archives of Insect Biochemistry and Physiology*, *47*, 119–125.
- Sichina, W. J. (2000). Characterization of polymers using TGA. *Manager*, 1–5.
- Sik, Y., Ho, W., Ihm, D., & Hudson, S. M. (2010). Effect of the degree of deacetylation on the thermal decomposition of chitin and chitosan nanofibers. *Carbohydrate Polymers*, *80*(1), 291–295.

- Simionato, J. I., Villalobos, L. D. G., Bulla, M. K., Coró, F. A. G., & Garcia, J. C. (2014). Application of chitin and chitosan extracted from silkworm chrysalides in the treatment of textile effluents contaminated with remazol dyes. *Acta Scientiarum. Technology*, 36(4), 693–698.
- Simionatto, L. (2006). The use of DSC curves to determine the acetylation degree of chitin/chitosan samples. *Thermochimica Acta*, 444, 128–133.
- Skřivanová, E., Marounek, M., Dlouhá, G., & Kaňka, J. (2005). Susceptibility of *Clostridium perfringens* to C2-C18 fatty acids. *Letters in Applied Microbiology*, 41(1), 77–81.
- Soon, C. Y., Tee, Y. B., Tan, C. H., Rosnita, A. T., & Khalina, A. (2018). Extraction and physicochemical characterization of chitin and chitosan from *Zophobas morio* larvae in varying sodium hydroxide concentration. *International Journal of Biological Macromolecules*, 108, 135–142.
- Spranghers, T., Michiels, J., Vrancx, J., Owyn, A., Eeckhout, M., De Clercq, P., & De Smet, S. (2018). Gut antimicrobial effects and nutritional value of black soldier fly (*Hermetia illucens* L.) prepupae for weaned piglets. *Animal Feed Science and Technology*, 235(June 2017), 33–42.
- Spranghers, T., Ottoboni, M., Klootwijk, C., Owyn, A., Deboosere, S., De Meulenaer, B., & De Smet, S. (2017). Nutritional composition of black soldier fly (*Hermetia illucens*) prepupae reared on different organic waste substrates. *Journal of the Science of Food and Agriculture*, 97(8), 2594–2600.
- Sripontan, Y., Juntavimon, T., Songin, S., & Chiu, C. I. (2017). Egg-trapping of black soldier fly, *Hermetia illucens* (L.) (Diptera : Stratiomyidae) with various wastes and the effects of environmental factors on egg-laying. *Khon Kaen Agriculture Journal*, 45(1), 179–184.
- Sun, K., & Li, Z. H. (2011). Preparations, properties and applications of chitosan based nanofibers fabricated by electrospinning. *Express Polymer Letters*, 5(4), 342–361.

- Suneeta, K., Rath, P., & Sri, H. K. A. (2016). Chitosan from shrimp shell (*Crangon crangon*) and fish scales (*Labeorohita*): extraction and characterization. *African Journal of Biotechnology*, *15*(24), 1258–1268.
- Surendra, K. C., Olivier, R., Tomberlin, J. K., Jha, R., & Khanal, S. K. (2016). Bioconversion of organic wastes into biodiesel and animal feed via insect farming. *Renewable Energy*, *98*, 197–202.
- Synowiecki, J., & Al-Khateeb, N. A. (2003). Production, properties, and some new applications of chitin and its derivatives. *Critical Reviews in Food Science and Nutrition*, *43*(2), 145–171.
- Tajik, H., Moradi, M., Rohani, S., Erfani, A., & Jalali, F. (2008). Preparation of chitosan from brine shrimp (*Artemia urmiana*) cyst shells and effects of different chemical processing sequences on the physicochemical and functional properties of the product. *Molecules*, *13*(6), 1263–1274.
- Thongngam, M., & McClements, D. J. (2004). Characterization of interactions between chitosan and an anionic surfactant. *Journal of Agricultural and Food Chemistry*, *52*(4), 987–991.
- Tolaimate, A., Desbrieres, J., Rhazi, M., & Alagui, A. (2003). Contribution to the preparation of chitins and chitosans with controlled physico-chemical properties. *Polymer*, *44*(26), 7939–7952.
- Tolaimate, A., Desbrières, J., Rhazi, M., Alagui, A., Vincendon, M., & Vottero, P. (2000). On the influence of deacetylation process on the physicochemical characteristics of chitosan from squid chitin. *Polymer*, *41*(7), 2463–2469.
- Tomberlin, J. K., Adler, P. H., & Myers, H. M. (2009). Development of the black soldier fly (Diptera: Stratiomyidae) in relation to temperature. *Environmental Entomology*, *38*(3), 930–4.
- Tomberlin, J. K., Sheppard, D. C., & Joyce, J. A. (2005). Black soldier fly (Diptera: Stratiomyidae) colonization of pig carrion in south Georgia. *Journal of Forensic Sciences*, *50*(1), 152–3.

- Torres-Giner, S., Ocio, M. J., & Lagaron, J. M. (2008). Development of active antimicrobial fiber based chitosan polysaccharide nanostructures using electrospinning. *Engineering in Life Sciences*, 8(3), 303–314.
- Tsigos, I., & Bouriotis, V. (1995). Purification and characterization of chitin deacetylase from *Colletotrichum lindemuthianum*. *The Journal of Biological Chemistry*, 270(44), 26286–91.
- van Huis, A. (2013). Potential of insects as food and feed in assuring food security. *Annual Review of Entomology*, 58(1), 563–583.
- Vasiliev, Y. M. (2015). Chitosan-based vaccine adjuvants: incomplete characterization complicates preclinical and clinical evaluation. *Expert Review of Vaccines*, 14(1), 37–53.
- Wang, W., Ouyang, K., Ouyang, J., Li, H., Lin, S., & Sun, H. (2004). Polymorphism of insulin-like growth factor I gene in six chicken breeds and its relationship with growth traits. *Asian-Australasian Journal of Animal Sciences*, 17(3), 301-304.
- Wang, X., & Hsiao, B. S. (2016). Electrospun nanofiber membranes. *Current Opinion in Chemical Engineering*, 12, 62–81.
- Wang, Y. S., & Shelomi, M. (2017). Review of black soldier fly (*Hermetia illucens*) as animal feed and human food. *Foods*, 6(10), 91.
- Wang, Y., Chang, Y., Yu, L., Zhang, C., Xu, X., Xue, Y., & Xue, C. (2013). Crystalline structure and thermal property characterization of chitin from Antarctic krill (*Euphausia superba*). *Carbohydrate Polymers*, 92(1), 90–97.
- Wanule, D., Balkhande, J. V., Ratnakar, P. U., Kulkarni, A. N., & Bhowate, C. S. (2014). Extraction and FTIR analysis of chitosan from american cockroach, *Periplaneta americana*. *International Journal of Engineering Science and Innovative Technology*, 3(3), 299–304.
- Waśko, A., Bulak, P., Polak-Berecka, M., Nowak, K., Polakowski, C., & Bieganski, A. (2016). The first report of the physicochemical structure of chitin isolated from *Hermetia illucens*. *International Journal of Biological Macromolecules*, 92, 316–320.

- Wysokowski, M., Bazhenov, V. V., Tsurkan, M. V., Galli, R., Stelling, A. L., Stöcker, H., & Ehrlich, H. (2013). Isolation and identification of chitin in three-dimensional skeleton of *Aplysina fistularis* marine sponge. *International Journal of Biological Macromolecules*, *62*, 94–100.
- Wysokowski, M., Petrenko, I., Stelling, A. L., Stawski, D., Jesionowski, T., & Ehrlich, H. (2015). Poriferan chitin as a versatile template for extreme biomimetics. *Polymers*, *7*(2), 235–265.
- Yen, M. T., & Mau, J. L. (2007). Physico-chemical characterization of fungal chitosan from shiitake stipes. *LWT - Food Science and Technology*, *40*(3), 472–479.
- Yen, M. T., Yang, J. H., & Mau, J. L. (2009). Physicochemical characterization of chitin and chitosan from crab shells. *Carbohydrate Polymers*, *75*(1), 15–21.
- Yeul, V. S., & Rayalu, S. S. (2013). Unprecedented chitin and chitosan: a chemical overview. *Journal of Polymers and the Environment*, *21*(2), 606–614.
- Yördem, O. S., Papila, M., & Menciloğlu, Y. Z. (2008). Effects of electrospinning parameters on polyacrylonitrile nanofiber diameter: An investigation by response surface methodology. *Materials & Design*, *29*(1), 34–44.
- Younes, I., & Rinaudo, M. (2015). Chitin and chitosan preparation from marine sources. structure, properties and applications. *Marine Drugs*, *13*(3), 1133–1174.
- Yu, G., Cheng, P., Chen, Y., Li, Y., Yang, Z., Chen, Y., & Tomberlin, J. K. (2011). Inoculating poultry manure with companion bacteria influences growth and development of black soldier fly (Diptera: Stratiomyidae) larvae. *Environmental Entomology*, *40*(1), 30–35.
- Yuan, X., Zhang, Y., Dong, C., & Sheng, J. (2004). Morphology of ultrafine polysulfone fibers prepared by electrospinning. *Polymer International*, *53*(11), 1704–1710.
- Zaku, S. G., Aguzue, S., & Thomas, S. A. (2011). Extraction and characterization of chitin ; a functional biopolymer obtained from scales of common carp fish (*Cyprinus carpio* l .): A lesser known source. *African Journal of Food Science*, *5*(8), 478–483.

- Zhang, Y., Chwee, T. L., Ramakrishna, S., & Huang, Z. M. (2005). Recent development of polymer nanofibers for biomedical and biotechnological applications. *Journal of Materials Science: Materials in Medicine*, *16*(10), 933–946.
- Zheng, H., Du, Y., Yu, J., Huang, R., & Zhang, L. (2001). Preparation and characterization of chitosan/poly(vinyl alcohol) blend fibers. *Journal of Applied Polymer Science*, *80*(13), 2558–2565.
- Zhou, G., Zhang, H., He, Y., & He, L. (2010). Identification of a chitin deacetylase producing bacteria isolated from soil and its fermentation optimization. *African Journal of Microbiology Research*, *4*(23), 2597–2603.
- Zhou, Z., Jiang, F., Lee, T. C., & Yue, T. (2013). Two-step preparation of nano-scaled magnetic chitosan particles using Triton X-100 reversed-phase water-in-oil microemulsion system. *Journal of Alloys and Compounds*, *581*, 843–848.
- Zhu, K. Y., Merzendorfer, H., Zhang, W., Zhang, J., & Muthukrishnan, S. (2016). Biosynthesis, Turnover, and Functions of Chitin in Insects. *Annual Review of Entomology*, *61*, 177–96.